# Synthesis and Stability of Ceramic-Carbonate Dual-Phase Membrane for Carbon Dioxide Separation

by

Tyler Norton

A Dissertation Presented in Partial Fulfillment
of the Requirements for the Degree
Doctor of Philosophy

Approved October 2013 by the
Graduate Supervisory Committee:

Jerry Y.S. Lin, Chair
Terry Alford
Mary Laura Lind
David Smith
Cesar Torres

ARIZONA STATE UNIVERSITY

December 2013

## ABSTRACT

Of the potential technologies for pre-combustion capture, membranes offer the advantages of being temperature resistant, able to handle large flow rates, and having a relatively small footprint. A significant amount of research has centered on the use of polymeric and microporous inorganic membranes to separate $CO_2$. These membranes, however, have limitations at high temperature resulting in poor permeation performance. To address these limitations, the use of a dense dual-phase membrane has been studied. These membranes are composed of conductive solid and conductive liquid phases that have the ability to selectively permeate $CO_2$ by forming carbonate ions that diffuse through the membrane at high temperature. The driving force for transport through the membrane is a $CO_2$ partial pressure gradient. The membrane provides a theoretically infinite selectivity.

To address stability of the ceramic-carbonate dual-phase membrane for $CO_2$ capture at high temperature, the ceramic phase of the membrane was studied and replaced with materials previously shown to be stable in harsh conditions. The permeation properties and stability of $La_{0.6}Sr_{0.4}Co_{0.8}Fe_{0.2}O_{3-\delta}$ (LSCF)-carbonate, $La_{0.85}Ce_{0.1}Ga_{0.3}Fe_{0.65}Al_{0.05}O_{3-\delta}$ (LCGFA)-carbonate, and $Ce_{0.8}Sm_{0.2}O_{1.9}$ (SDC)-carbonate membranes were examined under a wide range of experimental conditions at high temperature.

LSCF-carbonate membranes were shown to be unstable without the presence of $O_2$ due to reaction of $CO_2$ with the ceramic phase. In the presence of $O_2$, however, the membranes showed stable permeation behavior for more than one month at 900°C. LCGFA-carbonate membranes showed great chemical and permeation stability in the

presence of various conditions including exposure to $CH_4$ and $H_2$, however, the permeation performance was quite low when compared to membranes in the literature. Finally, SDC-carbonate membranes showed great chemical and permeation stability both in a $CO_2$:$N_2$ environment for more than two weeks at 900$^oC$ as well as more than one month of exposure to simulated syngas conditions at 700$^oC$. Ceramic phase chemical stability increased in the order of LSCF < LCGFA < SDC while permeation performance increased in the order of LCGFA < LSCF < SDC.

The following chapters are modified versions of papers published or to be submitted for publication:

Chapter 2

Norton, T.T., Lin, Y.S. (2012). Transient Oxygen Permeation and Surface Catalytic Properties of Lanthanum Cobaltite Membrane under Oxygen-Methane Gradient. *Industrial & Engineering Chemistry Research, 51*, 12917-12925.

Chapter 3

Norton, T.T., Ortiz-Landeros, J., Lin, Y.S. (2013). Stability of La-Sr-Co-Fe oxide-carbonate dual-phase membrane for $CO_2$ separation at high temperature. *Industrial & Engineering Chemistry Research*, submitted.

Chapter 4

Norton, T.T., Lin, Y.S. (2013). Ceramic-carbonate dual-phase membrane with improved chemical stability for carbon dioxide separation at high temperature. *Solid State Ionics*, submitted.

Chapter 5

Norton, T.T., Lu, Bo, Ortiz-Landeros, J., Lin, Y.S. (2013). High performance ceramic-carbonate dual-phase membrane for pre-combustion carbon dioxide capture at high temperature. In preparation.

To Jaime

Thank you for your love and support.
You push me to become better each day.
I wouldn't have made it this far without you.

ACKNOWLEDGMENTS

I would like to take this opportunity to thank my family for their love and support while I pursued my degree. In particular, my wife Jaime has been the greatest partner that anyone could ever dream of. Without her pushing me, I wouldn't have the opportunity to be where I am today. I would also like to thank my son Cooper, my parents, and my brother for their constant support and encouragement.

I would like to thank my advisor, Dr. Jerry Lin, for allowing me to join his group and for introducing me to academic research. Dr. Lin gave me the opportunity to do exciting research in an area that I truly enjoyed studying. I learned a great deal from him that I know I will use for the rest of my life, no matter where my career takes me. I appreciate the guidance and support that he gave to me throughout my time here.

I would like to thank Dr. Terry Alford, Dr. Mary Laura Lind, Dr. David Smith, and Dr. Cesar Torres for their willingness to serve on my committee and lend their expertise. I would also like to thank Fred Pena for his efforts and guidance in building and maintaining equipment for our laboratory.

Finally, I would like to thank all the current and former group members in Dr. Lin's group that I have had the pleasure to work with: Dr. Matthew Anderson, Dr. Jay Kniep, Dr. Shriya Seshadri, Dr. Carrie Eggen, Dr. Haibing Wang, Dr. Zebao Rui, Dr. Jose Ortiz-Landeros, Dr. Xiaoping Liang, Dr. Ding Wang, Teresa Rosa, Bo Lu, Xiaoli Ma, Nick Linneen, Alex Kasik, Defei Liu, Yang Liu, Dr. Xueliang Dong, Joshua James, Huifeng Zhang, and Stewart Mann.

I highly appreciate the US Department of Energy, the National Science Foundation, and Science Foundation Arizona for the financial support of this work.

TABLE OF CONTENTS

Page

APPENDIX

LIST OF TABLES

LIST OF FIGURES

# CHAPTER 1

# GENERAL INTRODUCTION

## 1.1 Introduction

The emission of carbon dioxide has become a significant environmental concern as the effect of greenhouse gases on global warming continues to be studied. In 2010, the United States was responsible for 6,865.5 million metric tons of $CO_2$ emissions from fossil fuels, accounting for 18% of the global $CO_2$ emissions into the environment [U.S. Environmental Protection Agency]. In an effort to reduce emissions, the application of carbon dioxide capture technologies at large point sources, like power plants, continues to be studied. The three main strategies considered for carbon capture from power plants include: post-combustion, oxy-fuel combustion, and pre-combustion. In post-combustion capture, $CO_2$ is separated from flue gas after fossil fuel combustion. In oxy-fuel combustion, oxygen replaces air during combustion, mainly producing $H_2O$ and $CO_2$, which is then separated. In pre-combustion capture, fossil fuels are reformed to produce syngas, which is mainly composed of CO and $H_2$. Syngas then undergoes water-gas shift reaction to produce more hydrogen, resulting in a high pressure $CO_2$ and $H_2$ stream, which is then separated. Pre-combustion capture offers the advantages of producing a high purity, carbon-free fuel as well as high pressure capture of $CO_2$. Of the potential technologies for pre-combustion capture, membranes offer the advantages of being temperature resistant, able to handle large flow rates, and have a relatively small footprint [Scholes et al., 2010].

Currently, the most commonly used methods of $CO_2$ separation are amine solvent absorption and cryogenic distillation from flue gas [Aaron & Tsouris, 2005]. While both

of these methods can achieve high separation purity, each has limitations. First, amine solvents are expensive and cannot provide continuous separation because they need to be regenerated. Second, cryogenic distillation is also expensive due to the large amount of energy required to cool gases for separation.

The use of membranes for pre-combustion $CO_2$ capture at high temperature is an attractive option due to its continuous nature that can handle large flow rates. A significant amount of research has centered on the use of polymeric membranes to separate $CO_2$ due to the cost and ease of manufacturing [Powell & Qiao; Bernardo et al., 2009; Scholes et al., 2010]. Polymers, however, are unable to handle elevated temperatures. Inorganic membranes, on the other hand, while more expensive, have been shown to have better mechanical, chemical, and thermal stability when compared to polymers [Hsieh, 1996; Lin, 2001].

This chapter will provide a review of the use of inorganic membranes for $CO_2$ separation from a gas mixture. Inorganic membranes have been shown to be able to withstand severe conditions such as high temperature and pressure as well as harsh chemical conditions when organic-based membranes would not be suitable. These membranes can be broken into two categories: porous and non-porous. A concise review of the current status of porous inorganic membranes for $CO_2$ separation followed by a detailed review of recently reported dense dual-phase ceramic-carbonate membranes for high temperature $CO_2$ separation. The chapter concludes by providing a review of the structure and stability of dense ceramic membranes for $O_2$ separation, which serve as the ceramic phase of the dual-phase membrane.

## 1.2 Porous Inorganic Membranes

Most research concerning inorganic membranes has focused on the use of microporous (less than 2 nm pores) membranes to separate $CO_2$ from $N_2$ by taking advantage of the difference in their kinetic diameter and solubility at temperatures below 400$^oC$ [Lin, 2001; Shekhawat et al. 2003, Bounaceur et al, 2006; Favre, 2007; Figueroa et al., 2008; Yang et al, 2008; Scholes et al., 2010; Anderson et al., 2012]. At low temperatures, separation of $CO_2$ from a gas mixture is controlled by the solubility difference in the membrane pores as diffusion properties for gases are similar [Anderson et al., 2012]. At higher temperatures, however, the solubility of gases are similar, so separation is controlled by diffusion properties, which results in separations that approach that predicted by Knudsen diffusion.

For the case of $CO_2$ and $H_2$ separation, the major focus has been applied to separation of smaller $H_2$ from larger $CO_2$, as the development of a porous inorganic membrane that is selective to the larger $CO_2$ while retaining the smaller $H_2$ is a significant challenge [Perry et al., 2006]. Porous inorganic membranes can only become $CO_2$ selective with respect to $H_2$ by either surface diffusion or capillary condensation [Scholes et al., 2010]. A few groups have reported success by modifying membrane surfaces with a polymer with $CO_2$ affinity in an attempt to maximize surface diffusion, however, this option isn't suitable for high temperature [Osada et al, 1999; Luebke & Pennline, 2003]. The uses of carbon, silica, and zeolite membranes, however, have been extensively studied as membranes for $CO_2$ separation from gas mixtures.

Carbon molecular sieve membranes rely on a carbon matrix with a controlled pore structure and morphology provided by the pyrolysis of polymer precursors on porous

substrates [Koresh & Sofer, 2006]. This controlled structure is achieved by adjusting the polymer precursors, the heating rate, and the pyrolysis temperature and atmosphere. These membranes show potential to effectively separate $CO_2$ from $N_2$ at low temperatures, but their effectiveness drops considerably with poor performance above 100$^oC$ [Anderson et al., 2012].

Microporous silica membranes are generally prepared by depositing a silica layer onto a porous support by either the sol-gel method or chemical vapor deposition (CVD) [Uhlhorn et al., 1989; Cooper & Lin, 2002]. Silica membranes prepared by the sol-gel method can be controlled by optimizing the sol concentration, dip-coating conditions, and using a smooth support with a uniform pore size to produce very thin membranes on the order of 100 nm. Silica membranes prepared by CVD are generally thicker as they rely on decomposition or oxidation of silica precursors in the pores or on the surface of a support [Uhlhorn et al., 1989]. In general, silica membranes achieve a permeance that is one to two orders of magnitude better than carbon membranes at the expense of a lower separation factor of $CO_2/N_2$ [Anderson et al., 2012]. As described for carbon membranes, separation performance of silica membranes significantly decreases at high temperature with poor performance above 300$^oC$.

Zeolites are crystalline aluminosilicates that are prepared by in situ nucleation and crystal growth or seeded nucleation and secondary growth of $TO_4$ tetrahedrals (T = Si or Al) on a macroporous support [Lin, 2001]. The pore size and quality of zeolite films relies on a controlled solution environment. Zeolite membranes show more promising separation capabilities than either carbon or silica membranes at low temperatures [Kusakabe et al., 1997]. In general, they achieve a permeance that is on the same order as

silica membranes, but with a higher separation factor of $CO_2/N_2$. Zeolite membranes also show a significant dependence of membrane performance with temperature, showing poor performance at 200°C and above [Anderson et al., 2012].

While microporous inorganic membranes offer greater chemical and thermal stability over polymeric membranes, they are still limited in effectiveness at relatively high temperatures (>500°C). To improve upon the limitations of polymer and microporous inorganic membranes for selective transport of $CO_2$ from a gas mixture at high temperature, the concept of a dense dual-phase membrane consisting of a metallic phase and a molten carbonate phase was proposed [Chung et al., 2005].

1.3 Dual-Phase Membrane

The idea for a dense carbon dioxide selective membrane was adapted from the concept of a molten carbonate fuel cell (MCFC) and was applied to the origination of the dual-phase membrane. This membrane consists of a solid support that is infiltrated with molten carbonate which has the ability to transport carbonate ions. Originally, the use of a stainless steel support was proposed due to its high electronic conductivity to facilitate the following reaction:

$$CO_2 + \frac{1}{2}O_2 + 2e^- \leftrightarrow CO_3^{=} \qquad (1.A)$$

At temperatures above the melting point of the carbonate phase, $CO_2$ and $O_2$ ionize and combine with electrons to form $CO_3^{=}$ at the membrane surface. A $CO_2$ partial pressure gradient across the membrane provides a driving force for the transport of carbonate ions through the molten carbonate phase of the membrane. On the permeate membrane surface, the reverse reaction takes place, releasing $CO_2$ and $O_2$. The membrane

is thought to provide a theoretically infinite selectivity over inert gases such as $N_2$ because of their inability to ionize.

Early research has shown that a metallic-carbonate dual-phase membrane can separate $CO_2$ from $N_2$ in the temperature range of 400-650$^oC$ [Chung et al., 2005]. A $CO_2$ permeance of 2.5 x $10^{-8}$ $mol \cdot s^{-1} \cdot m^{-2} \cdot Pa^{-1}$ was measured in the presence of oxygen with a $CO_2/N_2$ separation factor of 16 at 650$^oC$. At higher temperatures, however, reaction between the stainless-steel support and carbonate formed insulating $LiFeO_2$, which drastically reduced the electronic conductivity of the support. More recent work has improved the permeance through the metal-carbonate membrane by using a silver support. However, a maximum permeance is reached at 650$^oC$, followed by a similar drop in permeance at higher temperatures [Xu et al., 2012]. This is believed to be caused by loss of molten carbonate from the silver support.

Another limitation of the metal-carbonate dual-phase membrane is that while the liquid phase is able to transport carbonate ions, the metal support does not have the ability to transport oxygen ions. Therefore, $O_2$ must be present on the $CO_2$-rich side of the membrane in order for reaction 1 to take place when using a metal support. To improve upon these shortcomings, the use of an ionic conducting ceramic phase as the solid support of the dual-phase membrane was proposed [Anderson & Lin, 2006]. Dense ceramic membranes have been found to permeate oxygen under certain conditions [Sunarso et al., 2008; Leo et al., 2009; Zhang et al., 2011]. Mixed ionic and electronic conducting (MIEC) membranes allow the transport of both oxygen ions and electrons. Therefore, a porous ceramic support infiltrated with molten carbonate has the ability to transport oxygen and carbonate ions, respectively, as shown in Figure 1.1

$La_{0.6}Sr_{0.4}Co_{0.8}Fe_{0.2}O_{3-\delta}$. On the $CO_2$ rich surface of the membrane, $CO_2$ reacts with oxygen ions from the ceramic phase to form a carbonate ion, $CO_3^{=}$, as shown in the following reaction:

$$CO_2 + O^{=} \leftrightarrow CO_3^{=} \tag{1.B}$$

The molten carbonate phase transports the carbonate ion toward the $CO_2$ lean surface of the membrane where the reverse surface reaction takes place. The carbonate ion converts to $CO_2$, which is released, and $O^{=}$, which transports through the ceramic phase back towards the upstream surface of the membrane to maintain electronic neutrality. Carbon dioxide permeation is driven by the partial pressure gradient across the membrane. Recently, modeling work using this concept has been used to predict $CO_2$ transport through the dual-phase ceramic-carbonate membrane using ionic or mixed conducting ceramic supports [Wade et al., 2007; Rui et al., 2009].

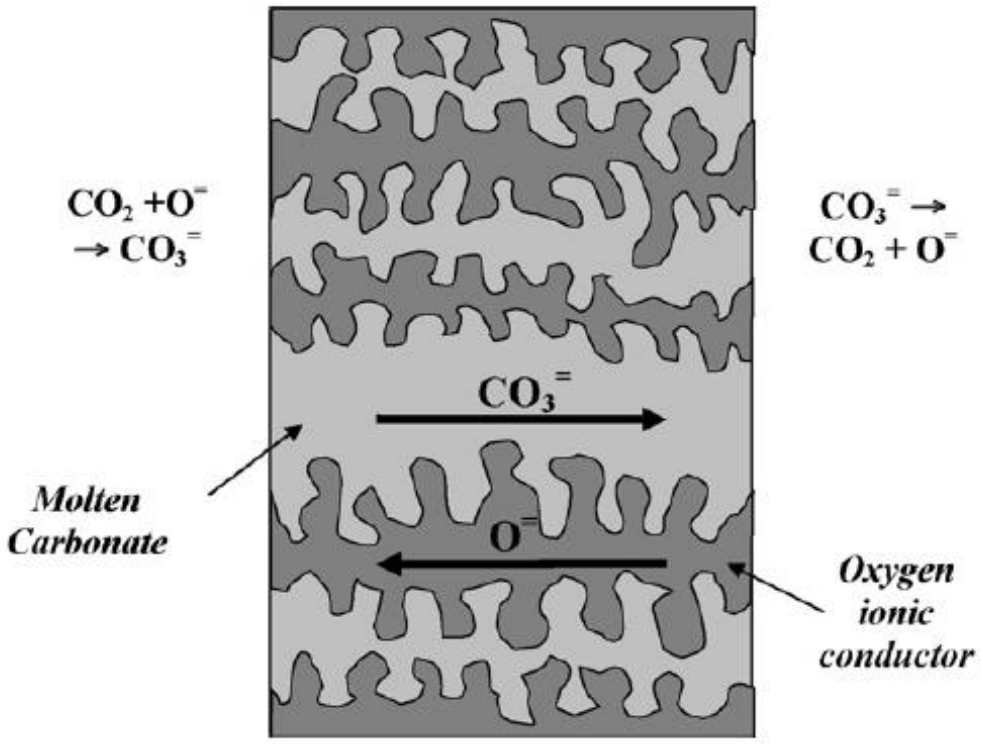


*Figure 1.1 Concept of ceramic-carbonate dual-phase membrane for $CO_2$ separation [Anderson & Lin, 2010].*

Experimentally, the first ceramic-carbonate dual-phase membrane was synthesized using the perovskite-type material $La_{0.6}Sr_{0.4}Co_{0.8}Fe_{0.2}O_{3-\delta}$ [Anderson & Lin, 2010]. This material was chosen because it has been shown to have a high electronic and oxygen ionic conductivity at high temperatures [Qu et al., 2004]. Using this support, the ceramic-carbonate dual-phase membrane has been shown to effectively separate $CO_2$ from an inert gas such as Ar or $N_2$ in the temperature range of 700-900ºC [Anderson & Lin, 2010]. A $CO_2$ permeance of 4.6 x $10^{-8}$ $mol \cdot s^{-1} \cdot m^{-2} \cdot Pa^{-1}$ was measured with a maximum $CO_2/N_2$ separation factor of 225 at 900ºC for a membrane with 0.75 mm thickness. The carbon dioxide permeance through membranes of varied thicknesses 0.375 mm to 3.0 mm was evaluated. Thinner membranes resulted in a lower bulk diffusion

resistance. However, the increase in $CO_2$ permeance was not proportional to the decrease in membrane thickness as predicted by the permeation model, as shown in Figure 1.2 [Rui et al., 2009].

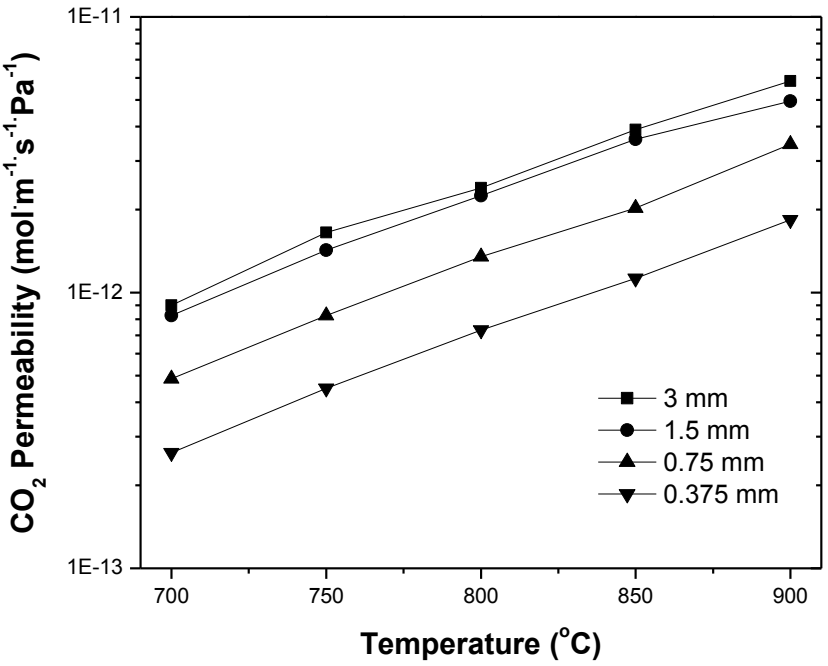


*Figure 1.2 Carbon dioxide permeability through LSCF-carbonate membranes of different thicknesses [Anderson & Lin, 2010]*

More recently, yttria-stabilized-zirconia (YSZ) of composition $Y_{0.16}Zr_{0.84}O_{2-\delta}$ (YSZ) and gadolinia doped ceria (GDC) of composition $Ce_{0.9}Gd_{0.1}O_{2-\delta}$ have been used as the ceramic phase of the dual-phase membranes [Wade et al., 2011]. YSZ- and GDC-carbonate membranes of 200-400 μm thickness have shown $CO_2$ permeances of $2\times10^{-8}$ and $3\times10^{-8}$ $mol{\cdot}Pa^{-1}{\cdot}s^{-1}{\cdot}m^{-2}$, respectively at 850°C. Constant membrane permeability through YSZ- and GDC-carbonate membranes was reported for membrane thicknesses between 200-400 μm for both materials, suggesting that $CO_2$ permeance is inversely

proportional to the membrane thickness. This contradicts the previous finding for LSCF-carbonate membranes.

$Bi_{1.5}Y_{0.3}Sm_{0.2}O_3$ (BYS) was recently chosen to serve as the ceramic phase of the dual-phase membrane because of its high ionic conductivity relative to LSCF and YSZ [Rui et al., 2012]. Due to wettability issues at the BYS/carbonate interface within the pores of the BYS support, a thin $\gamma$-$Al_2O_3$ film was introduced in an attempt to increase the wettability of the BYS surface. In addition, by controlling the thickness of the $\gamma$-$Al_2O_3$ film, the dual-phase membrane thickness could be reduced as molten carbonate is non-wettable to the BYS surface, and therefore does not infiltrate into the unmodified support. A maximum $CO_2$ permeance of $1\times10^{-8}$ $mol\cdot Pa^{-1}\cdot s^{-1}\cdot m^{-2}$ was measured for ~50 μm BYS-carbonate membranes at 650ºC. For the first time for the ceramic-carbonate membrane, the $CO_2$ permeation flux increased linearly with the logarithm of $CO_2$ concentration gradient across the membrane for BYS-carbonate membranes. This result is consistent with the model which assumes bulk diffusion controls $CO_2$ transport rate through the membrane.

In an attempt to improve the pore structure of the ceramic support for the dual-phase membrane, Zhang et al. used a combined co-precipitation and sacrificial-template synthesis method to prepare samarium doped ceria (SDC) supports of composition $Ce_{0.8}Sm_{0.2}O_{1.9}$ [Zhang et al., 2012]. SDC powder was first co-precipitated with NiO to form a homogeneous composite mixture [Zhang et al., 2011; Zhang et al., 2012]. The powder was pressed and sintered resulting in 1.2 mm thick pellets. The pellets were then reduced in pure $H_2$ at 800ºC for 10 hours to convert NiO to Ni followed by immersion in nitric acid to leach Ni out of the membranes. The porous SDC support was then

infiltrated with molten carbonate. SDC-carbonate membranes were exposed to a $CO_2$:$N_2$:$H_2$ feed mixture in a 10:10:1 ratio. Hydrogen was added to the system to lower the feed $O_2$ partial pressure to promote oxygen ion transport in the ceramic phase. A maximum $CO_2$ permeance of $2.9\times10^{-7}$ $mol\cdot Pa^{-1}\cdot s^{-1}\cdot m^{-2}$ was measured at 700°C, which was shown to be a significant improvement in the $CO_2$ permeation relative to the dual-phase membranes previously reported [Zhang et al., 2012]. The combination of new ceramic material, enhanced support pore structure, and addition of hydrogen to the $CO_2$-rich side of the membrane all likely contribute to the improved permeation behavior relative to other dual-phase membranes. In addition, $CO_2$ permeation was measured for membranes with different SDC:carbonate ratios in an attempt to determine the best ratio to optimize $CO_2$ permeation properties.

SDC supports with open porosities of 30, 35, 40, and 50% were infiltrated and tested [Zhang et al., 2012]. The permeation flux increased with decreasing SDC:carbonate ratios. Membranes with a 50:50 SDC:carbonate ratio has a permeation flux more than double that of the 60:40 membrane, more than three times higher than 65:35 membrane, and roughly seven times that of the 70:30 membrane. Finally, $CO_2$ permeation flux was shown to increase with increased $H_2$ concentration in the $CO_2$-rich side of the membrane. The addition of $H_2$ to the feed side of the membrane results in a dramatic increase of the $O_2$ partial pressure across the membrane at high temperature, which increases the ionic conductivity of the ceramic phase. Since the conductivity of SDC is lower than that for the carbonate phase, improving the oxygen ionic conductivity of this phase results in enhanced $CO_2$ permeation properties.

More recently, thin film YSZ-carbonate membranes on porous BYS supports have been developed [Lu & Lin, 2013]. By taking advantage of the non-wettable behavior previously reported for BYS, thin, asymmetric porous supports were prepared by preparing YSZ films on large pore BYS. Ceramic supports were immersed in molten carbonate, and only the YSZ films were infiltrated, resulting in a supported thin dual-phase membrane. A maximum $CO_2$ permeance of $7.7\times10^{-8}$ $mol\cdot Pa^{-1}\cdot s^{-1}\cdot m^{-2}$ was measured at 650°C for 10 μm thick membranes. This result shows an increase in $CO_2$ permeance over the previously reported YSZ-carbonate membrane by an order of magnitude, while the membrane thickness was decreased by a factor of 20-40. This, coupled with the fact that the apparent activation energy increases for the thin film, suggests that the surface exchange reaction contributes to the rate of permeation for the 10 μm thick membrane.

Figure 1.3 shows a comparison of the permeance and permeability of the dual-phase membranes reported in the literature [Anderson & Lin, 2010; Wade et al., 2011; Rui et al., 2012; Zhang et al., 2012; Lu & Lin, 2012]. Based on the permeance plot, SDC- and YSZ-carbonate membranes show the highest $CO_2$ permeation performance. However, when taking into account the membrane thickness, the relatively thicker SDC- and LSCF-carbonate membranes show the highest permeability relative to the previously tested materials. As previously discussed, SDC-carbonate membranes were prepared using a unique technique in an attempt to optimize the pore structure of the porous SDC supports [Zhang et al., 2012]. The addition of $H_2$ to the $CO_2$ rich feed gas to induce a larger oxygen partial pressure gradient across the membrane and increase ionic conductivity of the ceramic support also likely contributed to improved permeation

properties relative to the other dual-phase membranes reported. It is difficult, however, to quantify the effect of this contribution.

Table 1.1 shows a comparison of dual-phase membrane properties. Based on the literature to date, each dual-phase membrane has shown $CO_2$ transport has exponential dependence to increasing temperature. There are, however, conflicting reports as to the degree in which decreasing membrane thickness improves $CO_2$ permeation. While decreasing membrane thickness has been shown to result in an increase in $CO_2$ permeation, the effect hasn't been verified to be directly proportional to decreasing membrane thickness in all cases, as illustrated in Figure 1.2 for LSCF-carbonate membranes. In addition, little work has been done to determine the dependence of $CO_2$ permeation on the $CO_2$ partial pressure gradient across the membrane. Finally, long-term chemical and permeation stability of the dual-phase membrane remains a question that has yet to be addressed.

*Table 1.1 Comparison of properties of dual-phase membranes*

| | LSCF | YSZ | GDC | BYS | SDC | YSZ |
|---|---|---|---|---|---|---|
| Thickness (μm) | 1500 | 200-400 | 200-400 | 50 | 1200 | 10 |
| Temp Range (°C) | 700-900 | 500-850 | 500-850 | 500-650 | 550-700 | 500-650 |
| $E_A$ (kJ·mol$^{-1}$) | 88 | 84 | 77 | 113 | 74 | 106 |
| 700°C $CO_2$ Permeance ($10^{-9}$ mol·m$^{-2}$·s$^{-1}$·Pa$^{-1}$) | 5.0 | 7.3 | 2.5 | 19* | 290 | 210* |
| 700°C Permeability ($10^{-12}$ mol·m$^{-1}$·s$^{-1}$·Pa$^{-1}$) | 7.5 | 2.9 | 1.0 | 1.0* | 350 | 2.1* |
| Feed $CO_2$ Conc. | 0.50 | 0.50 | 0.50 | 0.50 | 0.48† | 0.25 |
| Feed Flow Rate (mL·min$^{-1}$) | 100 | 15 | 15 | 100 | 105 | 100 |
| Permeate Flow Rate (mL·min$^{-1}$) | 100 | 15 | 15 | 100 | 50 | 100 |
| Reference | Anderson & Lin, 2010 | Wade et al., 2011 | Wade et al., 2011 | Rui et al., 2012 | Zhang et al., 2012 | Lu & Lin, 2012 |

* Values were extrapolated based on permeance data and measured apparent activation energy.

† $H_2$ feed concentration of 4.8% added

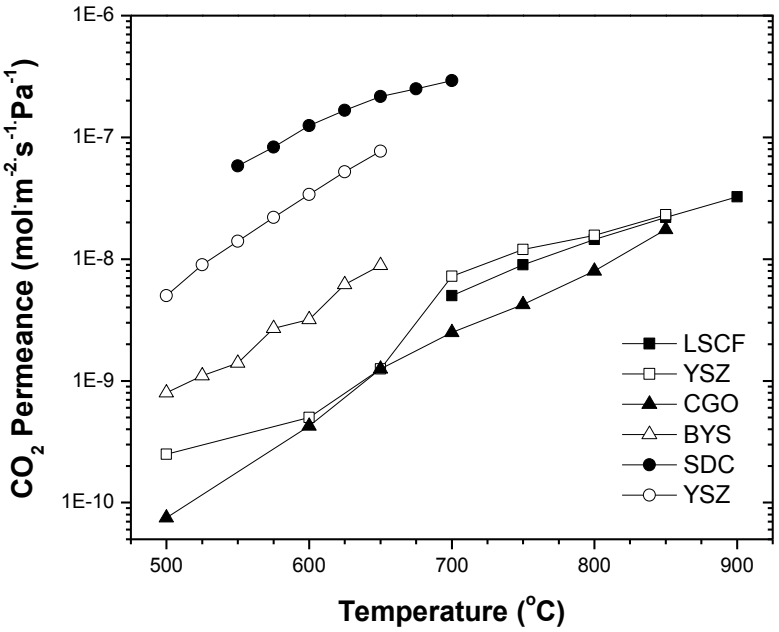


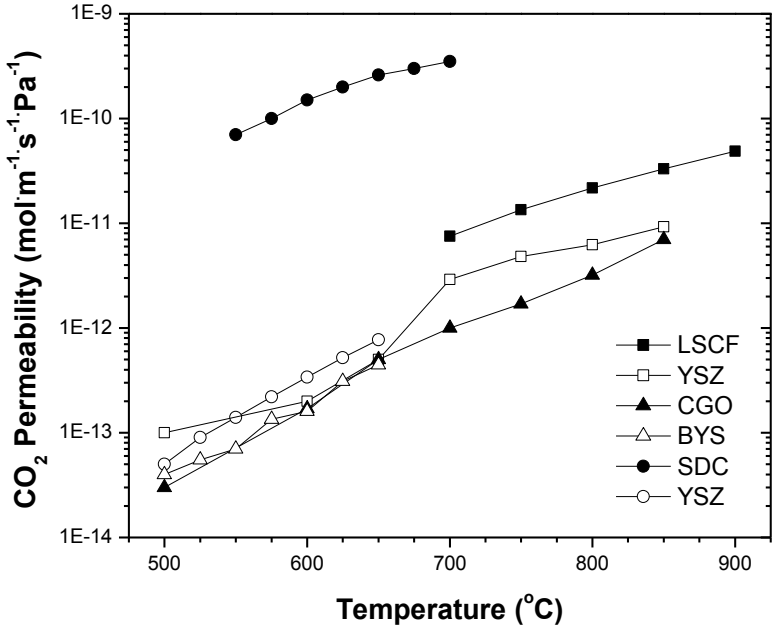


*Figure 1.3 Carbon dioxide (a) permeance and (b) permeability through ceramic-carbonate membranes published in the literature (Refer to Table 1.1)*

To address improving the performance and stability of the ceramic-carbonate dual-phase membrane, the material serving as the ceramic support should be optimized. This material should satisfy a number of conditions. The material must have high oxygen ionic conductivity, as oxygen is required for the formation of carbonate ions. The material must have long-term chemical stability at high temperatures in the presence of carbon dioxide and reducing gases such as methane, as well as having compatibility with the carbonate phase. The material must also exhibit high mechanical strength and an appropriate pore size in an effort to control the amount of the molten carbonate phase.

To maximize the performance and stability of the dual-phase membrane, it is necessary to examine different materials to serve as the solid ceramic support of the dual-phase membrane. In the ceramic-carbonate dual-phase membrane, transport relies on the conductivity of the ceramic and carbonate phases. As an example, Figure 1.4 shows the ionic conductivity of the molten carbonate and LSCF phases at different temperatures. In the temperature range of 400-950$^{o}$C, the carbonate conductivity of the molten carbonate phase ranges from between one to four orders of magnitude higher than the oxygen ionic conductivity of the LSCF phase. This large gap between the conductivities of the two phases provides an opportunity to increase the theoretical permeability of the membrane by improving the ceramic phase of the dual-phase membrane, as the transport mechanism is limited by the ionic conductivity of the ceramic phase. The materials that have drawn the most attention for selective oxygen transport are perovskite and fluorite type materials [Sunarso et al., 2008; Leo et al., 2009; Zhang et al., 2011]. The following review of the structure and stability of dense oxygen-conducting ceramic membranes aims to help identify potential materials that can serve as the ceramic phase of the ceramic-carbonate

membrane and withstand the harsh conditions associated with pre-combustion carbon dioxide capture at high temperature.

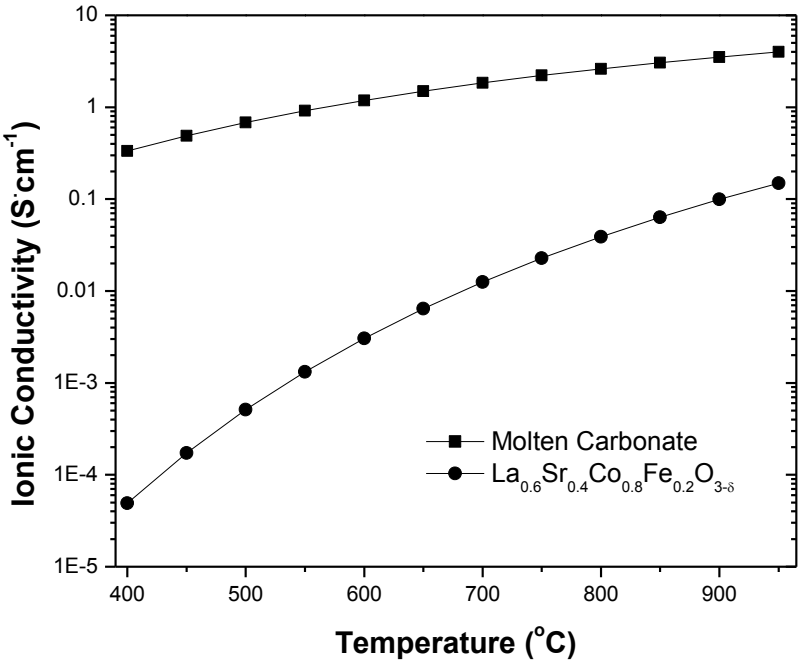


*Figure 1.4 Ionic conductivity of Li/Na/K molten carbonate mixture and the perovskite material $La_{0.6}Sr_{0.4}Co_{0.8}Fe_{0.2}O_{3-\delta}$ at different temperatures [Janz et al, 1979; Xu et al., 2004]*

1.4 Oxygen permeable membranes

As previously described, dense ceramic materials have been well studied as oxygen permeable membranes at high temperature [Sunarso et al., 2008; Leo et al., 2009; Zhang et al., 2011]. Mixed ionic and electronic conducting membranes allow the transport of both oxygen ions and electrons. The transport of oxygen for dense mixed-conducting ceramic membranes requires the presence of an oxygen partial pressure gradient across the membrane to provide a driving force. In a single-phase dense ceramic

membrane, the transport of oxygen ions through the membrane requires the movement of electrons in the opposite direction in order to remain electronically neutral. The transport of oxygen through mixed conducting membranes typically occurs via the following steps [Manning et al., 1996; Ishihara et al., 1998; Ruiz-Trejo et al., 1998; Lane and Kilner, 2000]:

1. Mass transfer of gaseous oxygen from the high pressure side to the membrane surface
2. Adsorption and dissociation of oxygen molecules into ions
3. Transport of oxygen ions through the membrane
4. Association of oxygen ions into oxygen molecules and desorption
5. Mass transfer of gaseous oxygen from the membrane surface to the low pressure side of the membrane

Of these steps, numbers 2-4 are considered to be the most important in terms of determining the rate of transport through the membrane, as steps 1 and 5 are simple mass transport processes in the gas phase. In dense ceramic membranes, either the surface reaction (steps 2 and 4), or bulk diffusion (step 3) provides the greatest resistance and limits the rate of oxygen permeation. In Steps 2 and 4, material properties affect the level of resistance for the surface exchange reaction. In step 3, the resistance for oxygen transport across the membrane is proportional to the membrane thickness. For a relatively thick membrane, the rate of oxygen diffusion will be dominated by bulk diffusion rather than the surface reaction. As the membrane thickness decreases, the surface exchange reaction rate stays the same, and oxygen permeation will increase. Once the membrane thickness is decreased to the point that the surface exchange reaction becomes the rate-

controlling step, there is no further benefit to decreasing the membrane thickness in terms of increasing oxygen permeance. This thickness is referred to as the characteristic thickness ($L_c$). This will depend on a number of factors including the membrane material and operating conditions. The $L_c$ for most dense ceramic membranes has typically been found in the range of 200-300 μm [Aasland et al., 2000]. As previously noted, the materials that have drawn the most attention for selective oxygen transport are perovskite and fluorite type materials [Sunarso et al., 2008; Leo et al., 2009; Zhang et al., 2011].

*1.4.1 Ceramic phase structure*

The fluorite structure, based on the material $CaF_2$, is a cubic structure with the general formula $AO_2$. This structure has anions in simple cubic packing with cations occupying half of the interstices in a structure that has a face-centered-cubic (fcc) packing. Doping of metal ions with a lower valence state leads to the formation of oxygen vacancies in the structure in order to maintain charge neutrality, and therefore, oxygen ionic conductivity. While doping with transition metal ions can provide electronic conductivity to the material, the oxygen ionic conductivity normally accounts for most of the total conductivity [Arashi & Naito, 1992; Nigara et al., 1995; Nigara et al, 1996; Han et al, 1997]. The electronic conductivity of fluorite structures ranges from $10^{-6}$-$10^{-4}$ $S \cdot cm^{-1}$ while the ionic conductivity ranges from 0.1 to 1 [Kniep & Lin, 2010].

The perovskite structure, which is based on the mineral $CaTiO_3$, is a cubic structure with the general formula $ABO_3$. In a unit cell, metal B cations are located at all eight corners, the metal A cation is located at the center of the cell, and oxygen ions are located in the center of the cell faces. B-site metal cations are traditionally transition metal cations, such as Fe, Co, Ni, or Cu [Burgraaf & Cot, 1996]. A-site cations are

usually rare earth, alkali, or alkaline earth ions, such as La, Na, Ca, Sr, or Ba. The shape of the crystal structure is determined by the relative sizes of the A and B-site metal cations, as predicted by the Goldschmidt factor [Goldschmidt, 1946]:

$$t = \frac{r_A + r_O}{\sqrt{2}(r_B + r_O)} \tag{1.1}$$

where $r_A$, $r_B$, and $r_O$ are the atomic radii of the A-site, B-site, and oxygen ions, respectively. Perovskite structures have been shown to be stable at factors between 0.75-1.0 [Cook & Sammells, 1991]. Above one, distortion leads to the formation of other crystal structures [Leo et al., 2009]. Oxygen transport through dense perovskite membranes relies on bulk diffusion of oxygen ions through the crystal structure. A traditional perovskite with a single A and B site metal cation is unlikely to conduct oxygen ions, as imperfections in the crystal structure resulting in oxygen vacancies are required to allow for diffusion of oxygen ions [Van Roosmalen & Corfunke, 1991; Steele, 1992; Adler et al., 2007].

In order to achieve a high ionic and electronic conductivity for perovskite structures, the A- and B-sites can be doped. Doping the A-site metal cation with a metal (such as La) with a lower valence state (such as Sr) increases the oxygen vacancy concentration of the material. Substitution of a lower valence metal cation (2+ vs. 3+) results in a charge imbalance for the material. To compensate, oxygen vacancies develop throughout the material and the valence state of transition metals occupying the B-site can change to account for the charge inequality [ten Elshof et al., 1995]. Doping of the B-site results mostly in an increase in the electronic conductivity of the material, as electronic conduction occurs via electron transfer between B-site metals with different

valence states. Therefore, it is desirable to have transition metal cations that are stable in many oxidation states. The choice of dopants, however, can have a dramatic effect on the chemical and mechanical properties of the material. The electronic conductivity of perovskite structures range from 10-1000 $S \cdot cm^{-1}$ and the ionic conductivity ranges from 0.01-0.1 $S \cdot cm^{-1}$ [Kniep & Lin, 2010]. The following review of the chemical and permeation stability of various fluorite and perovskite-type membranes under a wide range of harsh experimental conditions is necessary to narrow the focus in choosing an appropriate ceramic phase to serve as part of the dual-phase membrane.

*1.4.2 Ceramic Membrane Stability*

For practical application, ceramic membranes must be able to withstand process conditions and maintain chemical stability while maintaining high oxygen permeability. Fluorite-based materials have shown to be more stable than perovskite-type compounds in spite of their relatively low oxygen permeability. While perovskite-type materials have very high oxygen permeation fluxes, the alkaline-earth compounds that are responsible for the high ionic conductivity exhibit long-term stability problems in the presence of gases such as $CO_2$, $SO_2$ and $H_2O$ [Qiu et al., 1995; Shao et al, 2000; Yaremchenko et al., 1999; Kharton et al., 1999, Thursfield & Metcalf, 2007]. Surface reaction of these gases with oxides on the membrane surface leads to degradation of the perovskite structure and formation of secondary phases on the membrane surface.

Recently, many groups have reported on the stability of perovskite-type oxides in the presence of carbon dioxide and other carbon-containing gases [Pei et al, 1994; ten Elshof et al., 1995; ten Elshof et al., 1996; Tong et al., 2002]. In particular, Sr- and Co-containing perovskite-type oxides exposed to $CO_2$ and CO resulted in the formation of

carbonates on the membrane surface. After exposure to methane, $SrCo_{1-y}Fe_yO_x$ membranes form $SrCO_3$ as well as the presence of Fe and Co on the membrane surface [Pei et al., 1994]. $La_{0.6}Sr_{0.4}Co_{0.8}Fe_{0.2}O_{3-\delta}$ membranes showed an increase in the membrane surface area and surface roughness after exposure to $CH_4$ [ten Elshof et al., 1995]. In addition, the perovskite-type structure on the membrane surface had decomposed into $SrCO_3$ and $SrSO_4$ and La, Co, and Fe in a surface layer above the bulk perovskite phase that remained below. Later testing of $La_{1-x}Sr_xFeO_{3-\delta}$ membranes exposed to CO and $CO_2$ produced similar results with formation of SrO and $SrCO_3$ on the membrane surface and an increase in surface area and surface roughness was observed [ten Elshof et al., 1996]. Carbonate formation was apparent on the surface of $BaCo_{0.4}Fe_{0.4}Zr_{0.2}O_{3-\delta}$ membranes [Tong et al., 2002]. After 400 hours of exposure to ambient air containing water and carbon dioxide, the oxygen permeation flux of $Ba_{0.5}Sr_{0.5}Co_{0.8}Fe_{0.2}O_{3-\delta}$ membranes was shown to decrease by roughly 35%. In another series of studies, it was reported that oxygen permeation flux through Mg-, Ca-, Sr-, and Ba-based perovskites decreased by roughly 30-50% after 100 hours in the presence of a few percentage points of water and a few parts per million of carbon dioxide [Carolan et al., 1993a; Carolan et al, 1993b; Carolan et al, 1993c]. Finally, $BaCo_{0.4}Fe_{0.4}Zr_{0.2}O_{3-\delta}$ membranes showed relative stability in the presence of $CO_2$ on the oxygen-rich side of the membrane, as it had a small effect on the oxygen permeation flux [Tong et al., 2002]. However, when carbon dioxide is introduced to the oxygen-lean side of the membrane the oxygen permeation flux drops dramatically, resulting from the interaction of carbon dioxide with the membrane surface, causing the formation of carbonates on the surface. In this case, the presence of oxygen lessens this effect.

Various strategies have been attempted to improve the chemical stability of ceramic membranes. Specific B-site doping of perovskites with Zr has been shown to improve chemical stability of membranes in $CO_2$ and $H_2O$ environments [Tong et al., 2002; Caro et al., 2006; Taniguchi et al., 2001]. However, this method results in a lower overall oxygen permeation flux. Another common strategy is to develop Co-free materials to improve the chemical stability of materials, as Co readily reacts with $CO_2$ in addition to being easily reduced at high temperatures [Bouwmeester, 2003]. Recently reported cobalt-free materials with good chemical stability include: $BaCe_{0.15}Fe_{0.85}O_{3-\delta}$, $La_{0.85}Ce_{0.1}Ga_{0.3}Fe_{0.65}Al_{0.05}O_{3-\delta}$, $(La_{1-x}Ca_x)_{1.01}FeO_{3-\delta}$, $Ba_{0.5}Sr_{0.5}Zn_{0.2}Fe_{0.8}O_{3-\delta}$, and $Sr_{2-x}La_xGa_{2-y}Fe_yO_{5+\delta}$ [Schwartz et al., 2000; Schwartz et al., 2001; Dyer et al., 2002; Zhu et al., 2004; Wang et al., 2005; Zhu et al., 2006; Dong et al., 2009]. The removal of Co has proven to be an effective method to improve chemical stability without significant change to the oxygen permeation properties for certain material compositions, while others show lower oxygen permeation flux. Another option that has been recently explored is introducing higher valence cations to either the A-site or B-site [Prado et al., 2004; Yang et al., 2005; Ishihara et al., 2000; Kharton et al., 2000]. Overall, this method demonstrated improvement of the structural stability at the expense of oxygen permeation flux due to a decrease in electronic conductivity. Finally, partial substitution of A- or B-site cations with ions of a larger radius has shown to upgrade chemical stability while maintaining oxygen permeation flux in the case of partial substitution of Ba for Sr in $SrCo_{0.8}Fe_{0.2}O_{3-\delta}$ and Sc for Co in $SrCoO_{3-\delta}$ [Shao et al., 2000, Zeng et al., 2008].

## 1.5 Research objectives and significance

This dissertation will present the findings of a systematic study of the stability of the ceramic phase of the ceramic-carbonate dual-phase membrane for $CO_2$ capture at high temperature. The three main objectives are: (1) to determine permeation stability of the previously studied LSCF and LSCF-carbonate dual-phase membrane, (2) to identify a stable ceramic material to serve as the support of the dual-phase membrane in an effort to verify the permeation mechanism of the dual-phase membrane, and (3) to test the chemical and permeation stability of identified stable ceramic-carbonate membrane under simulated pre-combustion conditions at high temperature.

*Objective 1*

In order to determine the permeation stability of membranes containing $La_{0.6}Sr_{0.4}Co_{0.8}Fe_{0.2}O_{3-\delta}$ (LSCF), porous disk supports and dense membranes were synthesized by the citrate method. Porous supports were infiltrated with a molten carbonate mixture to form a dense dual-phase membrane. LSCF and LSCF-carbonate membranes were characterized using room temperature helium permeance measurements to ensure that membrane samples were dense. The chemical structure and phases present in LSCF were identified and analyzed using X-ray diffraction throughout the study. A high temperature gas permeation system was used to determine the oxygen permeation through dense LSCF in both inert and reducing environment at high temperature. The same system was used to determine the carbon dioxide permeation properties of LSCF-carbonate under varying experimental conditions at high temperature. The experimental results from both sets of experiments were used to verify the permeation stability of the ceramic phase under a wide range of experimental conditions and were used to compare to those predicted by theoretical permeation models.

*Objective 2*

In an effort to verify the permeation mechanism of the dual-phase membrane that results in selective $CO_2$ separation, the use of a stable ceramic phase was introduced in the dual-phase membrane. In objective 1, the permeation properties of LSCF and LSCF-carbonate membranes were studied under experimental conditions to determine the permeation stability of LSCF-containing membranes. In objective 2, the perovskite material LCGFA served as the ceramic phase of the new LCGFA-carbonate dual-phase membrane. In an attempt to verify the proposed permeation mechanism, a number of experimental conditions were varied when measuring high temperature $CO_2$ permeation properties of LCGFA-carbonate membranes. The effect of membrane thickness provided information about the rate of bulk diffusion versus surface reaction. In addition, the system temperature and $CO_2$ partial pressure gradient was varied to provide information about the effect the driving force has on the permeation properties. The permeation stability of the dual-phase membrane was examined under constant experimental conditions in a $CO_2$:$N_2$ feed. Finally, the chemical stability of LCGFA-carbonate was examined by exposing membrane samples to a wide range of experimental conditions at high temperature and examining the chemical structure using X-ray diffraction upon completion.

*Objective 3*

The final objective of this work was to demonstrate the use of a dual-phase membrane to separate $CO_2$ from a simulated syngas mixture. In objective 3, the fluorite material samarium doped ceria (SDC) of composition $Ce_{0.8}Sm_{0.2}O_{1.9}$ served as the ceramic phase of the SDC-carbonate dual-phase membrane. In addition to providing a

comprehensive study of the permeation properties of the membrane under large $CO_2$ gradients as was shown for LCGFA-carbonate membranes in objective 2, SDC-carbonate membranes were tested under simulated syngas conditions in a wide temperature range. In addition, the long-term chemical and permeation stability of the membrane was examined under constant experimental conditions at high temperature.

The research objectives listed above present a significant contribution to dual-phase membrane research. Systematic studies of membrane stability and permeation properties under various experimental conditions will have a meaningful contribution to the membrane community as the capabilities and potential application of these membranes continue to be studied. Early studies on ceramic-carbonate membranes have focused on proving the concept of $CO_2$ separation from dense dual-phase membranes, but lack further study of material stability and long-term permeation performance. In addition, as these studies looked to prove the concept of the dual-phase membrane, little has been done beyond $CO_2/N_2$ separation.

## 1.6 Structure of the dissertation

Each chapter of this dissertation serves to address one of the previously mentioned objectives. Chapters 2 and 3 address objective 1 in examining the permeation stability of LSCF-containing membranes at high temperature. Chapter 2 examines the effect inert and reducing conditions have on the long-term oxygen permeation properties of dense LSCF membranes at high temperature. Chapter 3 looks at the carbon dioxide permeation stability of LSCF-carbonate membranes under different experimental conditions at high temperature. Chapter 4 addresses Objective 2 by developing a new LCGFA-carbonate membrane to verify the transport mechanism of the dual-phase

membrane as well as providing a chemical and permeation stability study under varying experimental conditions. Objective 3 is addressed in Chapter 5 where the permeation properties and stability of SDC-carbonate membranes are measured under $CO_2$:$N_2$ and simulated syngas environments at high temperature. Chapter 6 summarizes the work reported in this thesis and provides recommendations for future advancement of the stability and permeation performance of the dual-phase membrane for $CO_2$ capture.

# CHAPTER 2

# TRANSIENT OXYGEN PERMEATION AND SURFACE CATALYTIC PROPERTIES OF LANTHANUM COBALTITE MEMBRANE UNDER OXYGEN-METHANE GRADIENT

## 2.1 Introduction

Perovskite-type ceramics for oxygen separation have been shown to react when exposed to reducing conditions at high temperature, especially in the case of Sr- and Co-containing materials [Pei et al, 1994; ten Elshof et al., 1995; ten Elshof et al., 1996; Tong et al., 2002]. However, there is little evidence that this surface reaction and degradation goes beyond the membrane surface (10-20 μm). Therefore, the true effect of surface degradation on the long-term permeation properties of oxygen conducting membranes at high temperature remains in question. In this chapter, the permeation properties and long-term stability of dense $La_{0.6}Sr_{0.4}Co_{0.8}Fe_{0.2}O_{3-\delta}$ membranes in inert and reducing environments are investigated.

Ionic and electronic conducting dense ceramic membranes have been extensively studied as a means to separate oxygen from a wide range of experimental conditions at high temperature [Sunarso et al., 2008; Leo et al., 2009; Zhang et al., 2011]. In the membrane reactor applications, air is fed to one side of the membrane and a hydrocarbon (such as methane) is fed to the other side which is often packed with a catalyst. The membrane permits the permeation of oxygen resulting in the separation of air in the feed. It also controls distribution of oxygen, or the way oxygen interacts with hydrocarbons, improving the selectivity or heat-distribution in the reaction side [Li, 2008]. Most studies on these membranes were focused on the effects of composition and operation conditions

on oxygen permeation or catalytic reactions [Sunarso et al., 2008; Leo et al., 2009; Zhang et al., 2011]. Only limited studies have been reported on stability of these membranes under such a large oxygen partial gradient, such as air/methane, in spite of its great importance to industrial applications [Sunarso et al., 2008].

Stability issues for perovskite membranes include short-term stability in response to a change in the surrounding gases and the long-term stability under steady-state operating conditions. Short-term stability refers to a membrane change when it is subjected to a change in its surroundings (such as a change in oxygen pressure gradient from air/air to air/methane, or a change in temperature). The oxygen vacancy concentration profile in the membrane changes in response to a change in its surroundings. In the case of an increased oxygen vacancy gradient, an increase in oxygen permeation flux is observed experimentally [Zeng et al., 1998; Li et al., 1999]. This change may also lead to membrane fracture due to increased mechanical strain [Pei et al., 1994]. Zolochevsky et al. recently reported stress development of the membranes due to the change of the surrounding conditions [Zolochevsky et al., 2012]. These membrane changes usually occur in the first few hours after a change of the surrounding conditions.

The long term stability refers to the membrane change under steady-state conditions with a fixed oxygen gradient across the membrane beyond the initial transient hours described above. Some research groups have reported steady state operation of mixed-conducting ceramic membranes under an oxygen/methane gradient, such as Ba-Sr-Co-Fe oxide for several hundred up to 2200 hours [Shao et al., 2001; Zhu et al., 2008]. Other groups reported changes of the oxygen permeation fluxes for perovskite type ceramic membranes, especially in the initial several ten hours prior to the establishment

of the steady state operation during the long term stability studies [ten Elshof et al., 1995; Xu & Thomson, 1998; Tsai et al., 1997; Dong et al., 2001; Trunec & Cihlar, 2006; Zhu et al., 2006; Luo et al., 2010].

Thermodynamically, it is known that metal oxides consisting of later transition and alkaline-earth metals may have a tendency to react with a reducing gas such as methane at high temperature. When a perovskite metal oxide ceramic membrane is exposed to an oxygen/methane gradient, the thermodynamic driving force for the reaction between the membrane surface and methane can lead to chemical and structural changes of the surface as well as the bulk of the membrane. However, different from metal oxide particulates surrounded by a reducing gas, oxygen from the opposite membrane surface can permeate towards the surface exposed to methane, increasing oxygen potential in the gas in contact with the membrane [Lin & Zeng, 1996]. Thus, the membrane under an oxygen/methane gradient might initially experience a change in structure and eventually reach a steady-state depending on the relative flux of oxygen and membrane material properties. These changes include formation of a porous layer consisting of $SrCO_3$ on the membrane exposed to methane for La-Sr-Co-Fe membranes [ten Elshof et al., 1995; Xu & Thomson, 1998]. Eventually, the membrane might reach a steady state operation because a sufficient amount of oxygen is supplied from the feed side. However, no experimental study has been reported investigating such a transient process during the long term stability study of perovskite-type ceramic membrane under an oxygen/methane gradient.

The objective of this chapter is to investigate the transient oxygen permeation and surface catalytic properties of a mixed-conducting ceramic membrane under an

oxygen/methane gradient for an extended period of time. Lanthanum cobaltite perovskite-type ceramic membrane of composition $La_{0.6}Sr_{0.4}Co_{0.8}Fe_{0.2}O_{3-\delta}$ (LSCF) was selected in this work because the material has been well studied in the membrane literature. In the experimental work the membrane was exposed to an oxygen feed and pure methane sweep with an empty permeate chamber (not packed with an oxidation catalyst) to avoid possible changes of the catalyst during the transient process. This would allow the study of changing membrane properties for an extended period of time.

## 2.2 Experimental Methods

### *2.2.1 Preparation and characterization of dense $La_{0.6}Sr_{0.4}Co_{0.8}Fe_{0.2}O_{3-\delta}$ membranes*

$La_{0.6}Sr_{0.4}Co_{0.8}Fe_{0.2}O_{3-\delta}$ (LSCF) powder was synthesized via the liquid citrate method [Yin & Lin, 2007]. Stoichiometric amounts of metal nitrate precursors $La(NO_3)_3{\cdot}6H_2O$ (99.9%, Alfa Aesar), $Sr(NO_3)_2$ (99.0%, Alfa Aesar), $Co(NO_3)_3{\cdot}6H_2O$ (98.0%, Alfa Aesar), and $Fe(NO_3)_3{\cdot}9H_2O$ (98.0%, Alfa Aesar) were weighed out in a 0.05 mole basis and mixed with a 50 percent excess of citric acid (99.5%, Alfa Aesar). The precursors were dissolved in 1000 mL of de-ionized water and heated to 105$^{o}$C and covered for four hours to prevent evaporation and promote polymerization. Evaporation was then implemented by uncovering and heating the solution at 110$^{o}$C for 3-4 hours. The resulting viscous solution was dried in a furnace (Thermolyne, 46100) at 110$^{o}$C for 24 hours. Self-ignition of the dried gel was then performed at 400$^{o}$C to burn out the organic compounds. The resulting powder was then ground with a mortar and pestle to reduce the particle size. The powder was then calcined at 600$^{o}$C in air for 20 hours with heating and cooling ramping rates of $2^{o}C{\cdot}min^{-1}$. The calcined powder was again ground using a mortar and pestle.

Approximately 3 grams of powder were placed in a 30 mm stainless steel mold and pressed to 160 MPa for 5 minutes using a hydraulic press (Carver, Model #3853). The green disks were then sintered at 1200$^{o}$C for 24 hours with heating and cooling ramping rates of 2$^{o}$C·min$^{-1}$ resulting in a dense LSCF disk support. An unsteady-state helium permeation system was used to verify the gas tightness of the membrane. The phase structure of the LSCF powder and membrane was characterized using X-ray diffraction (XRD) (Bruker, $CuK_{\alpha 1}$) evaluated in the 2θ range from 20$^{o}$ to 80$^{o}$.

*2.2.2 Oxygen permeation measurements*

A Probostat high temperature permeation system (Probostat, Norwegian Electro Ceramics AS) was used for oxygen permeation experiments as previously described by Kniep et al. [Kniep et al., 2010]. Figure 2.1 shows the schematic drawing of the oxygen permeation setup. For each experiment an alumina spacer attached to a spring force assembly, a dense LSCF disk membrane, and a silver seal were placed on top of a 20 mm alumina tube, which was then enclosed by a 40 mm diameter alumina tube. The assembled apparatus was then placed in a vertical tube furnace and heated to approximately 950$^{o}$C to reach the softening temperature of silver at a ramping rate of 1$^{o}$C·min$^{-1}$. Once the softening point of silver was reached, the spring assembly attached to the alumina spacer above the disk membrane forced the membrane into the silver ring forming a seal between the membrane and the 20 mm alumina tube. Argon was then introduced inside the 20 mm alumina tube, serving as the sweep gas at the bottom of the membrane, while helium was introduced to the space between the two alumina tubes, serving as the feed gas to the top of the membrane. The quality of the seal was determined by measuring the helium content in the argon sweep gas using a gas

chromatograph (Agilent, 6890N). After reaching minimization of helium leakage the system was cooled to either 700ºC or 900ºC at a rate of 1ºC·min$^{-1}$.

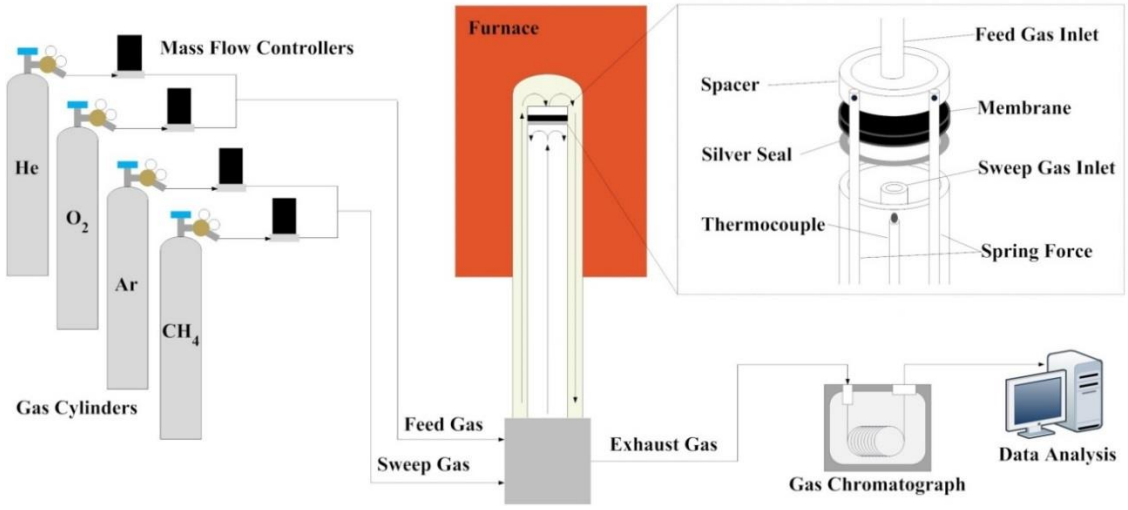


*Figure 2.1 Experimental high temperature oxygen permeation setup*

For oxygen permeation experiments, the feed gas consisted of a variable oxygen flow mixed with a balance of helium to reach 100 mL·min$^{-1}$ for an oxygen partial pressure varying between 0.2-1.0 atm. Pure argon or pure methane was flowed as the sweep gas at a flow rate range between 25-200 mL·min$^{-1}$. The temperature was varied between 700-900ºC. Gas flow rates were regulated using mass flow controllers (MKS, Model 1179) and a four-channel readout (MKS, Type 247). Samples were taken three hours after a change in gas composition and one hour after a temperature change to allow the system to reach steady state. A mass balance on the measured sweep side gases was used to calculate the oxygen permeation flux through each membrane. The oxygen error in the sweep gas caused by air leaks when sampling, along with seal leaks, were corrected by measuring the presence of nitrogen and helium, respectively, and subtracting

the corresponding oxygen from the calculated oxygen permeation flux. The error in determining the oxygen permeation flux using this procedure is approximately $\pm$ 10%.

For experiments with the reducing methane gas, the permeate chamber was not packed with a catalyst so the reaction between permeated oxygen and methane was influenced by the membrane surface only. The oxygen permeation flux was measured by accounting for all of the oxygen containing components in the sweep gas. In the sweep side gas, $O_2$, $CH_4$, He, $N_2$, $H_2$, CO, $CO_2$, $H_2O$, $C_2H_4$, and $C_2H_6$ were measured using an Agilent Technologies 6890N gas chromatograph (GC) with TCD detector and Alltech Hayesep DB 100/120 column (30' x 1/8" x 0.85" SS) with an argon carrier gas. The amount of nitrogen was used to indicate leakage through the sampling syringe while the amount of helium in the sweep was used to correct for the oxygen leak through the seal. The seal leakage was on the order of 0.01 $mL \cdot cm^{-2} min^{-1}$ He throughout experimentation. All gases except for water were measured with the gas chromatograph. Carbon and hydrogen balances were used to determine the water content. The oxygen permeation flux was calculated from the oxygen containing species: $O_2$, CO, $CO_2$, and $H_2O$.

The permeation experiments under oxygen/methane gradient were conducted at low methane conversion (1-5%) to maintain relatively constant methane partial pressure (~ 1 atm) in the sweep side. Therefore, oxygen conversion, defined as the ratio of the oxygen consumed in the reaction to the amount permeated, was used to indicate the reactivity of the membrane surface as well as oxygen chemical potential in the gas near the membrane surface. The oxygen conversion was calculated:

$$X_{O_2} = \frac{oxygen\ in\ products\ in\ permeate}{total\ moles\ of\ oxygen\ in\ permeate} \tag{2.1}$$

where the $O_2$ in products refers to the oxygen content of CO, $CO_2$, and $H_2O$. The selectivity of each carbon based products was found by calculating the moles of methane reacted of each carbon containing product relative to the total amount of carbon containing products. Equation 2.2 shows an example for calculating the selectivity of $CO_2$:

$$S_{CO_2} = \frac{moles\ of\ CO_2}{total\ moles\ of\ CH_4\ reacted} \tag{2.2}$$

where the total moles of $CH_4$ reacted includes the formation of $CO_2$, CO, $C_2H_4$, and $C_2H_6$.

## 2.3 Results and Discussion

### *2.3.1 Properties of Fresh Membranes*

Oxygen permeation properties of fresh LSCF membranes under various conditions were first measured shortly after exposing the membrane to experimental conditions. This data is compared with the results of previous work and serves as the basis for examining transient oxygen permeation properties of the membrane under an oxygen/methane gradient for an extended period of time. Figure 2.2 is an Arrhenius plot showing oxygen permeation flux for a fresh LSCF membrane in an argon and methane sweep gas environment measured in the temperature range of 700-900$^o$C. The oxygen permeation flux with a methane and argon sweep at 900$^o$C is found to be 0.91 and 0.48 $ml \cdot cm^{-2} \cdot min^{-1}$, respectively.

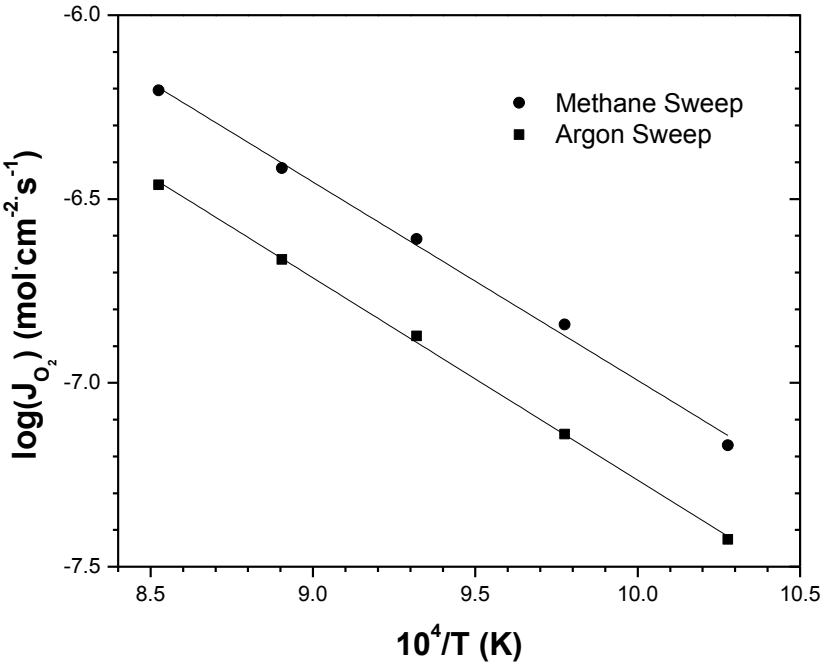


*Figure 2.2 Arrhenius plot showing the influence of temperature on the oxygen permeation flux for fresh $La_{0.6}Sr_{0.4}Co_{0.8}Fe_{0.2}O_{3-\delta}$ membranes with a methane and argon sweep gas (system temperature = 700-900°C, $O_2$/He flow rate = 100 mL·min$^{-1}$, Ar or $CH_4$ sweep flow rate = 100 mL·min$^{-1}$)*

Table 2.1 compares the oxygen permeation value in an inert sweep environment to literature values for the same composition under similar conditions. The oxygen permeation flux in this work is found to be higher than those reported by different research groups. A number of parameters, including different permeation conditions, microstructure differences, and sealing conditions help to improve the permeation properties of this membrane. For both cases with an argon or methane sweep, oxygen flux increases with a logarithmic dependence to increasing temperature, as shown by the Arrhenius plot. The calculated apparent activation energies are each found to be 103

$kJ \cdot mol^{-1}$, which is within the range for apparent activation energy reported for La-Sr-Co-Fe oxide membranes [Sunarso et al., 2008; Zeng et al., 1998].

*Table 2.1 Oxygen permeation flux of $La_{0.6}Sr_{0.4}Co_{0.8}Fe_{0.2}O_{3-\delta}$ membranes in inert sweep gas*

| $J_{O2}$ ($mL \cdot cm^{-2} \cdot s^{-1}$) | Temp. ($^oC$) | Thickness (mm) | Feed $P'_{O2}$ (atm) | $E_A$ ($kJ \cdot mol^{-1}$) | Reference |
|---|---|---|---|---|---|
| 0.2 | 900 | 1.0 | 0.21 | - | Teraoka et al., 2002 |
| 0.15 | 900 | 0.98 | 0.21 | 130-140 | Ten Elshof et al. 1995 |
| 0.1 | 900 | 1.5 | 0.21 | 115 | Yuan et al., 2006 |
| 0.48 | 900 | 1.5 | 0.20 | 103 | This work |

Figure 2.3 shows the oxygen conversion as well as the selectivity of the carbon containing products of the reaction between permeated oxygen and methane in the temperature range of 700-900$^o$C. The $CO_2$ selectivity at 700$^o$C is very close to 1 as very little CO and $C_2H_X$ products are formed. The LSCF surface is known catalytically active for combustion reaction at high temperature [Lin & Zeng, 1996]. Since no other catalyst was packed in the membrane permeation setup, only the LSCF membrane surface was there to catalyze the combustion reaction, which explains the observed high $CO_2$ selectivity. As the temperature increases, an increase in the $C_2H_X$ selectivity is found as it reaches approximately 35% at 900$^o$C as the CO selectivity remains less than 5%. The oxygen conversion, which is a measure of the permeated oxygen that reacts with methane on the sweep side of the membrane, increases with temperature.

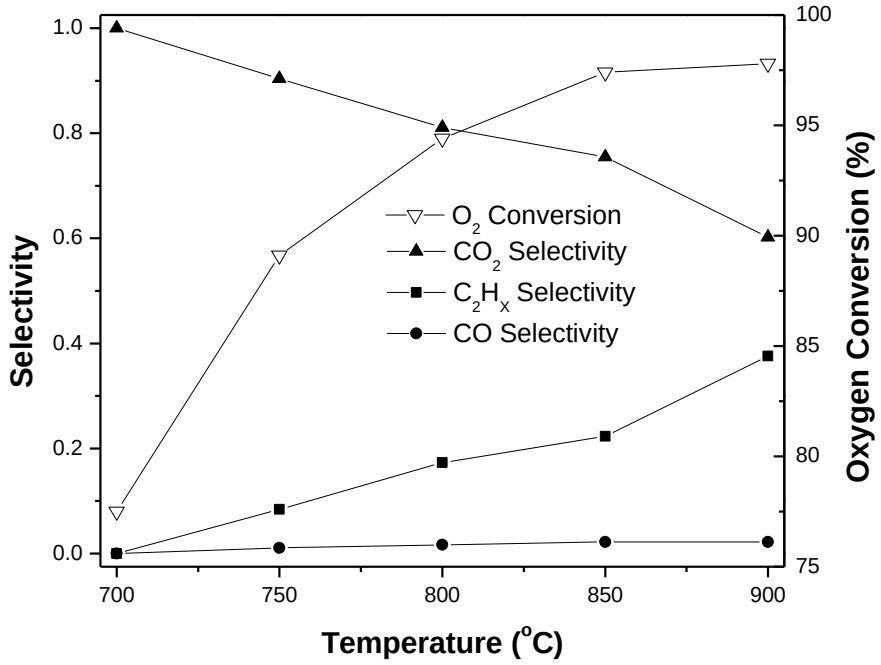


*Figure 2.3 Influence of temperature on the carbon product selectivity and oxygen conversion of a 1.5 mm $La_{0.6}Sr_{0.4}Co_{0.8}Fe_{0.2}O_{3-\delta}$ membranes with a methane sweep gas (same experimental conditions as Figure 2.2)*

Figure 2.4 shows oxygen permeation flux as a function of varying oxygen partial pressure in the feed gas with argon or methane as the sweep gas. The oxygen permeation flux increases for both the argon and methane sweep gases as the oxygen partial pressure increases. Figure 2.5 shows oxygen permeation flux as a function of sweep flow rate for both an argon and methane sweep gas. For the sweep flow rates tested, oxygen permeation flux increases with increased sweep flow rate for both argon and methane. At a sweep flow rate of 200 $mL \cdot min^{-1}$, a maximum oxygen permeation flux of 0.36 and 1.75 $mL \cdot cm^{-2} \cdot min^{-1}$ is measured in argon and methane, respectively.

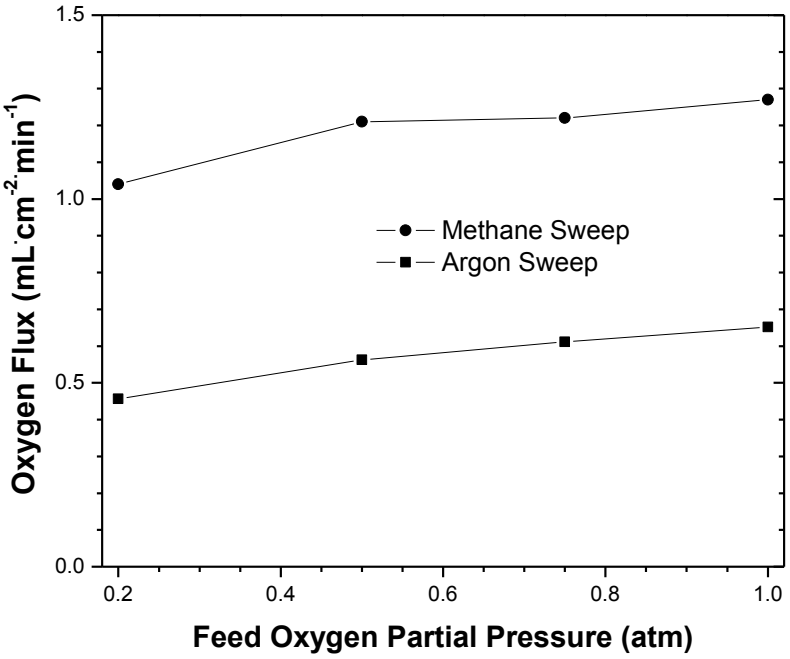


*Figure 2.4 Influence of feed oxygen partial pressure on the oxygen permeation flux of a 1.5 mm $La_{0.6}Sr_{0.4}Co_{0.8}Fe_{0.2}O_{3-\delta}$ membrane with an argon and methane sweep gas (system temperature = 900°C, $O_2$/He flow rate = 100 $mL \cdot min^{-1}$, Ar or $CH_4$ sweep flow rate = 100 $mL \cdot min^{-1}$)*

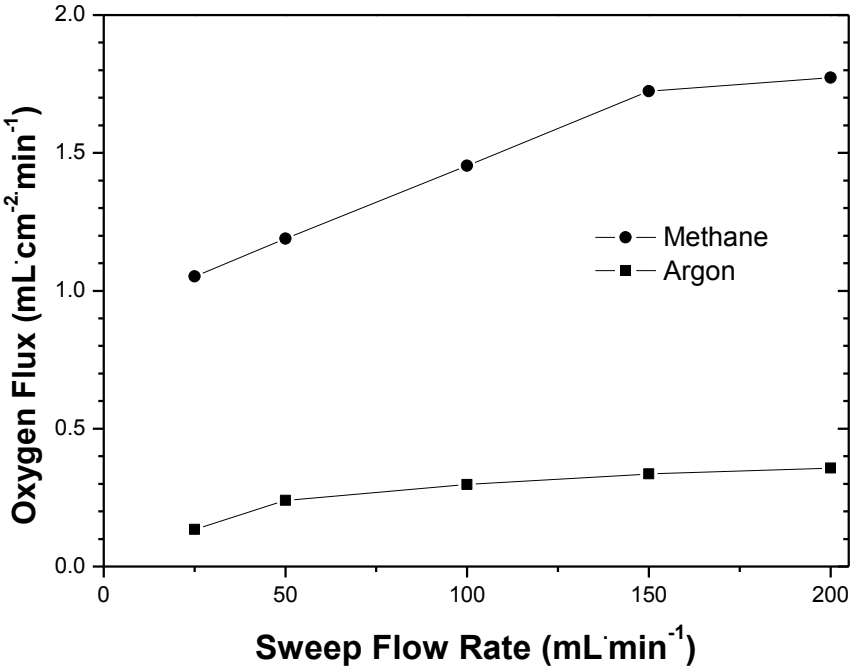


*Figure 2.5 Influence of argon or methane sweep flow rate on the oxygen permeation flux of a 1.5 mm $La_{0.6}Sr_{0.4}Co_{0.8}Fe_{0.2}O_{3-\delta}$ membranes (system temperature = 900°C, $O_2$ inlet concentration = 20%, $O_2$/He flow rate = 100 mL·min$^{-1}$, Ar or $CH_4$ sweep flow rate = 25-200 mL·min$^{-1}$)*

Oxygen permeation flux through a thick LSCF membrane controlled by oxygen ionic conduction in the bulk phase of the membrane is described by:

$$J_{O_2} = \frac{RT\sigma_i^o}{8F^2L}\left(\frac{1}{P''^n_{O_2}} - \frac{1}{P'^n_{O_2}}\right) \tag{2.3}$$

where $P'_{O_2}$ and $P''_{O_2}$ are the feed and sweep side oxygen partial pressures, respectively, $\sigma_i^o$ is the oxygen ionic conductivity at a reference oxygen partial pressure (normally 1 atm), $F$ is Faraday's constant, $L$ is the membrane thickness, and $n$ is a positive exponent constant that is determined by the dependence of the oxygen ionic conductivity on

oxygen partial pressure for LSCF [Yuan et al., 2006; Qi et al., 2000]. For a LSCF membrane at a given temperature, a higher feed oxygen partial pressure ($P'_{O_2}$), or a faster sweep gas flow rate (and hence the lower the oxygen partial pressure in the sweep gas ($P''_{O_2}$), would give a larger driving force for oxygen permeation, as shown in Equation 2.3, and therefore, a higher oxygen permeation flux [Akin et al., 2001]. Concerning oxygen partial pressure in the sweep gas, oxygen partial pressure is on the order of $10^{-4}$ atm in inert gas such as argon, depending on the purity of the gas and relative flow rate of oxygen permeation and sweep gas. The oxygen partial pressure of a reducing gas such as methane is less than $10^{-10}$ atm depending on the reaction conditions [Akin et al., 2001]. This explains higher oxygen permeation flux with methane than argon as the sweep gas.

The temperature dependence of oxygen permeation flux with argon sweep gives an apparent activation energy that is the same as for oxygen ionic conduction for LSCF (103 kJ/mol), as shown by Equation 2.3 because the effects of the variations in ($P''_{O_2}$) at different temperature on permeation flux can be neglected [Akin et al., 2001]. With methane as the sweep, $P''_{O_2}$ depends on the chemical reaction in the permeate side [Rui et al., 2009]. With methane, the following major reactions may take place on the permeate side:

$$2CH_4 + O_2 \leftrightarrow C_2H_4 + 2H_2O \qquad (2.A)$$

$$CH_4 + 2O_2 \leftrightarrow CO_2 + 2H_2O \qquad (2.B)$$

$$CH_4 + \frac{1}{2}O_2 \leftrightarrow CO + 2H_2 \qquad (2.C)$$

$$CH_4 + CO_2 \leftrightarrow 2CO + 2H_2 \qquad (2.D)$$

$$CH_4 + H_2O \leftrightarrow CO + 3H_2 \qquad (2.E)$$

Reactions 2.A-2.3C are exothermic, while reactions 2.D and 2.E are endothermic. As shown in Figure 2.3 and summarized in Table 2.2, as the temperature increase from 700 to 900°C, oxygen conversion and $C_2H_X$ ($C_2H_4$ + $C_2H_6$) selectivity increases respectively from 78 to 98% and 0 to 38% , while the $CO_2$ decreases from 100 to 60% and CO selectivity remains essentially zero. This shows that the LSCF surface becomes more active for the reactions and selective for $C_2H_X$ as temperature increases, consistent with the results on the catalytic properties of the LSCF pellets [Lin & Zeng, 1996].

*Table 2.2 Comparison of $O_2$ permeation flux and reaction product selectivity for LSCF membrane with methane as the sweep at two temperatures*

| Measurement | 700°C | 900°C |
|---|---|---|
| $O_2$ Flux ($mL \cdot cm^{-2} \cdot min^{-1}$) | 0.10 | 0.91 |
| $O_2$ conversion $Xo_2$ | 0.78 | 0.98 |
| $C_2$ selectivity $S_{C2HX}$ | 0.00 | 0.38 |
| CO selectivity $S_{CO}$ | 0.00 | 0.38 |
| $CO_2$ selectivity $S_{CO2}$ | 1.00 | 0.60 |

Qualitatively, the downstream oxygen partial pressure $P"_{O_2}$ decreases with increasing oxygen conversion (consumption of the permeated oxygen) [Akin et al., 2001]. It also depends on reactor flow conditions and reaction kinetics represented by the selectivity for various products [Rui et al., 2009]. Figure 2.2 shows that with methane as the sweep the oxygen permeation flux increases approximately one order of magnitude from 0.1 to over 0.9 $mL \cdot cm^{-2} \cdot min^{-1}$. The fact that the apparent activation energy for oxygen permeation with methane as the sweep is the same as that with argon as the

sweep indicates that the effects of the variations in $P''_{O_2}$ due to different reactivity at different temperature on oxygen permeation flux can be neglected in the temperature range studied.

*2.3.2 Transient and Steady State Properties of Membrane during Oxygen Permeation*

Figure 2.6 shows oxygen permeation flux of an LSCF membrane with methane as the sweep gas as a function of time at 900°C over the course of more than 430 h. As shown, the oxygen permeation flux increases for the first 55 hours and reaches a maximum of 2.27 $mL \cdot cm^{-2} \cdot min^{-1}$ followed by a decrease before reaching a steady-state value of approximately 1.80 $mL \cdot cm^{-2} \cdot min^{-1}$ after 200 h. A similar trend has been documented for dense perovskite-type ceramic hydrogen permeable $SrCe_{0.75}Zr_{0.2}Tm_{0.05}O_{3-\delta}$ at 900°C in a $H_2$/He and $O_2$/Ar feed and sweep arrangement, respectively, requiring approximately 100 hours to reach a steady-state value [Kniep et al., 2010]. This trend was attributed to the formation of non-perovskite metal oxide phases on the membrane surface exposed to hydrogen. Moreover, previous work by Xu and Thomson has shown that a $La_{0.6}Sr_{0.4}Co_{0.2}Fe_{0.8}O_{3-\delta}$ membrane exposed to an air/methane gradient had an increase in oxygen permeation flux for the first 36 hours before reaching a steady-state value until completion of the experiment after 50 hours at 850°C [Xu & Thomson, 1998]. The increase in oxygen flux was explained by a decrease in the membrane thickness due to an etching phenomenon on the membrane surface exposed to methane. Stress caused by thermal expansion led to the membrane surface being reduced to the point that it de-sintered to relieve stress. Ultimately, the membrane of Xu and Thomson maintained good mechanical integrity and no cracks or defects developed.

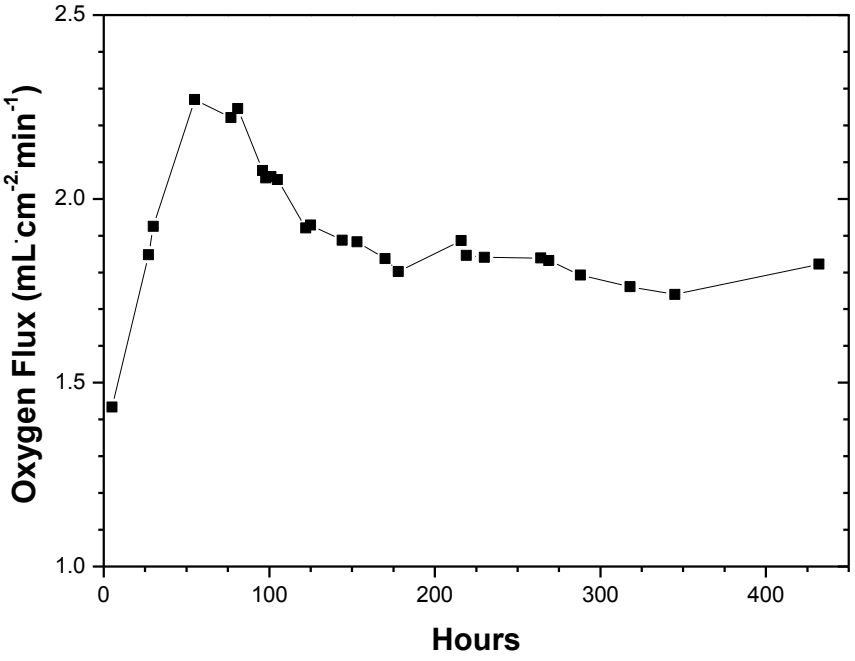


*Figure 2.6 Stability of oxygen permeation flux of a 1.5 mm $La_{0.6}Sr_{0.4}Co_{0.8}Fe_{0.2}O_{3-\delta}$ membrane with a methane sweep gas (system temperature = 900°C, $O_2$ inlet concentration = 20%, $O_2$/He flow rate = 100 mL·min$^{-1}$, sweep flow rate = 100 mL·min$^{-1}$)*

Figure 2.7 shows that the selectivity of carbon based products does not appear to reach steady-state for approximately 200 h. Initially, there is a significant $C_2H_X$ selectivity, which drastically drops from 36% to 3% over the course of the first 55 h before stabilizing at approximately 5%. The CO selectivity increases from 0 to 45% in the first 55 h before stabilizing at approximately 31%. $CO_2$ selectivity drops slightly for the first 55 h before climbing and reaching a steady-state value of approximately 64%. The oxygen conversion increases slightly from 99% to maximum 100% at 55 h and then drops to about 99.5% at the steady state. The changes in oxygen permeation flux and other reaction parameters are summarized in Table 2.3. Previous work for LSCF of

similar composition has shown a same trend of the $C_2H_X$ selectivity decreasing from 40% to 10% after testing for 40 h [Xu & Thomson, 1998]. It is clear that the surface catalytic properties for LSCF membranes change upon exposure to methane but eventually reach steady state.

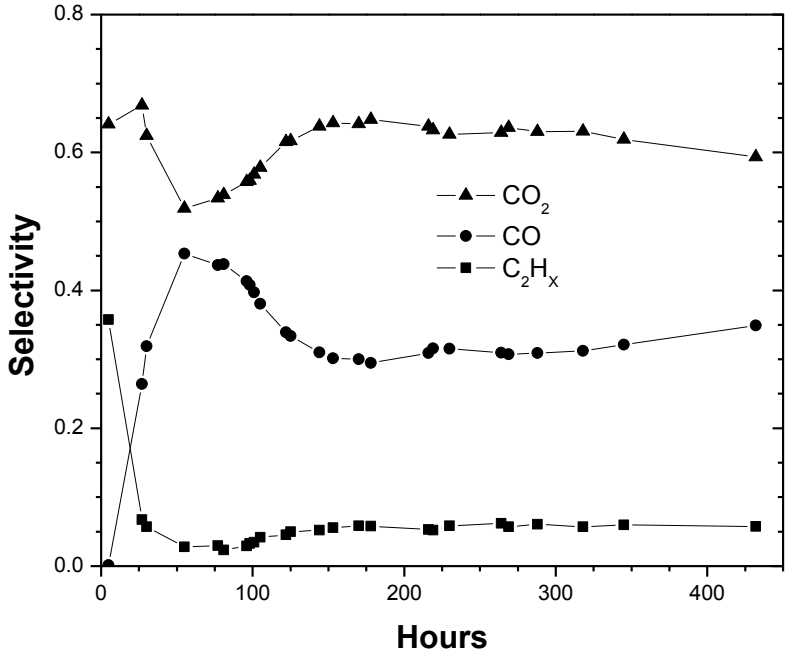


*Figure 2.7 Stability of the reaction of permeated oxygen with methane (system conditions same as Figure 2.6)*

*Table 2.3 Comparison of $O_2$ permeation flux and reaction product selectivity with increased exposure to experimental conditions at 900$^oC$*

| Measurement | Fresh (0-10 h) | Peak (~55 h) | Steady-State (215 h) |
|---|---|---|---|
| $O_2$ Flux ($mL \cdot cm^{-2} \cdot min^{-1}$) | 1.43 | 2.27 | 1.89 |
| $O_2$ conversion $Xo_2$ | 0.98 | 0.99 | 0.99 |
| $C_2$ selectivity $S_{C2Hx}$ | 0.36 | 0.03 | 0.05 |
| CO selectivity $S_{CO}$ | 0.00 | 0.45 | 0.31 |
| $CO_2$ selectivity $S_{CO2}$ | 0.64 | 0.52 | 0.64 |

Figure 2.8 compares the temperature effect on oxygen permeation for the LSCF membrane with methane as the sweep gas in the fresh state (first 5 h) and the steady states (215 h and 290 h). Within the experimental errors, the slopes of these three data sets shown in Figure 2.8 are very close, giving an approximate apparent activation energy of about 103 kJ/mol. Figures 2.9-2.11 compare the catalytic properties of the LSCF membrane with methane as the sweep gas in the steady state (aged membrane) with that at the initial state (fresh membrane) under various conditions. For both the aged and fresh membranes, the oxygen conversion, CO and $C_2H_X$ selectivity increase, and $CO_2$ selectivity decreases with increasing temperature, as shown in Figure 2.9. The effects of the feed oxygen partial pressure and sweep gas flow rates on various selectivities are similar for the aged and fresh membranes. The results shown in Figures 2.8-2.11 suggest that the oxygen permeation mechanisms for the LSCF membrane in the fresh state and those in the transient and final steady states are similar and can be described by Equation 2.1.

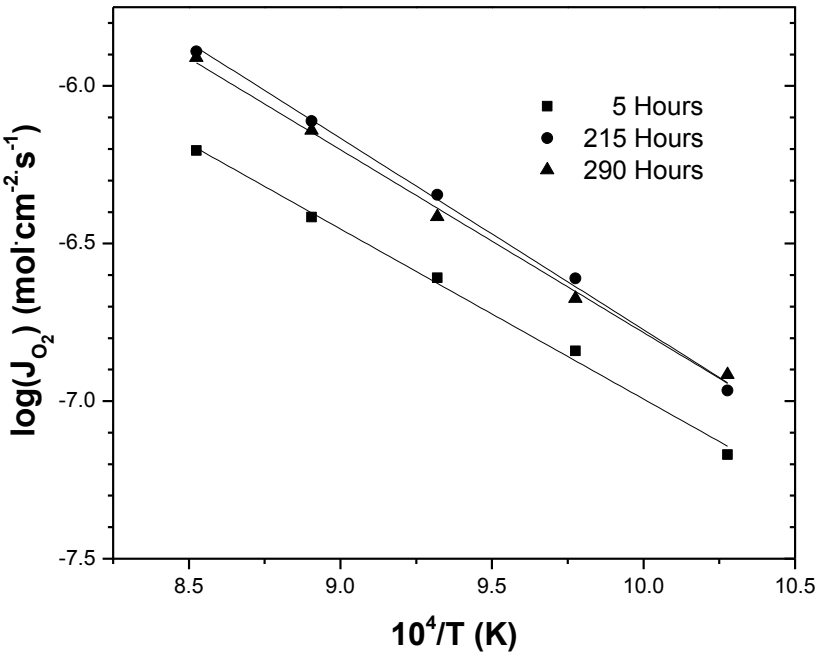


*Figure 2.8 Arrhenius plot of the oxygen permeation flux of $La_{0.6}Sr_{0.4}Co_{0.8}Fe_{0.2}O_{3-\delta}$ membranes after exposure to methane at different times*

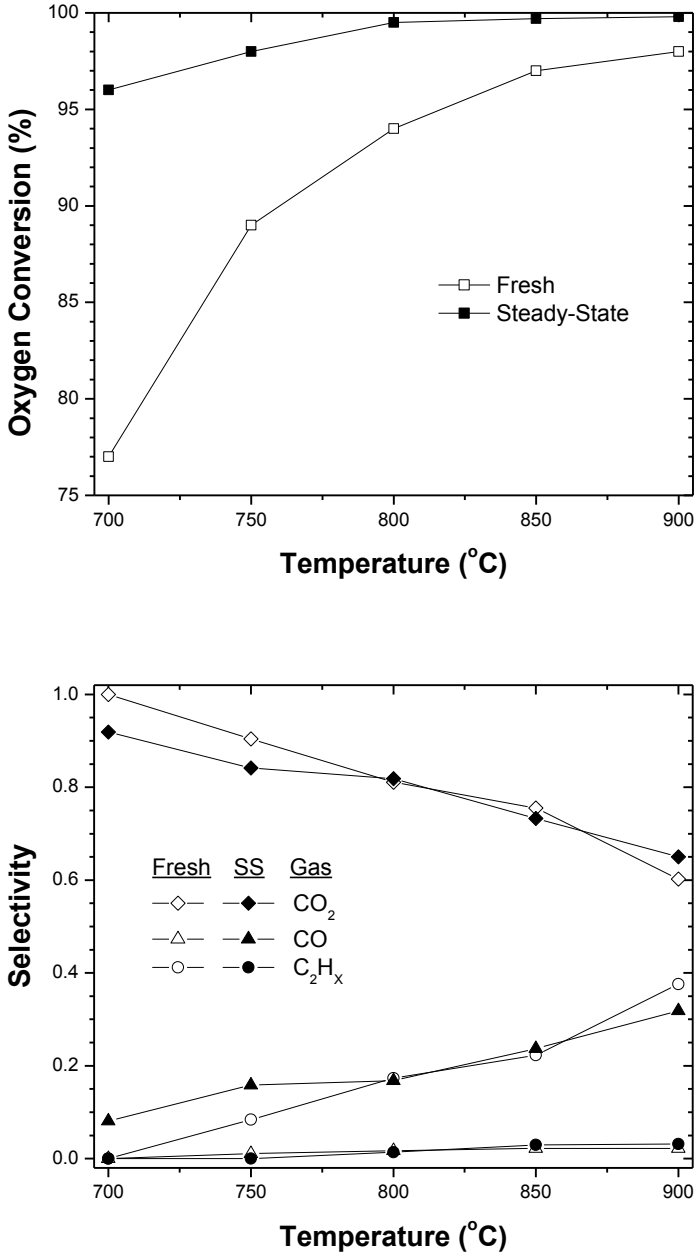


*Figure 2.9 Effect of temperature on the (a) oxygen conversion and (b) selectivity of fresh LSCF and steady-state (450 h) LSCF membranes with methane as the sweep*

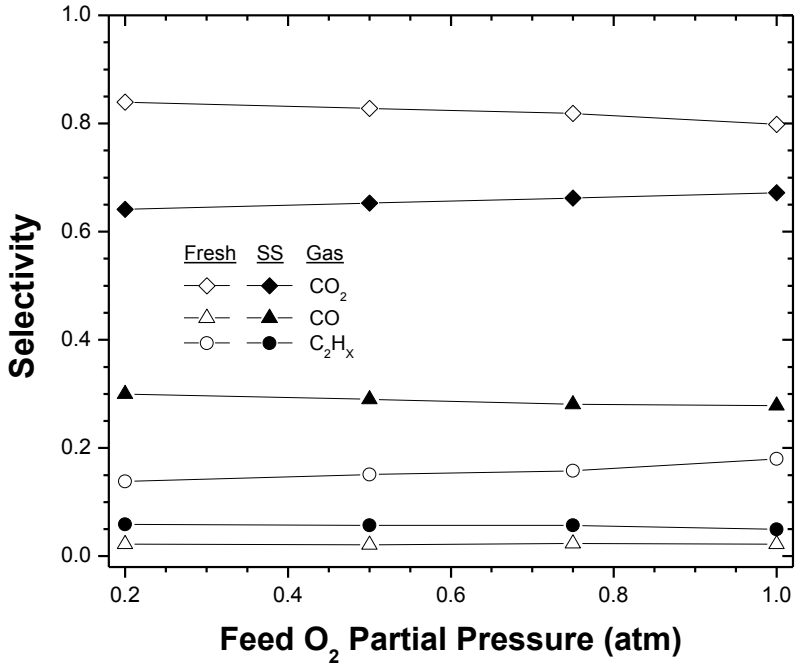


*Figure 2.10 Effect of feed $O_2$ partial pressure on the selectivity of dense LSCF on fresh and steady-state membranes*

The aged LSCF membrane at steady state has a higher oxygen permeation flux than the fresh membrane probably because the aged membrane surface is more active for reaction (as indicated by a higher oxygen conversion) and selective for CO than the fresh membrane. Thus the aged membrane would give a lower $P''_{O_2}$, which is determined by the reactivity in the permeate side, resulting in a higher driving force for oxygen permeation [Rui et al., 2011]. It appears that $P''_{O_2}$ is a strong function of CO selectivity because oxygen permeation flux under constant temperature correlates well with CO selectivity as shown in Figure 2.7. Clearly the transient behavior and subsequent steady state for oxygen permeation and catalytic properties for the LSCF membrane are related to a change on the membrane surface exposed to methane at high temperatures. However,

such changes in catalytic properties cause a change in the reactivity in the permeate side, and therefore, the downstream oxygen partial pressure. This is responsible for the observed changing oxygen permeation flux.

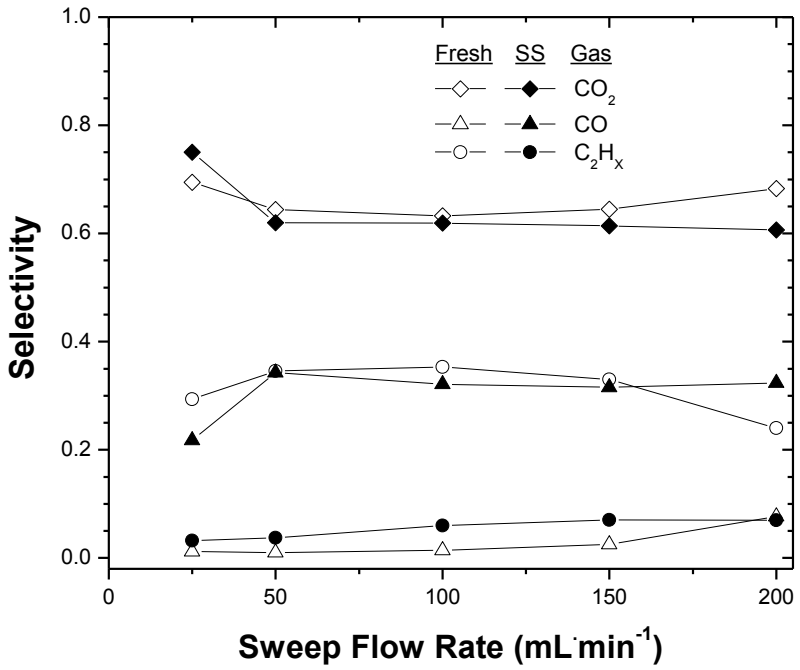


*Figure 2.11 Effect of sweep flow rate on the selectivity of dense LSCF on fresh and steady-state membranes*

Figure 2.12 shows XRD patterns of the LSCF at various stages. The XRD pattern of the fresh membrane prior to being used in an experiment shows a fully developed perovskite-type structure in good agreement with Anderson & Lin, who also prepared dense LSCF membranes using the citrate method sintered at 1200$^{o}$C [Anderson et al., 2010]. The membrane surface exposed to oxygen for 450 h remains in the perovskite structure. The membrane surface exposed to methane for 100 h also has a perovskite-structure with peaks present at 23, 33, 41, 47, 59, 69, and 79$^{o}$, with no clear formation of

$La_2O_3$, $LaFeO_3$, or $Co_2O_3$. This indicates that the change in the surface properties up to 100 h were not detectable by XRD. The oxygen feed side of the membrane remains in the same perovskite structure after the exposure of the membrane to oxygen/methane gradient for more than 450 h. However, the XRD pattern of the membrane surface exposed to methane for more than 450 h shows formation of $SrCO_3$ with peaks at 31, 37, and 44° and CoO with peaks present at 43 and 65°, which is consistent with previous perovskite materials exposed to an air/methane gradient [Pei et al., 1994; ten Elshof et al., 1995; ten Elshof et al., 1996].

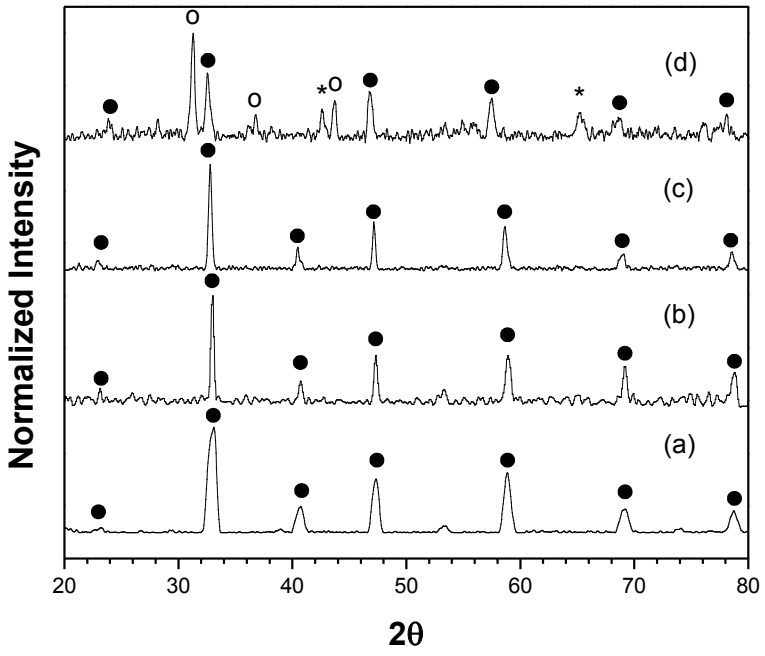


*Figure 2.12 XRD patterns of LSCF membranes (a) fresh, (b) permeate surface after 100 hours exposed to methane, (c) feed surface after 450 hours exposed to air, and (d) permeate surface after 450 h exposed to methane (Peak identifications: • = $La_{0.6}Sr_{0.4}Co_{0.8}Fe_{0.2}O_{3-\delta}$, o = $SrCO_3$, and * = CoO)*

Figure 2.13 shows a SEM micrograph of the feed and sweep surfaces and cross section of the membrane exposed to methane for 450 h. The feed side shows a dense surface with a well-defined grain boundary. The sweep surface exposed to methane for 450 h is clearly porous. The XRD pattern (Figure 2.12) of the membrane surface exposed to methane for 450 h show quite intensive peaks of the perovskite structure for the membrane underneath the porous layer. This suggests that the porous layer is sufficiently thin so that X-rays can still penetrate. This is verified by analyzing the cross section by SEM. The cross section shows a porous thickness between 40-100μm, which is representative of the sweep surface. Therefore, the change in oxygen permeation flux is not caused by the change in dense membrane thickness as predicted by Equation 2.3 as this leads to less than 10% decrease in thickness.

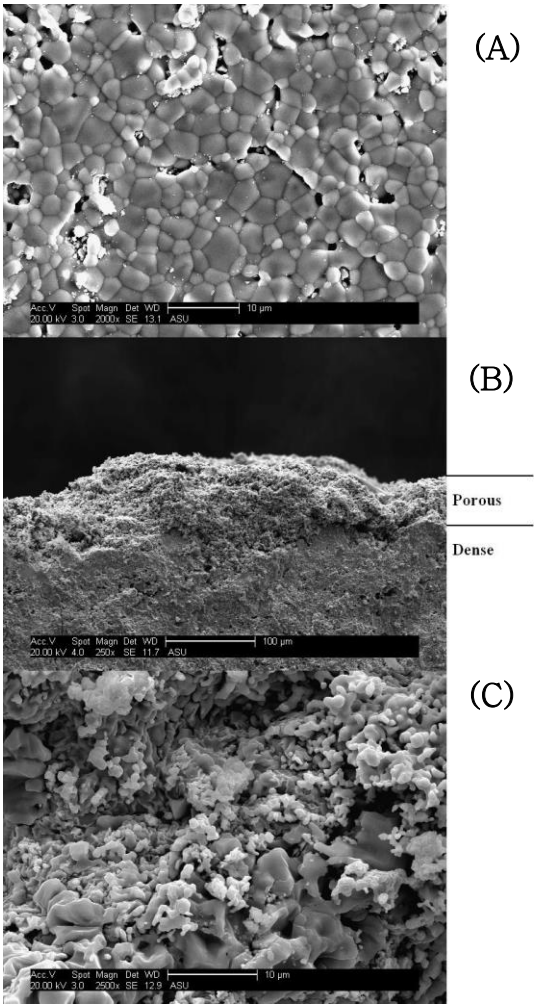


*Figure 2.13 SEM images of LSCF membrane (a) feed surface (b) cross section, and (c) sweep surface after exposure to methane for 450 hours.*

## 2.4 Conclusions

Oxygen permeation flux and surface catalytic properties of $La_{0.6}Sr_{0.4}Co_{0.8}Fe_{0.2}O_{3-\delta}$ (LSCF) membrane in an oxygen/methane gradient were measured for an extended period of time to examine the transient characteristics of the mixed-conducting membranes. Upon exposure to an oxygen/methane gradient the oxygen permeation flux of the membrane increases to a maximum at around 55 h, then decreases and reaches a steady state value after around 200 h. The surface catalytic properties of the membrane exposed

to methane also change with the exposure time in the similar fashion. In spite of these changes, the apparent activation energy for oxygen permeation for the membranes at various stages of the transient study is nearly constant indicating no change in oxygen permeation mechanism. Upon exposure to methane the membrane surface becomes more active for reaction with increased selectivity for carbon monoxide formation upon exposure to methane. This lowers oxygen partial pressure in the permeate side and increases the driving force for oxygen permeation. The maximum and steady state flux is approximately 60% and 30% higher than the initial flux of the fresh membrane, respectively. Under the studied experimental conditions the membrane can reach a steady state for continuous operation. Further discussion of the stability of LSCF continues in Chapter 3 as the steady-state permeation properties of LSCF-carbonate dual-phase membranes in various experimental conditions are addressed.

# CHAPTER 3

# STABILITY OF LA-SR-CO-FE OXIDE-CARBONATE DUAL-PHASE MEMBRANES FOR CARBON DIOXIDE SEPARATION AT HIGH TEMPERATURES

## 3.1 Introduction

The emission of $CO_2$ into the atmosphere has become an issue of significant concern as its effect on the environment continues to be studied. Current technologies for $CO_2$ capture are focused on low temperature separation [Anderson et al., 2012]. However, the ability to separate $CO_2$ at elevated temperatures offers many benefits. Current research on $CO_2$ selective membranes centers around polymeric and microporous inorganic membranes [Powell and Qiao, 2006, Bernardo et al., 2009; Hsieh, 1996, Lin, 2001]. While both methods have shown promising results, their effectiveness is limited at high temperatures.

To improve upon the limitations of polymer and microporous inorganic membranes at high temperatures, the concept of a dual-phase membrane consisting of a metallic phase and a molten carbonate phase was proposed [Chung et al., 2005]. However, at higher temperatures, reaction between the stainless-steel support and carbonate formed insulating $LiFeO_2$, which drastically reduced the electronic conductivity of the support. More recent work for silver-carbonate membranes has showed improved performance, however, the membrane is unstable as molted carbonate is continuously lost from the silver support at high temperature. [Xu et al., 2012].

Another limitation of the metal-carbonate dual-phase membrane is that $O_2$ is required on the $CO_2$ rich side of the membrane in order to permeate $CO_2$, as the metal support does not have the ability to transport oxygen ions. To address these

shortcomings, the use of an ionic conducting ceramic phase as the solid support of the dual-phase membrane was proposed [Anderson and Lin, 2006]. To briefly review, a porous ceramic support infiltrated with molten carbonate has the ability to transport oxygen and carbonate ions, respectively [Anderson and Lin, 2010]. On the $CO_2$ rich surface of the membrane, $CO_2$ reacts with oxygen ions from the ceramic phase to form a carbonate ion, $CO_3^{=}$. The molten carbonate phase transports the carbonate ion toward the $CO_2$ lean surface of the membrane where the reverse surface reaction takes place. The carbonate ion converts to $CO_2$, which is released, and $O^{=}$, which transports through the ceramic phase back towards the upstream surface of the membrane to maintain electronic neutrality. Carbon dioxide permeation is driven by the partial pressure gradient across the membrane.

The first ceramic-carbonate dual-phase membrane was synthesized using LSCF ceramic supports [Anderson and Lin, 2010]. In addition to the previous LSCF-carbonate study, this material was chosen because it has been well studied as an oxygen conducting membrane as well as shown to have a high electronic and oxygen ionic conductivity at high temperatures. LSCF has shown to be an effective ceramic material to serve as the support for the dual-phase membrane. Ortiz-Landeros et al. recently studied the effects of the structure of solid (LSCF) and pore (carbonate) phases on carbon transport in the LSCF-carbonate dual-phase membrane and identified the optimum structure to give maximum $CO_2$ permeance through the membrane [Ortiz-Landeros et al., 2013]. Anderson and Lin also demonstrated that the LSCF-carbonate membrane could be used in a membrane reactor that couples separation of CO2 from flue gas and methane dry reforming reaction to produce syngas [Anderson and Lin, 2013].

In Chapter 2, the stability of oxygen permeation flux through $La_{0.6}Sr_{0.4}Co_{0.8}Fe_{0.2}O_{3-\delta}$ (LSCF) membranes was measured in inert and reducing conditions. It was found that while the surface of LSCF shows signs of decomposition into $SrCO_3$ and CoO when exposed to a reducing gas, oxygen permeation through the membrane reaches steady-state for continuous operation with an appreciable permeation flux on the order of 1.8 $mL \cdot cm^{-2} \cdot min^{-1}$ at 900°C. In Chapter 3, carbon dioxide permeation flux stability for LSCF-carbonate membranes will be presented in an oxygen-lean and oxygen-rich environment.

The objective of Chapter 3 is to study the stability and permeation performance of the LSCF-carbonate membrane at high temperature under various experimental conditions. While this material has been well studied as an oxygen-conducting membrane, a study examining the chemical and permeation stability of the dual-phase membrane after long-term exposure to experimental conditions at high temperature has yet to be conducted.

## 3.2 Experimental Methods

### *3.2.1 Preparation of porous $La_{0.6}Sr_{0.4}Co_{0.8}Fe_{0.2}O_{3-\delta}$ supports*

$La_{0.6}Sr_{0.4}Co_{0.8}Fe_{0.2}O_{3-\delta}$ (LSCF) powder was synthesized via the liquid citrate method previously described in detail in Chapter 2. To summarize, stoichiometric amounts of metal nitrate precursors were weighed out in a 0.05 mole basis and mixed with an excess of citric acid. The precursors were dissolved in de-ionized water and heated and covered to prevent evaporation and promote polymerization followed by evaporation. The resulting viscous solution was dried in a furnace for 24 hours. Self-ignition of the dried gel was then performed to burn out the organic compounds. The

resulting powder was then ground with a mortar and pestle to reduce the particle size. The powder was then calcined at 600$^{o}$C in air for 20 hours with heating and cooling ramping rates of 2$^{o}$C·min$^{-1}$. The calcined powder was again ground using a mortar and pestle. Porous membrane supports were prepared by the method previously described by Anderson and Lin [Anderson & Lin, 2010]. Approximately 3 grams of powder was placed in a 30 mm stainless steel mold and pressed to 160 mPa for 5 minutes using a hydraulic press (Carver, Model #3853). The green disks were then sintered at 900$^{o}$C for 24 hours with heating and cooling ramping rates of 2$^{o}$C·min$^{-1}$ resulting in porous LSCF disk supports.

*3.2.2 Synthesis of $La_{0.6}Sr_{0.4}Co_{0.8}Fe_{0.2}O_{3-\delta}$-carbonate dual phase membrane*

Synthesis of LSCF-carbonate dual-phase membranes was achieved by direct infiltration of molten carbonate into the pores of sintered LSCF support via the direct infiltration technique previously described by Chung et al [Chung et al., 2005]. The carbonate powders $Li_2CO_3$ (99.2%, Fischer Scientific), $Na_2CO_3$ (99.9%, Fischer Scientific), and $K_2CO_3$ (99.8%, Fischer Scientific) were weighed out in a 42.5/32.5/25 mol% ratio, respectively, and heated to 550$^{o}$C in a furnace. Porous ceramic supports were preheated above the molten carbonate mixture to prevent thermal shock prior to being lowered into contact with carbonate. Supports were left in contact with molten carbonate for 5-10 minutes to ensure complete infiltration via capillary force. The membrane was then lifted and slowly removed from the furnace and cooled. Residual carbonate on the membrane surface was removed using SiC polishing paper.

*3.2.3 Characterization of ceramic supports and ceramic-carbonate dual-phase membranes*

Room temperature helium permeation was used to determine the average pore size of porous supports as well as verifying the gas tightness of dense ceramic and ceramic-carbonate dual-phase membranes. The phase structure of the LSCF powder and membranes were characterized using X-ray diffraction (XRD) (Bruker, $CuK_{\alpha 1}$) evaluated in the 2θ range of $20^o$ to $80^o$. Scanning electron microscopy (SEM) imaging was performed to confirm the porous nature of ceramic supports as well as the dense nature of dense ceramic and ceramic-carbonate samples.

*3.2.4 Carbon dioxide permeation measurements*

Previous studies on $CO_2$ permeation through LSCF-carbonate membranes were conducted in a custom-built high temperature permeation setup using a ceramic-glass seal [Anderson & Lin, 2010, Ortiz-Landeros et al., 2013, Anderson and Lin, 2013]. In this study, a Probostat high temperature permeation system (Probostat, Norwegian Electro Ceramics AS), with a silver seal was used for carbon dioxide permeation experiments. Figure 3.1 shows a schematic drawing of the carbon dioxide permeation setup. For each experiment an alumina spacer attached to a spring force assembly, a dense LSCF-carbonate disk membrane, and silver seal were placed on top of a 20 mm alumina tube, which was then enclosed by a 40 mm diameter alumina tube. Argon was introduced inside the 20 mm alumina tube serving as the sweep gas at the bottom of the membrane while carbon dioxide and nitrogen was introduced to the space between the two alumina tubes, serving as the feed gas to the top of the membrane. The assembled apparatus was then placed in a vertical tube furnace and was heated to approximately $950^oC$ to reach the

softening temperature of silver at a ramping rate of $1^{o}C \cdot min^{-1}$. Once the softening point of silver was reached, the spring assembly attached to the alumina spacer above the disk membrane forced the membrane into the silver ring forming a seal between the membrane and the 20 mm alumina tube. The quality of the seal was determined by measuring the nitrogen content in the argon sweep gas using an Agilent Technologies 7890A gas chromatograph (GC) with TCD detector and Alltech Hayesep DB 100/120 column (30 ft × 1/8 in. × 0.85 in. SS). After reaching minimization of helium leakage, the system was cooled to either 700°C or 900°C at a rate of $1^{o}C \cdot min^{-1}$.

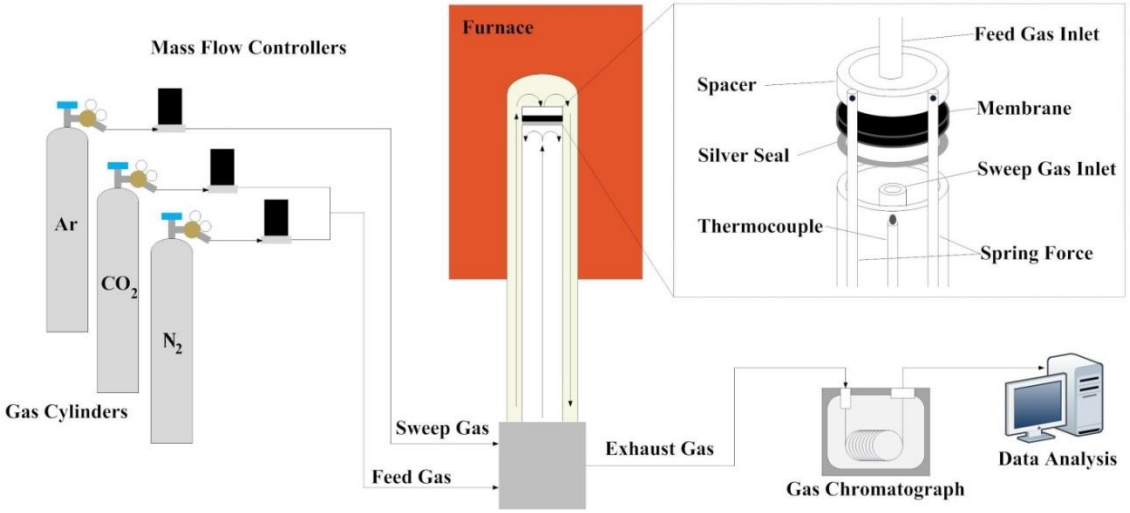


*Figure 3.1 Experimental high temperature carbon dioxide permeation setup*

For carbon dioxide permeation experiments, the feed gas consisted of a variable carbon dioxide flow mixed with a balance of nitrogen to reach 100 $mL \cdot min^{-1}$ for a carbon dioxide partial pressure varying between 0.1-0.9 atm. Argon was flowed as the sweep gas at a flow rate range between 25-200 $mL \cdot min^{-1}$. The temperature was varied between 700-900°C. Gas flow rates were regulated using mass flow controllers (MKS, Model 1179) and a four-channel readout (MKS, Type 247. Samples were taken three hours after a

change in gas composition and one hour after a temperature change to allow the system to reach steady state. Table 3.1 shows the system parameters for tests with varying temperature, carbon dioxide partial pressure, and sweep flow rate. A mass balance on the measured sweep side gases was used to calculate the carbon dioxide permeation flux through each membrane. The carbon dioxide error in the permeate gas caused by seal leaks was corrected by measuring the presence of nitrogen and subtracting the corresponding carbon dioxide from the calculated carbon dioxide permeation flux. The error in determining the carbon dioxide permeation flux using this procedure is approximately $\pm$ 10%.

*Table 3.1 System parameters for carbon dioxide permeation flux experiments*

| Variable Parameter | System Temp ($^oC$) | Feed $CO_2$ Partial Pressure (atm) | Sweep Flow ($mL \cdot min^{-1}$) |
|---|---|---|---|
| Temperature | 700-900 | 0.5 | 100 |
| $CO_2$ Partial Pressure | 900 | 0.1-0.9 | 100 |
| Sweep Flow Rate | 900 | 0.5 | 25-200 |
| Stability | 900 | 0.5 | 100 |

## 3.3 Results and Discussion

### *3.3.1 High temperature $CO_2$ permeation measurements without $O_2$*

Figure 3.2 shows the $CO_2$ permeation of LSCF-carbonate membranes exposed to constant experimental conditions at temperatures of 800, 850, and 900$^o$C for as long as 110 hours. For all three temperatures, the $CO_2$ permeation flux decreases significantly after initial exposure to experimental conditions. Initial measurements at each temperature are shown 10-15 hours after exposure to experimental conditions due to the long period of time it takes to seal these membranes. In Figure 3.2, time zero represents

the point in time when the membrane reaches its desired testing temperature. For example, hour 0 represents the point in time when membrane 1 first reaches 900$^{o}$C. The time between 0 hours and when measurements are first taken is the time required to seal the membrane. Based on the behavior of the $CO_2$ permeation after initial measurements were taken, it is assumed that the permeation flux after initial exposure is significantly higher than what is measured after 10-15 hours. The instability and large drop-off in $CO_2$ permeation flux through the LSCF-carbonate membrane at high temperature is caused by the instability of the ceramic support in highly concentrated $CO_2$ environments. Previous work on LSCF membranes of the same composition as a dense membrane for oxygen separation has shown a sharp decrease in $O_2$ permeance under highly concentrated $CO_2$ exposure when compared to testing conditions that do not include $CO_2$ [Tan et al., 2012].

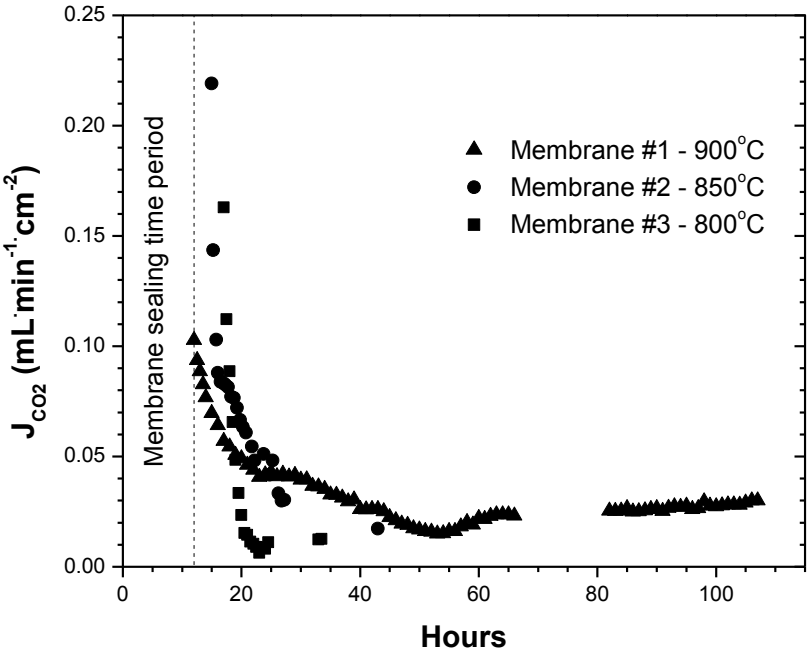


*Figure 3.2 Time dependence of $CO_2$ permeation flux of three LSCF-carbonate membranes at different permeation temperatures (thickness = 1.0 mm, feed gas is equimolar $CO_2$:$N_2$, sweep gas is pure He, feed and sweep flow rate = 100 mL·min$^{-1}$, both feed and sweep gases at 1 atm, T = 800-900°C)*

Recent studies on dense MIEC membranes for oxygen separation have shown that the presence of $CO_2$ has a significant poisoning effect on the oxygen permeability of these membranes at high temperature [Waindich et al., 2009, Yi et al., 2010, Yi and Schroeder, 2011, Tan et al., 2012]. For mixed conducting membranes, oxygen separation relies on a surface exchange reaction between molecular oxygen and oxygen vacancies in the perovskite structure. In the presence of $CO_2$, however, alkaline earth metals readily react with $CO_2$ at high temperature, resulting in the formation of a carbonate layer on the membrane surface. This surface layer inhibits the surface exchange reaction, resulting in a decrease in the oxygen permeability. This is also a concern for the dual-phase

membrane, as the formation of a carbonate layer on the ceramic phase of the dual-phase membrane surface would limit $CO_2$ permeability of the membrane. In the case of the ceramic-carbonate membrane, a carbonate layer would limit the surface reaction between $CO_2$ and lattice oxygen in the ceramic phase, which is required in order to form a permeable carbonate ion in the carbonate phase.

As shown in Figure 3.2, after approximately 65 hours of exposure at 900°C, the $CO_2$ permeation measured through the LSCF-carbonate membrane achieved a steady-state value of approximately 0.03 $mL \cdot min^{-1} \cdot cm^{-2}$. In an attempt to verify the proposed transport mechanism of the dual-phase membrane, steady-state $CO_2$ permeation was necessary to test the effect of varying experimental conditions. Recent work by Rui et al. proposes a model for $CO_2$ permeation through ceramic-carbonate membranes at high temperature based on conductive ceramic and carbonate phases of the dual-phase membrane [Rui et al., 2009]. Carbon dioxide permeation flux through a bulk dual-phase membrane is described by:

$$J_{CO_2} = \frac{\alpha RT}{4F^2 L} ln\left(\frac{P"_{CO_2}}{P'_{CO_2}}\right) \tag{3.1}$$

where α is a permeance coefficient (or referred to as total conductance [Ortiz-Landeros et al., 2013] is defined by:

$$\alpha = \frac{\left(\frac{\varepsilon}{\tau}\right)_p \sigma_c \left(\frac{\varepsilon}{\tau}\right)_s \sigma_i}{\left(\frac{\varepsilon}{\tau}\right)_p \sigma_c + \left(\frac{\varepsilon}{\tau}\right)_s \sigma_i} \tag{3.2}$$

In Equation 3.1, R is the ideal gas constant, T is the system temperature, F is Faraday's constant, L is the membrane thickness, and P' and P" are the $CO_2$ partial pressures of the feed and sweep gas, respectively. In Equation 3.2, p and s are subscripts used to identify the volume fraction to tortuosity ratio of the support pores and solid phases, respectively,

while $\sigma_c$ and $\sigma_i$ represent the carbonate conductivity of the carbonate phase and oxygen ionic conductivity of the ceramic phases, respectively. For $CO_2$ permeation without oxygen through LSCF-carbonate membrane, since $\sigma_i << \sigma_c$, Equation 3.2 shows that the flux is controlled by oxygen ion conductivity of the LSCF phase.

The effect of system temperature and $CO_2$ partial pressure was measured after the $CO_2$ permeation reached a steady state. Figure 3.3 shows the effect of temperature on a 1.0 mm thick membrane exposed to a 50:50 $CO_2$ and $N_2$ feed mixture with a He sweep with feed and sweep flow rates of 100 $mL \cdot min^{-1}$ each in the temperature range of 700-900ºC. A maximum permeation flux of 0.02 and 0.051 $mL \cdot cm^{-2} \cdot min^{-1}$ was measured at 700 and 900ºC, respectively. As shown by the Arrhenius plot, $CO_2$ permeation exhibits an exponential dependence to increasing temperature. Both the oxygen ionic conductivity of the ceramic phase and the carbonate ionic conductivity of the molten carbonate phase increase exponentially with increasing temperature. Therefore, the permeance coefficient $\alpha$ defined in Equation 3.2 increases exponentially with increasing temperature, resulting in the carbon dioxide permeance to increase exponentially with increasing temperature, as shown in Equation 3.1. The apparent activation energy is calculated to be 144 $kJ \cdot mol^{-1}$. Early work on LSCF-carbonate membranes have measured an apparent activation energy ranging from 86-90 $kJ \cdot mol^{-1}$ under similar testing conditions [Anderson and Lin, 2010]. However, these membranes were tested immediately after exposure to experimental conditions and prior to degradation of the membrane surface. This large increase in the apparent activation energy suggests that as the membrane surface degrades, the energy required for the surface exchange reaction between $CO_2$ and lattice oxygen increases.

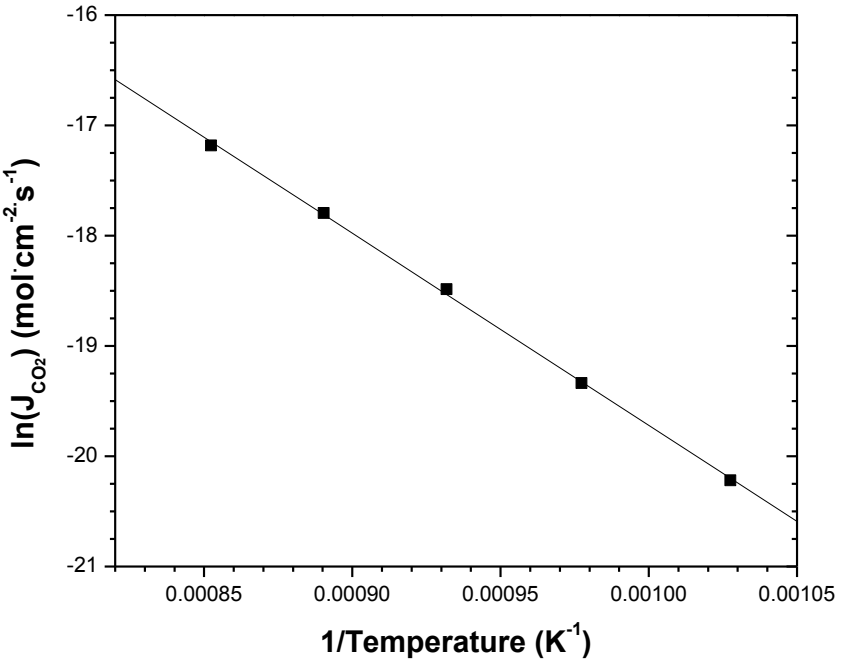


*Figure 3.3 Effect of temperature on $CO_2$ permeation flux of LSCF-carbonate membrane (membrane #1) of 1.0 mm thickness (feed and sweep flow rate = 100 $mL \cdot min^{-1}$, feed $CO_2$ = 0.5 atm, T = 700-900°C, in 70-80 hr after exposure to permeation gas as shown in Figure 2)*

Figure 3.4 shows the effect of varying the $CO_2$ partial pressure across the membrane on the $CO_2$ permeation flux of the LSCF-carbonate membrane. The $CO_2$ partial pressure gradient was varied by changing the feed $CO_2$ partial pressure from 0.25 to 0.90 atm. The effect of increasing the $CO_2$ partial pressure across the membrane results in a larger driving force, and therefore, an increase in $CO_2$ permeation flux as predicted by Equation 3.1. This verifies the prediction that $CO_2$ permeation is proportional to the logarithmic $CO_2$ partial pressure gradient across the membrane.

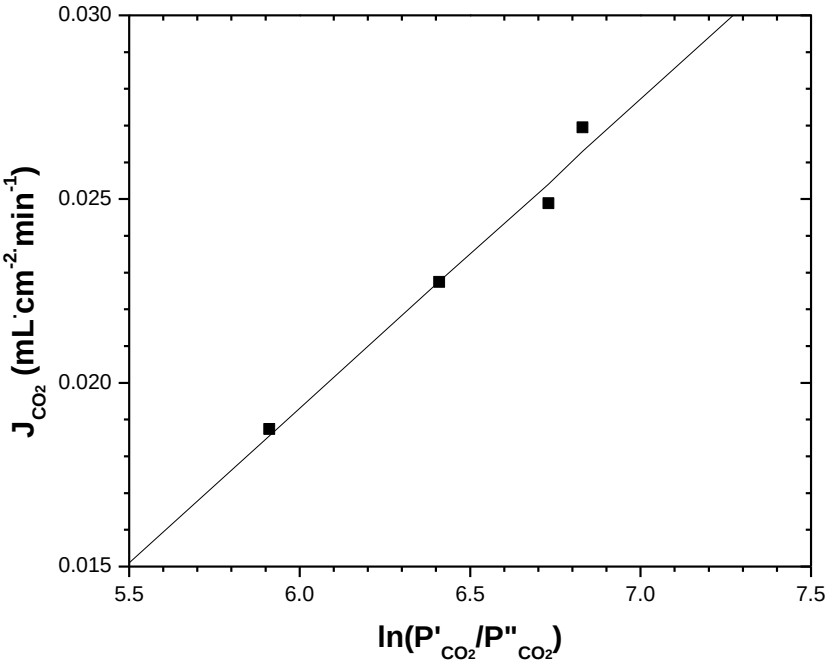


*Figure 3.4 Effect of $CO_2$ partial pressure gradient on $CO_2$ permeation flux of LSCF-carbonate membrane (thickness = 1.0 mm, feed and sweep flow rate = 100 mL·min$^{-1}$, feed $CO_2$ = 0.25-0.9 atm, T = 900$^o$C)*

Figure 3.5 shows the XRD patterns of the membrane exposed to experimental conditions for 110 hours at 900$^o$C. On the feed side of the membrane it is difficult to discern any phase other than $SrCO_3$. On the sweep side, we see the perovskite peaks corresponding to LSCF as well as the formation of CoO. In LSCF, Sr, which occupies the A-site of the perovskite structure with La, is prone to reacting with $CO_2$ to form $SrCO_3$ at elevated temperatures. Subsequently, the loss of A-site Sr from the perovskite can then lead to further decomposition of the ceramic structure, resulting in the formation of additional secondary phases such as CoO. In the presence of $O_2$, however, $SrCO_3$ decomposes into oxides at temperatures above 800$^o$C [Liu et al., 2002]. Therefore, a solid-state reaction can lead to the recovery of the perovskite structure, as has been

previously shown for dense LSCF for oxygen separation [Tan et al., 2012). To address the problem of LSCF-carbonate membrane stability, the introduction of oxygen to the feed side of the membrane is proposed. This will, however, result in changing the transport mechanism, as only electrons will be required from the ceramic support to form carbonate ions.

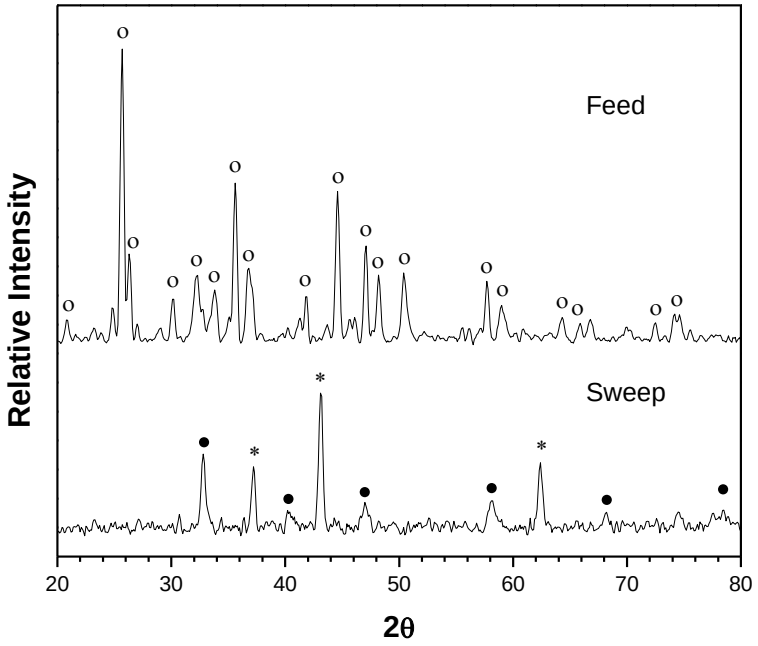


*Figure 3.5 XRD patterns of LSCF-carbonate samples exposed to a feed mixture of $CO_2$ and $N_2$ at temperatures ranging from 850-950$^oC$ for 110 hours (peak identification: • = LSCF, * = CoO, $^o$ = $SrCO_3$)*

*3.3.2 High temperature $CO_2$ permeation measurements with $O_2$*

In the presence of $CO_2$ and $O_2$ on the membrane surface, as opposed to relying on the ionic conductivity of the ceramic support, the electronic conductivity is used to facilitate the following reaction:

$$CO_2 + \frac{1}{2}O_2 + 2e^- \leftrightarrow CO_3^= \quad (3.A)$$

In this case, $CO_2$ and $O_2$ ionize and combine with electrons to form $CO_3^=$ at the membrane surface. $O_2$ and $CO_2$ partial pressure gradients across the membrane each provide driving forces for the transport of carbonate ions through the molten carbonate phase of the membrane. On the permeate membrane surface, the reverse reaction takes place, releasing $CO_2$ and $O_2$. If the electronic conductivity of the ceramic phase is much greater than its ionic conductivity of the ceramic phase and carbonate ionic conductivity of carbonate phase, $CO_2$ permeation flux with oxygen through the ceramic-carbonate phase will be controlled by carbonate ionic conductivity in the carbonate phase.

Figure 3.6 shows the long-term stability of LSCF-carbonate membranes exposed to a $CO_2$ and $O_2$ partial pressure gradient. The membrane exhibits remarkable stability in the temperature range of 850-950$^o$C when compared to the membrane exposed only to $CO_2$ and $N_2$ as shown in Figure 3.2. The $CO_2$ permeation stability in the presence of a $CO_2$ and $O_2$ feed is stable due to the structural stability of LSCF in the presence of oxygen. As previously discussed, when adding $O_2$ to the feed side of the membrane, it reacts with $CO_2$ at the ceramic-carbonate interface, to form carbonate ions, which diffuse through the membrane as shown in Reaction 1. In addition, however, $O_2$ also ionizes at the ceramic surface, and diffuses through the ceramic phase of the membrane due to the driving force provided by the oxygen partial pressure gradient across the membrane. This helps maintain the chemical stability of the ceramic phase of the membrane. The dual-phase membrane maintains a high mechanical structure and remained continuous for approximately 600 hours at temperatures between 850-950$^o$C.

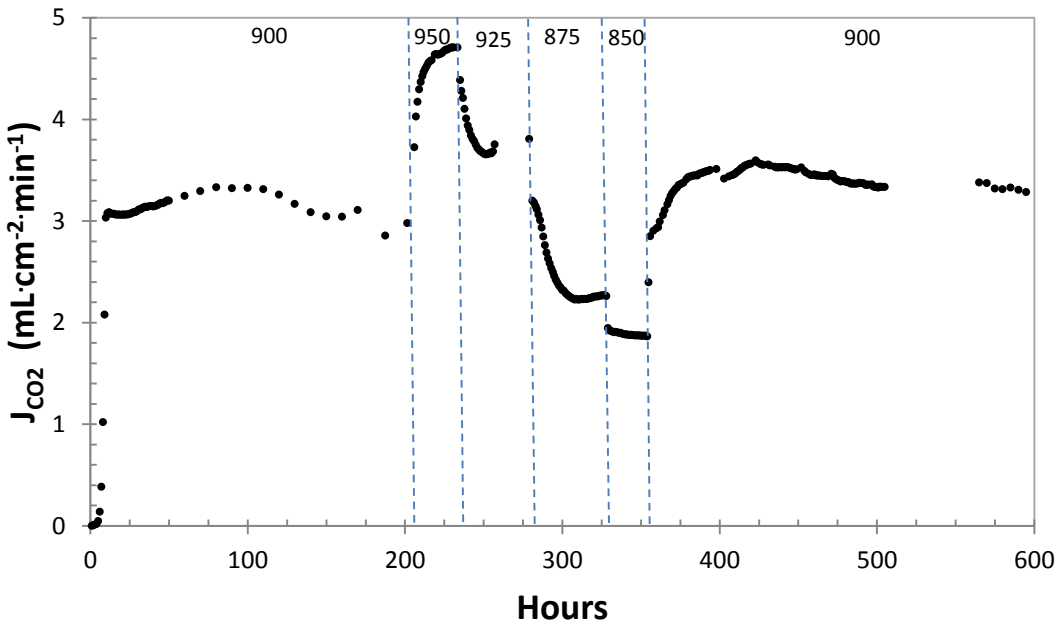


*Figure 3.6 Time dependence of $CO_2$ permeation flux of LSCF-carbonate membranes (thickness = 1.0 mm, feed and sweep flow rate = 100 mL·min$^{-1}$, feed $CO_2$ = 0.5 atm, feed $O_2$ = 0.25 atm, T = 850-950$^o$C)*

The $CO_2$ permeation flux ranges from approximately 2.0 mL·cm$^{-2}$·min$^{-1}$ to 4.8 mL·cm$^{-2}$·min$^{-1}$ at 850 and 950$^o$C, respectively. In the sweep effluent $O_2$ was also measured, from which the oxygen permeation flux was calculated to be about 50% of the $CO_2$ flux measured. This confirms that $CO_2$ permeation mechanism through ceramic-carbonate membrane with the ceramic phase having higher electronic conductivity. Compared to Figure 3.3, Figure 3.6 shows that the $CO_2$ permeation flux with oxygen in the feed is larger than initial CO2 permeation flux without oxygen by one order of magnitude at 900$^o$C. Prior to the introduction of oxygen, the rate limiting step of carbonate ion transport was the oxygen ionic conductivity of the ceramic phase. After the introduction of oxygen to the system, carbonate formation on the membrane surface no longer relies on the oxygen ion transport through the ceramic phase. Rather, electrons

from the ceramic phase are now required to facilitate the reaction between $CO_2$ and $O_2$ at the membrane surface. Since the electronic conductivity of the LSCF ceramic phase (~1000 S/cm at 900$^oC$) is much greater than the oxygen ionic conductivity of LSCF phase (~0.1 S/cm) or carbonate ionic conductivity of the carbonate phase (~ 3.5 S/cm), the carbonate ion diffusion rate through the membrane becomes limited by the ionic conductivity of the molten carbonate phase [Rui et al., 2009]. Thus, $CO_2$ permeance with oxygen through LSCF-carbonate is controlled by carbonate ionic conductivity in the carbonate phase, which is about 10-20 times that of oxygen ionic conductivity in the LSCF phase. Oxygen ionic conductivity controls $CO_2$ permeation flux in the LSCF-carbonate membrane when oxygen is not present.

Figure 3.7 shows the effect of temperature on $CO_2$ permeation flux of the membrane under the same range of temperatures. The $CO_2$ permeation again exhibits an exponential dependence to increasing temperature. The apparent activation energy is calculated to be 108 $kJ \cdot mol^{-1}$. The change in transport mechanism previously described results in the decrease in apparent activation energy relative to what was measured for the membrane that was not exposed to $O_2$, as shown in Figure 3.3.

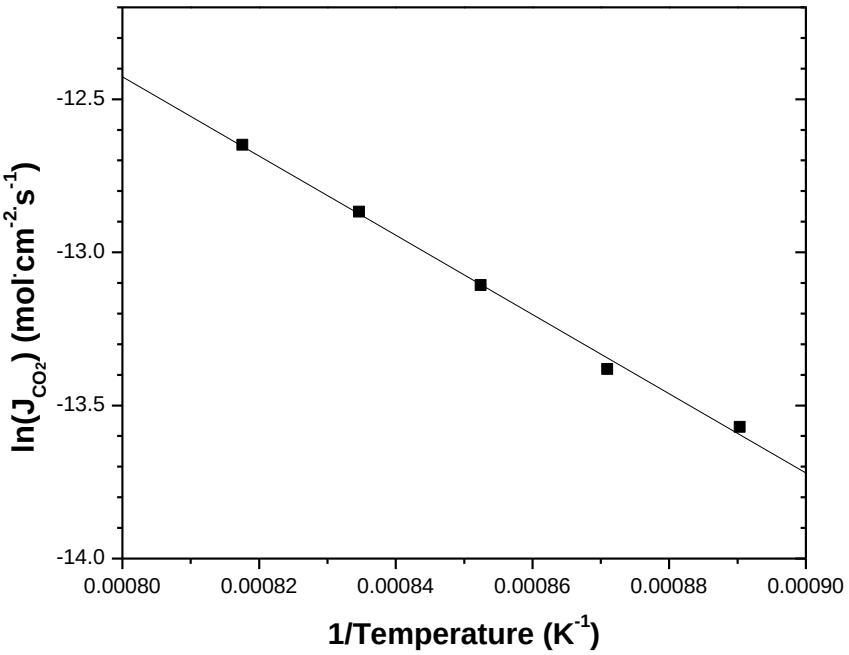


*Figure 3.7 Effect of temperature on $CO_2$ permeation flux of LSCF-carbonate membranes of 1.0 mm thickness (feed and sweep flow rate = 100 mL·min$^{-1}$, feed $CO_2$ = 0.5 atm, feed $O_2$ = 0.25 atm, T = 850-950$^oC$)*

Figure 8 shows the XRD pattern of the feed and sweep side of the membrane exposed to a $CO_2$ and $O_2$ gradient for one month. Both sides of the membrane still show the presence of a fully developed perovskite structure. In addition, the presence of CoO is found on both sides of the membrane. SEM images of the feed and sweep side of the membrane are shown in Figure 3.9. The feed-side surface of the membrane still shows a dense dual-phase network while the sweep side of the membrane shows a porous structure. The SEM image of the cross section of the membrane in Figure 3.10 apparently shows a more porous region in the sweep side and a denser region on the feed side. In

contrast, the XRD patterns in Figure 3.8 show presence of carbonate phases on both surfaces.

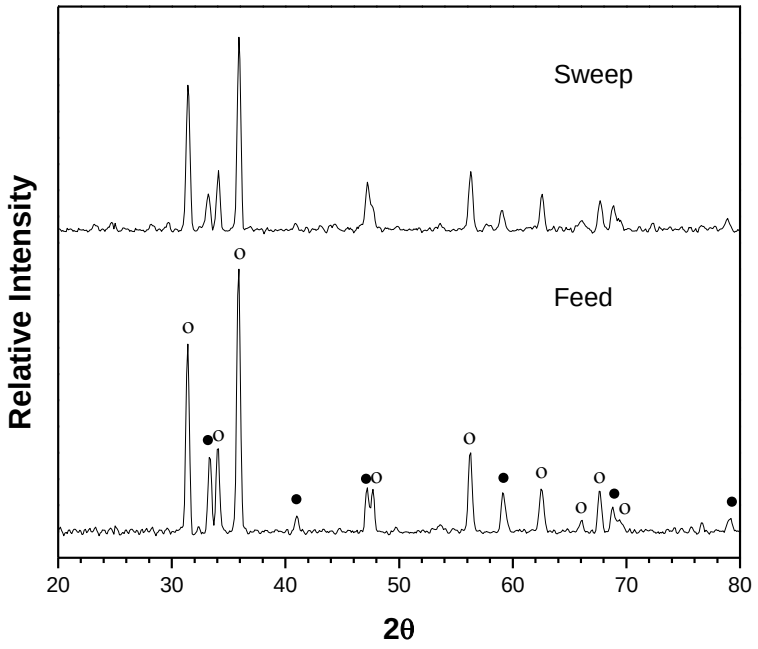


*Figure 3.8 XRD patterns of LSCF-carbonate samples exposed to a feed mixture of $CO_2$ and $O_2$ at temperatures ranging from 850-950°C for 600 hours (peak identification: • = LSCF, o = CoO)*

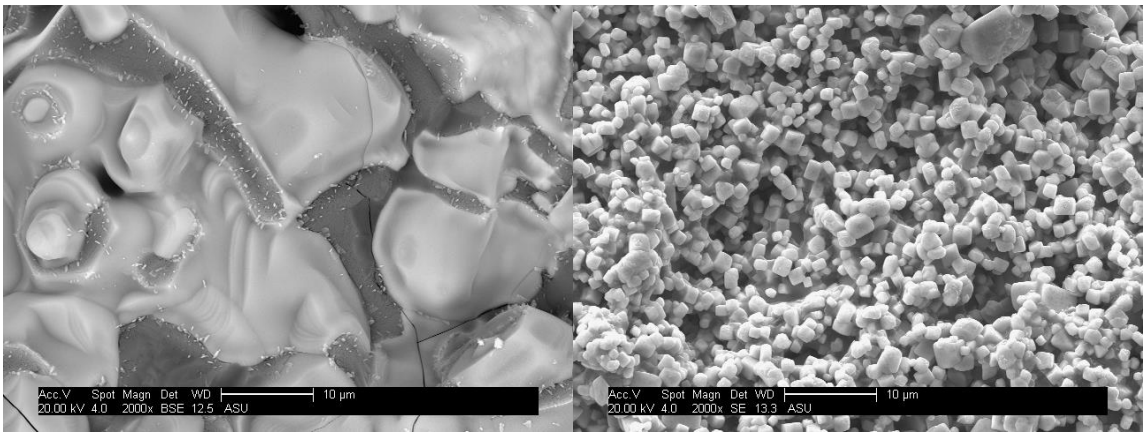


*Figure 3.9 SEM analysis of the (a) feed and (b) sweep side of the LSCF-carbonate membrane after one month exposure to $CO_2$ and $O_2$ partial pressure gradients at high temperature*

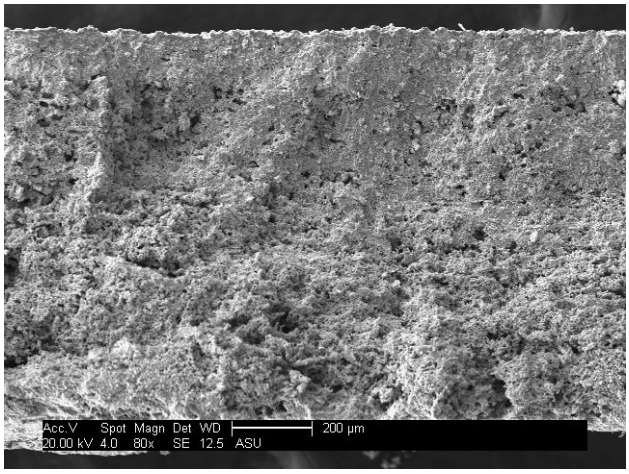


*Figure 3.10 Cross section of the LSCF-carbonate membrane after one month exposure to $CO_2$ and $O_2$ partial pressure gradients at high temperature*

As shown in Figure 3.6, when changing the permeation system temperature, it takes the system approximately 24 hours to reach steady state. It is possible that the carbonate in the sweep side decomposes when the $CO_2$ pressure is lower than the equilibrium carbonate decomposition $CO_2$ partial pressure for the molten carbonate. Since the equilibrium decomposition $CO_2$ decreases with increasing temperature, higher

temperatures favor decomposition. Thus, the effective thickness of the dense dual-phase membrane may be smaller than the initial thickness of the membrane, and may change with permeation temperature, or the molten carbonate thickness changes in the LSCF-carbonate membrane at high temperature. As temperature increases, molten carbonate decomposes into metal oxides and $CO_2$ is released due to the higher decomposition partial pressure of molten carbonate at increased temperatures. This decreases the total membrane thickness, resulting in a continually increasing permeation flux before reaching steady state. When the temperature decreases, the reverse takes place and the effective membrane thickness decreases. This is observed by a continually decreasing $CO_2$ permeation flux for approximately 24 hours after decreasing the system temperature. This result also complicates the measurement of the apparent activation energy due to the fact that the membrane thickness changes as a function of system temperature. While the molten carbonate phase thickness changes at different temperatures, the membrane achieves continuous operation for at least 600 hours.

### 3.4 Discussion of $CO_2$ Permeation Stability

In the case of $CO_2$ permeation without the presence of oxygen, the data presented in Figure 3.6 show $CO_2$ permeation instability that has not been reported for previous LSCF-carbonate permeation studies [Anderson & Lin, 2010, Anderson & Lin, 2013, Ortiz-Landeros et al., 2013]. As previously mentioned, these studies used a different sealing procedure in a custom-built permeation setup, which allowed for permeation measurements to be concluded within 10 hours of exposure to experimental conditions at high temperature. In the case of the sealing procedure used in this study, permeation measurements did not start until 10 hours or more of exposure to experimental

conditions. In an effort to confirm the results presented here, membrane stability was examined in the custom-made permeation setup using a ceramic-glass seal at 850 and 900°C. In the first 10 hours of exposure, approximately a 20% drop in the permeation flux is measured under constant experimental conditions. After 50 hours of exposure, a nearly 80% drop from the initial permeation flux is measured, confirming the trend observed in Figure 3.6.

The stability of the ceramic-carbonate membranes to a large extent depends on the stability of the oxide ceramic phase in $CO_2$ atmosphere. The present study shows that presence of oxygen in the feed gas would enhance the stability of LSCF. The carbonate phase in the downstream side might be decomposed, depending on the permeation temperature and carbon dioxide partial pressure in the downstream side. However, $CO_2$ permeating from the feed side can ensure a stable carbonate phase in the most part of the membrane, as found in this study. To obtain stable ceramic-carbonate membranes, it is important to use an oxygen ionic or mixed-conducting ceramic oxide with high oxygen ionic conductivity, which is stable in carbon dioxide atmosphere at high temperatures. This finding has led our efforts to identify $CO_2$ ionic or mixed conducting perovskite and fluorite structured ceramics for the ceramic-carbonate dual-phase membranes. These results will be reported in near future.

## 3.5 Conclusions

$CO_2$ permeation properties of $La_{0.6}Sr_{0.4}Co_{0.8}Fe_{0.2}O_{3-\delta}$ (LSCF)-carbonate membranes in a $CO_2$/He gradient were measured with and without the presence of $O_2$ to examine the long-term permeation stability of the dual-phase membrane. Upon exposure to a $CO_2$/He gradient, the $CO_2$ permeation flux decreased considerably for temperatures

ranging from 800-900°C before reaching steady state after approximately 65 hours. This is caused by reaction of the ceramic phase with $CO_2$ on the membrane surface, resulting in the formation of a carbonate layer which inhibits the surface exchange reaction between $CO_2$ and lattice oxygen. The addition of $O_2$ on the feed side of the membrane with $CO_2$ improves the membrane stability as the presence of oxygen inhibits carbonate reaction with the LSCF, ensuring its perovskite structure with desired ionic conductivity. With the presence of oxygen the change in transport mechanism results in an increase of $CO_2$ permeation flux by almost two orders of magnitude to 3.0 $mL \cdot cm^{-2} \cdot min^{-1}$ at 900°C when compared to the initial $CO_2$/He gradient. Long term operation with oxygen in the feed gas could result in development of a stable porous structure in the membrane near the sweep gas side. LSCF-carbonate membranes exposed to a $CO_2$ and $O_2$ gradient result in high, stable $CO_2$ permeation at temperatures between 850-950°C for continuous operation. The results suggest that identifying oxygen ionic or mixed-conducting ceramic material stable in $CO_2$ is critical to preparation of the dual-phase membranes for stable operation in $CO_2$ permeation. In Chapter 4, the stability of the ceramic phase of the dual-phase membrane is addressed, as a $CO_2$-tolerant perovskite-type material is synthesized into a new dual-phase membrane. The $CO_2$ permeation properties and chemical stability of the membrane are examined under a wide range of experimental conditions.

# CHAPTER 4

# CERAMIC-CARBONATE DUAL-PHASE MEMBRANE WITH IMPROVED CHEMICAL STABILITY FOR CARBON DIOXIDE SEPARATION AT HIGH TEMPERATURE

## 4.1 Introduction

In Chapter 3, the stability of $CO_2$ permeation flux through $La_{0.6}Sr_{0.4}Co_{0.8}Fe_{0.2}O_{3-\delta}$ (LSCF)-carbonate membranes was measured in $CO_2$ rich environments with and without $O_2$. Without the presence of $O_2$, $CO_2$ permeation rapidly decreased due to a reaction between LSCF and $CO_2$, resulting in the formation of $SrCO_3$ and CoO, which prevented oxygen ions from reaching the LSCF surface to react with $CO_2$ to form carbonate ions that can transport through the membrane. In the presence of $O_2$, however, $CO_2$ permeation remained stable for more than one month of exposure. In Chapter 4, the use of a new perovskite-phase in the dual-phase membrane to address stability concerns is described.

In order to improve the stability of the ceramic-carbonate dual-phase membrane, the material serving as the ceramic support should be optimized. This material should satisfy a number of conditions. The material must be an oxygen ion conductor, as oxygen is required for the formation of carbonate ions. The material must have long-term chemical stability at high temperatures in the presence of carbon dioxide and reducing gases such as hydrogen, as well as having compatibility with the carbonate phase. The material must also exhibit high mechanical strength and an appropriate pore size in an effort to control the amount of the molten carbonate phase.

Previous work has shown that ceramic membranes containing alkaline-earth elements are unstable in $CO_2$ environments, as they often react with $CO_2$ to form metal carbonates [Yi et al., 2005; Yang et al., 2006; Yan et al., 2007; Arnold et al., 2007]. In particular, Sr- and Co-containing materials have been studied as they have been shown to be reactive in the presence of carbon species and reducing environments. This was confirmed by earlier work with LSCF-carbonate dual-phase membranes described in Chapter 3, as a $SrCO_3$ layer was found on membranes exposed to high $CO_2$ concentrations without the presence of $O_2$. In addition, A-site deficient ceramic materials are reported to be resistant to $CO_2$ exposure at high temperature [Carolan et al., 1996, Dong et al., 2009].

The alkaline-earth metal-free and A-site-deficient perovskite-type ceramic material of composition $La_{0.85}Ce_{0.1}Ga_{0.3}Fe_{0.65}Al_{0.05}O_{3-\delta}$ (LCGFA) was chosen as the ceramic support for a new ceramic-carbonate membrane. Previous work has shown this ceramic material to be a $CO_2$-tolerant dense membrane for $O_2$ separation at high temperature [Dong et al., 2009]. A ternary carbonate mixture composed of lithium, sodium, and potassium carbonates was chosen as the molten carbonate phase. The objective of this work is to synthesize a new dual-phase membrane and examine the thermal and chemical stability as well as investigate the long-term $CO_2$ permeation stability and performance under various experimental conditions at high temperature.

## 4.2 Experimental Methods

### *4.2.1 Preparation of porous and dense $La_{0.85}Ce_{0.1}Ga_{0.3}Fe_{0.65}Al_{0.05}O_{3-\delta}$ supports*

$La_{0.85}Ce_{0.1}Ga_{0.3}Fe_{0.65}Al_{0.05}O_{3-\delta}$ (LCGFA) powder was prepared based on the method previously described by Dong et al. [Dong et al., 2009]. LCGFA powder was

synthesized by the solid-state method. Stoichiometric amounts of $La_2O_3$ (99.99%, Sigma-Aldrich), $CeO_2$ (99.9%, Sigma-Aldrich), $Ga_2O_3$ (99.99%, Sigma Aldrich), $Fe_2O_3$ (99.945%, Alfa Aesar), and $Al_2O_3$ (99.999%, Sigma-Aldrich) were mixed and ball-milled in ethanol for 24 hours. The resulting slurry was heated at 100$^oC$ until dried and the resulting powder was then ground with a mortar and pestle to reduce the particle size. The powder was then calcined at 950$^oC$ for 10 hours with heating and cooling ramp rates of 2$^oC \cdot min^{-1}$. The calcined LCGFA powder was again ground in a mortar and pestle and 4.4 grams were weighed and pressed in a 25 mm drive at 115 MPa for 5 minutes using a hydraulic press (Carver, Model #3853). The green disks were then sintered at temperatures ranging from 950-1200$^oC$ for 24 hours with heating and cooling ramping rates of 2$^oC \cdot min^{-1}$ resulting in porous LCGFA disk supports.

*4.2.2 Synthesis of $La_{0.85}Ce_{0.1}Ga_{0.3}Fe_{0.65}Al_{0.05}O_{3-\delta}$ -carbonate dual phase membrane*

Synthesis of LCGFA-carbonate dual-phase membranes was achieved by direct infiltration of molten carbonate into the pores of sintered LCGFA support via the direct infiltration technique previously described by Chung et al. [Chung et al, 2005]. The carbonate powders $Li_2CO_3$ (99.2%, Fischer Scientific), $Na_2CO_3$ (99.9%, Fischer Scientific), and $K_2CO_3$ (99.8%, Fischer Scientific) were weighed out in a 42.5/32.5/25 mol% ratio, respectively, and heated to 550$^oC$ in a furnace. Porous ceramic supports were preheated above the molten carbonate mixture to prevent thermal shock prior to being lowered into contact with the carbonate. Supports were left in contact with molten carbonate for 5-10 minutes to ensure complete infiltration via capillary force. The membrane was then lifted and slowly removed from the furnace and cooled. Residual carbonate on the membrane surface was removed using SiC polishing paper.

*4.2.3 Characterization of ceramic supports and ceramic-carbonate dual-phase membranes*

The porosity of the membranes was measured by the Archimedean method described by Harry & Johnson [Harry & Johnson, 2004]. In this method, membrane samples were weighed at three stages: dry, immersed in liquid nitrogen (measured once the weight reached steady state), and saturated in liquid nitrogen (measured once immediately lifted from liquid $N_2$). Using these three weights, the porosity of the sample can be estimated using the Archimedean principle by using the following equation:

$$P = \frac{S - D}{S - I} \tag{4.1}$$

where P is the porosity fraction, S is the saturated sample weight, D is the dry sample weight, and I is the immersed sample weight. Three samples corresponding to each sintering temperature were each measured four times to establish a mean porosity. Room temperature helium permeation was used to determine the average pore size of porous supports as well as verifying the gas tightness of dense ceramic and ceramic-carbonate dual-phase membranes. The phase structure of the LCGFA powder and membranes were characterized using X-ray diffraction (XRD) (Bruker, $CuK_{\alpha 1}$) evaluated in the 2θ range of 20-80$^o$. Scanning electron microscopy (SEM) imaging was performed to confirm the porous nature of ceramic supports as well as the dense nature of ceramic-carbonate samples.

*4.2.4 Chemical stability testing of ceramic-carbonate membranes at high temperature*

Dual-phase LCGFA-carbonate membrane disks were exposed to simulated experimental conditions to determine the chemical and thermal stability under a wide

variety of experimental conditions at different temperatures. Prepared membrane samples were exposed to four different gas environments, each at three different temperatures. Samples were placed in a tube furnace with a heating and cooling ramping rate of $5^{o}C \cdot min^{-1}$ with a gas flow rate of 25 $mL \cdot min^{-1}$ at 600, 750, and 900°C and held for 24 hours. Samples were exposed to pure $CO_2$, pure $N_2$, the $CO_2$ equilibrium partial pressure, and simulated syngas composed of 50% $CH_4$, 20% CO, 20% $H_2$, and 10% $CO_2$. The $CO_2$ equilibrium partial pressure is based on the decomposition partial pressure of the chosen carbonate mixture, and is 0.1, 1.5, and 9.3% at 600, 750, and 900°C, respectively [Janz et al., 1979]. The composition of each test is summarized in Table 4.1. Analysis of the effect of simulated experimental conditions on the phase structure of the dual-phase membrane samples was done by XRD.

*Table 4.1 Gas composition of stability testing experiments*

| Gases | $CO_2$ (600-900°C) | $N_2$ (600-900°C) | $CO_2$ Equilibrium Partial Pressure (600°C) | (750°C) | (900°C) | Syngas (600-900°C) |
|---|---|---|---|---|---|---|
| $CO_2$ | 100% | - | 0.1% | 1.5% | 9.3% | 10% |
| $N_2$ | - | 100% | 99.9% | 98.5% | 90.7% | - |
| $CH_4$ | - | - | - | - | - | 50% |
| CO | - | - | - | - | - | 20% |
| $H_2$ | - | - | - | - | - | 20% |

*4.2.5 Carbon dioxide permeation measurements*

A Probostat high temperature permeation system (Probostat, Norwegian Electro Ceramics AS) was used for carbon dioxide permeation experiments [Norton et al., 2013]. For each experiment an alumina spacer attached to a spring force assembly, a dense LCGFA-carbonate disk membrane, and a silver seal were placed on top of a 20 mm

alumina tube, which was then enclosed by a 40 mm diameter alumina tube. Argon was introduced inside the 20 mm alumina tube serving as the sweep gas at the bottom of the membrane while carbon dioxide and nitrogen was introduced to the space between the two alumina tubes serving as the feed gas to the top of the membrane. The assembled apparatus was then placed in a vertical tube furnace and was heated to approximately 950$^{o}$C to reach the softening temperature of silver at a ramping rate of 1$^{o}$C·min$^{-1}$. Once the softening point of silver was reached, the spring assembly attached to the alumina spacer above the disk membrane forced the membrane into the silver ring forming a seal between the membrane and the 20 mm alumina tube. The quality of the seal was determined by measuring the nitrogen content in the argon sweep gas using an Agilent Technologies 7890A gas chromatograph (GC) with TCD detector and Alltech Hayesep DB 100/120 column (30 ft × 1/8 in. × 0.85 in. SS). After reaching minimization of helium leakage the system was cooled to either 700$^{o}$C or 900$^{o}$C at a rate of 1$^{o}$C·min$^{-1}$.

For carbon dioxide permeation experiments, the feed gas consisted of a variable carbon dioxide flow mixed with a balance of helium to reach 100 mL·min$^{-1}$ for a $CO_2$ partial pressure varying between 0.1-0.9 atm. The temperature was varied between 700-900$^{o}$C. Gas flow rates were regulated using mass flow controllers (MKS, Model 1179) and a four-channel readout (MKS, Type 247). Samples were taken three hours after a change in gas composition and one hour after a temperature change to allow the system to reach steady state. Table 4.2 shows the system parameters for tests with varying temperature, $CO_2$ partial pressure, and stability measurements. A mass balance on the measured sweep side gases was used to calculate the $CO_2$ permeation flux through each membrane. The $CO_2$ error in the permeate gas caused by seal leaks were corrected by

measuring the presence of He and subtracting the corresponding $CO_2$ from the calculated permeation flux. The error in determining the $CO_2$ permeation flux using this procedure is approximately $\pm$ 10%.

*Table 4.2 System parameters for carbon dioxide permeation flux experiments*

| Variable Parameter | System Temp ($^oC$) | Feed $CO_2$ Partial Pressure (atm) | Sweep Flow ($mL \cdot min^{-1}$) |
|---|---|---|---|
| Temperature | 500-900 | 0.5 | 100 |
| $CO_2$ Partial Pressure | 900 | 0.1-0.9 | 100 |
| Stability | 900 | 0.5 | 100 |

## 4.3 Results and Discussion

### *4.3.1 Membrane Synthesis*

In an effort to create a porous ceramic support for the dual-phase membrane, LCGFA samples were prepared and sintered in 50 degree intervals from 950-1200$^o$C. A minimum sintering temperature of 950$^o$C was chosen as this is the minimum temperature required when sealing membranes at high temperature as previously described. Figure 4.1 shows XRD patterns of the LCGFA powder after calcination along with membrane supports prepared at each sintering temperature. The XRD pattern of the powder and membrane supports prepared by the solid-state method confirms the presence of a fully developed perovskite phase, with a very small presence of $CeO_2$ phase. This indicates that the calcination temperature of 950$^o$C is sufficient to achieve the desired perovskite structure. The presence of $CeO_2$ peaks, as well as the decrease in intensity when comparing prepared membranes with powder, is consistent with previous results for this ceramic material used to make dense membranes at higher sintering temperatures [Dong et al., 2009]. The XRD results confirm that supports sintered within the temperature

range in question would be suitable for selection of the dual-phase membrane based on the desired formation of a fully developed perovskite structure.

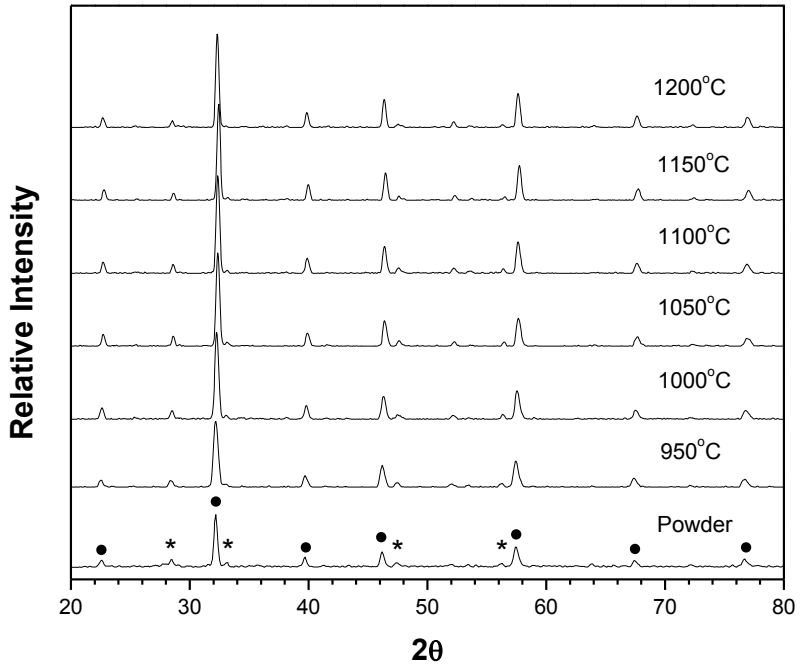


*Figure 4.1 XRD patterns of LCGFA powder and porous supports sintered in 50°C intervals from 950-1200°C (peak identification: • = perovskite, * = $CeO_2$ phase)*

Figure 4.2 shows the porosity of LCGFA membrane support samples prepared at sintering temperatures from 1000-1200°C as measured by a non-destructive liquid nitrogen Archimedean method. An increase in the sintering temperature results in a decrease in the support porosity. At 1000°C, an open porosity of 48% is measured followed by a decrease with increasing sintering temperature until reaching 22% at 1200°C. It is desirable to have a sufficiently high porosity in order to ensure connected pores through the entire thickness of the membrane support as $CO_2$ separation relies on transport through the molten carbonate phase which fills the void space of the ceramic

supports. Previous work has shown that a porosity of 40-50% resulted in maximum $CO_2$ permeation performance for $La_{0.6}Sr_{0.4}Co_{0.8}Fe_{0.2}O_{3-\delta}$-carbonate membranes at high temperature [Ortiz-Landeros et al, 2013]. Since the porosity significantly decreased to below 30% for supports sintered at 1150°C and higher, the choice of an appropriate support was narrowed down to those sintered from 1000-1100°C.

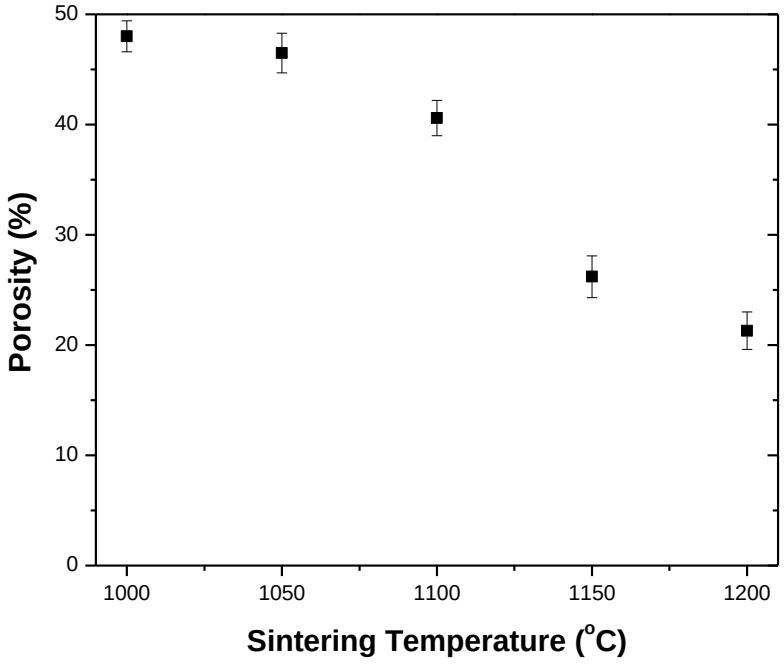


*Figure 4.2 Open porosity of LCGFA supports sintered at various sintering temperatures as measured by the Archimedean method*

In order to determine the connected porosity of the membrane supports, room temperature helium permeance testing was done for each sintering temperature. Helium permeance of supports sintered between 950-1100°C were found to be on the order of $10^{-6}$ $mol \cdot m^{-2} \cdot s^{-1} \cdot Pa^{-1}$ while supports sintered above 1100°C were at least one order of magnitude lower. Samples also exhibited an increase in support strength with increased

sintering temperature as supports sintered at 950°C were brittle and cracked easily upon handling. The open and connected porosity of supports sintered between 1000-1100°C were comparable while mechanical strength improved with increasing temperature. Therefore, based on the need for a support with highly connected porosity as well as high mechanical strength, LCGFA supports prepared at a sintering temperature of 1100°C were chosen to use for synthesis of the dual-phase membrane.

Figure 4.3 shows helium permeance versus the average pressure across the membrane for a sample sintered at 1100°C. By correlating the permeance data to the following Knudsen and viscous flow equations, the pore structure and other parameters can be estimated [Lin and Burggraaf, 1993; Kim & Lin, 1999]:

$$\frac{F}{L} = \alpha + \beta P_{avg} \tag{4.2}$$

$$\alpha = 1.06 \frac{\varepsilon}{\tau} \frac{r_p}{L\sqrt{RTM_w}} \tag{4.3}$$

$$\beta = 0.125 \frac{\varepsilon}{\tau} \frac{r_p^2}{L\mu RT} \tag{4.4}$$

where $F$ is the support permeance ($mol \cdot m^{-2} \cdot s^{-1} \cdot Pa^{-1}$) , $L$ is the support thickness (m), $P_{avg}$ is the average pressure (Pa) across the support, $\varepsilon$ and $\tau$ represent the support porosity and tortuosity, $r_p$ is the average pore radius (m), $R$ is the gas constant ($m^3 \cdot mol^{-1} \cdot Pa^{-1} \cdot K^{-1}$), $T$ is the temperature (K), and $M_w$ and $\mu$ are the molecular weight ($kg \cdot mol^{-1}$) and viscosity ($kg \cdot m^{-1} \cdot s^{-1}$) of the permeate gas helium, respectively. The average pore size and porosity to tortuosity ratio were then obtained using equations 4.2-4.4. The parameters are shown in Table 4.3. As shown, the LCGFA support sintered at 1100°C has an average pore radius of 145 nm and a porosity to tortuosity ratio of 0.134. Based on the estimated open

porosity of 40% based on the results shown in Figure 4.2, this corresponds to a tortuosity of approximately 3.0. Figure 4.4 shows (a) the surface morphology, and (b) the cross section, of the membrane support sintered at 1100$^{o}$C. The surface appears to have higher porosity than that of the bulk support. The pore size appears to vary throughout the support, but on average, the pore size is consistent with the value estimated using helium permeation data. Similar findings were reported for porous $La_{0.6}Sr_{0.4}Co_{0.2}Fe_{0.2}O_{3-\delta}$ and $Bi_{1.5}Y_{0.3}Sm_{0.2}O_3$ using similar characterization techniques [Anderson & Lin; 2010, Rui et al., 2012].

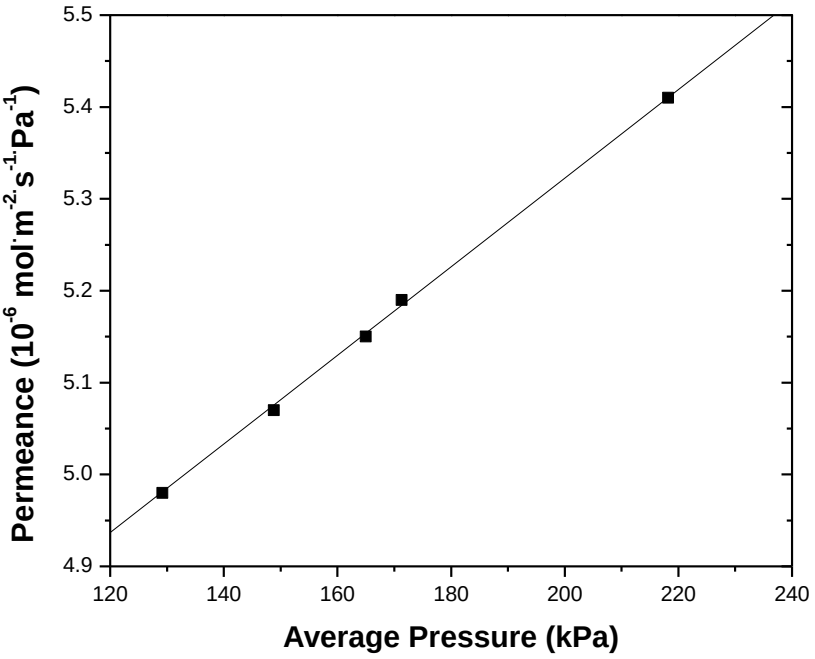


*Figure 4.3 Steady state helium permeance versus average pressure of LCGFA support used to determine the average pore radius of the support sintered at 1100$^{o}$C*

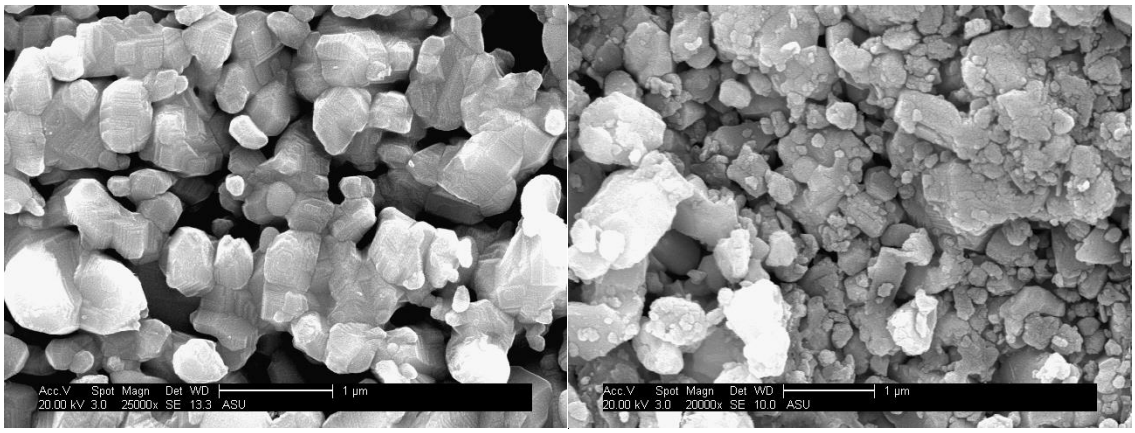


*Figure 4.4 SEM of LCGFA support (a) surface and (b) cross section sintered at 1100°C*

*Table 4.3 Helium permeation data and parameters to determine support pore properties*

| | |
|---|---|
| $A$ | $4.36 \times 10^{-6}$ |
| $B$ | $4.82 \times 10^{-12}$ |
| $L$ (m) | $1.5 \times 10^{-3}$ |
| $R$ ($m^3 \cdot mol^{-1} \cdot Pa^{-1} \cdot K^{-1}$) | 8.314 |
| $T$ (K) | 298 |
| $M_w$ ($kg \cdot mol^{-1}$) | $4.0 \times 10^{-3}$ |
| $\mu$ ($kg \cdot m^{-1} \cdot s^{-1}$) | $1.96 \times 10^{-5}$ |
| $r_p$ (m) | $1.45 \times 10^{-7}$ |
| $\varepsilon/\tau$ | 0.134 |

After preparing LCGFA supports with the desired pore structure, the supports were infiltrated with molten carbonate at 550°C. After cooling the membranes to room temperature, helium permeance testing was done again to confirm the dense nature of the membranes. Dual-phase membranes show a decrease in helium permeance by four orders of magnitude from $10^{-6}$ to $10^{-10}$ $mol \cdot m^{-2} \cdot s^{-1} \cdot Pa^{-1}$ when compared to porous supports, confirming complete infiltration of the support pores.

*4.3.2 Chemical Stability in Simulated Experimental Conditions*

Figure 4.5 shows the XRD patterns of LCGFA-carbonate membrane disk surfaces exposed to a pure $N_2$ environment as well as a pure $CO_2$ environment each at 600, 750, and 900$^oC$ for 24 hours in an effort to determine the stability of the dual-phase membrane in atmospheres with very low $O_2$ concentrations in addition to high $CO_2$ concentrations. The LCGFA-carbonate membrane samples show a perovskite structure in both the pure $N_2$ and pure $CO_2$ environments at each temperature tested. The results are consistent with those reported by Dong et al. [Dong et al., 2009], which showed dense LCGFA to be a $CO_2$ tolerant mixed conducting membrane for $O_2$ separation at high temperature. LCGFA was reported to have high $CO_2$ tolerance because it is alkaline-earth metal free and A-site deficient oxide.

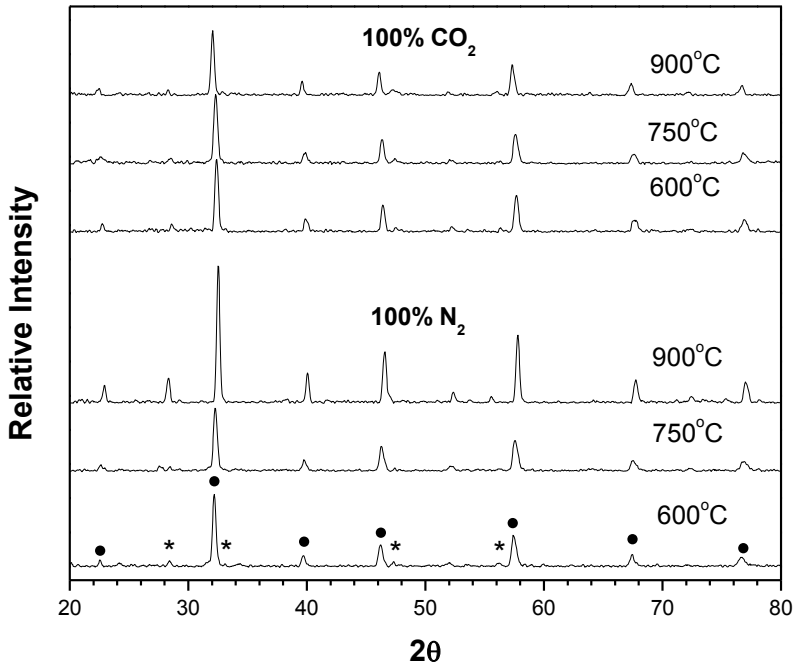


*Figure 4.5 XRD patterns of SDC-carbonate samples exposed to pure $CO_2$ and pure $N_2$ each at temperatures of 600, 750, and 900°C for 24 hours (peak identification: • = perovskite, * = $CeO_2$ phase)*

In addition to being tolerant to $CO_2$, dual-phase membranes must maintain structural stability and performance under low $CO_2$ partial pressures and reducing conditions in order to serve as an alternative for pre-combustion $CO_2$ capture. Figure 4.6 shows the XRD patterns of LCGFA-carbonate membranes exposed to the decomposition partial pressure of $CO_2$ of the molten carbonate as well as simulated syngas each at 600, 750, and 900°C for 24 hours. The LCGFA-carbonate membranes maintain their perovskite structure after 24 hours. This confirms previous work for dense LCGFA that has shown structural stability in the presence of $H_2$ [Dong et al., 2009]. Earlier stability studies conducted on $La_{0.6}Sr_{0.4}Co_{0.8}Fe_{0.2}O_{3-\delta}$ -carbonate membranes have shown the

formation of secondary phases on the membrane surface at high temperature when exposed to similar experimental conditions [Norton et al., 2013].

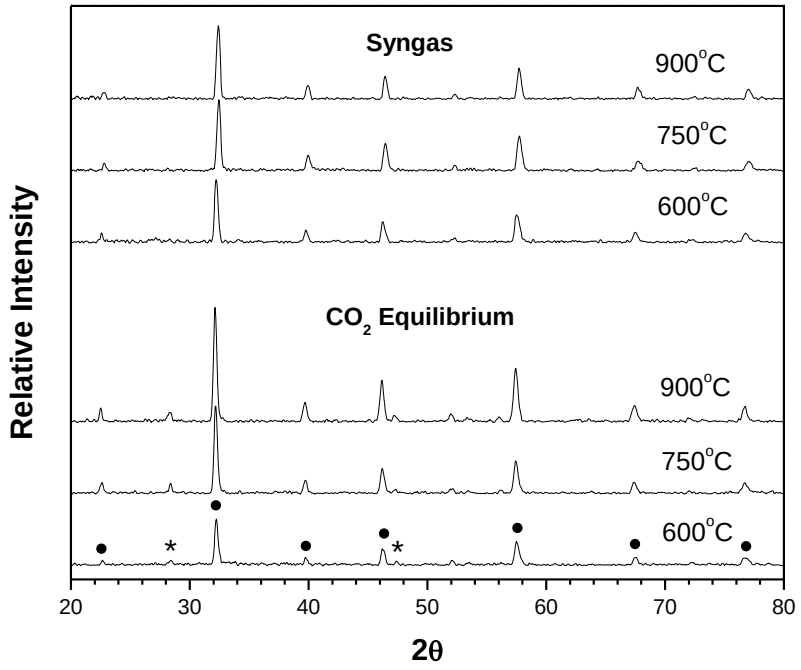


*Figure 4.6 XRD patterns of SDC-carbonate samples exposed to simulated syngas and the molten carbonate $CO_2$ equilibrium partial pressure each at temperatures of 600, 750, and 900°C for 24 hours (peak identification: • = perovskite, * = $CeO_2$ phase)*

*4.3.3 High Temperature $CO_2$ Permeation Measurements*

Carbon dioxide permeation properties of LCGFA-carbonate dual-phase membranes were first studied under changing temperature conditions. The feed $CO_2$ partial pressure was kept constant at 0.5 atm with a balance of He. Figure 4.7 shows the carbon dioxide permeation flux for two different LCGFA-carbonate membrane thicknesses measured in the temperature range of 700-900°C. A maximum permeation flux of 0.044 and 0.024 $mL \cdot cm^{-2} \cdot min^{-1}$ was measured for 0.75 and 1.5 mm thick

membranes, respectively, at 900°C. The measured downstream $CO_2$ partial pressure is given in Table 4.4. For both membrane thicknesses, carbon dioxide flux exhibits an exponential dependence to increasing temperature as verified by the linear behavior of the Arrhenius plot. The calculated apparent activation energies are found to be 96 $kJ \cdot mol^{-1}$ for both membrane thicknesses. The fact that the activation energy remains constant as membrane thickness is decreased indicates that the carbon dioxide permeation is controlled by bulk diffusion rather than the surface reaction. This is confirmed by the fact that the measured permeation flux of $CO_2$ effectively doubles for the entire temperature range tested when decreasing the membrane thickness from 1.5 to 0.75 mm.

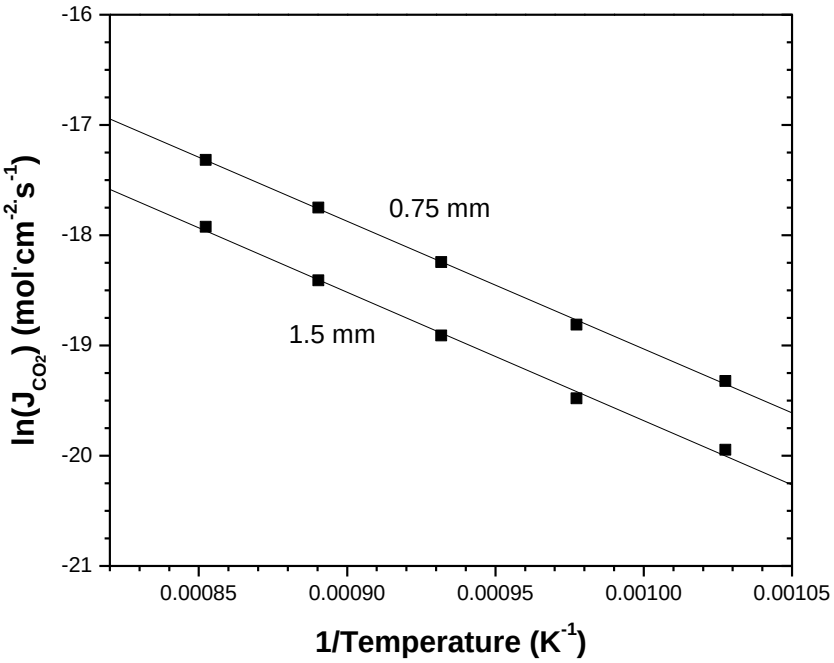


*Figure 4.7 Effect of temperature on $CO_2$ permeation flux of LCGFA-carbonate membranes of 0.75 and 1.5 mm thickness (feed and sweep flow rate = 100 $mL \cdot min^{-1}$, feed $CO_2$ = 0.5 atm, T = 700-900°C)*

*Table 4.4 Downstream $CO_2$ partial pressure for 0.75 and 1.5 mm thick membranes*

| Temperature ($^oC$) | $P''_{CO_2}$ for 0.75 mm (Pa) | $P''_{CO_2}$ for 1.5 mm (Pa) |
|---|---|---|
| 700 | 22 | 12 |
| 750 | 36 | 19 |
| 800 | 64 | 33 |
| 850 | 105 | 54 |
| 900 | 161 | 88 |

Based on the proposed transport mechanism previously described, the dense dual-phase membrane is only permeable to $CO_2$ [Anderson and Lin, 2010]. Any measured gas in the permeate stream from the feed side other than $CO_2$, therefore, results from either a membrane defect or leakage from the membrane seal. The concentration of He in the permeate stream at the highest measured leakage rate 1 x $10^{-5}$, or 10 ppm at 900$^o$C, while the lowest measured permeate $CO_2$ concentration remained at least two orders of magnitude higher.

A model for $CO_2$ permeation through ceramic-carbonate membranes at high temperature based on driving forces provided by the oxygen ion conducting phase of the ceramic support as well as the carbonate ion conducting phase of the molten carbonate has been reported [Rui et al., 2009]. Carbon dioxide permeation flux through a bulk dual-phase membrane is described by:

$$J_{CO_2} = \frac{\alpha RT}{4F^2 L} ln\left(\frac{P''_{CO_2}}{P'_{CO_2}}\right) \tag{4.5}$$

where α is a permeance coefficient (or referred to as total conductance) defined by:

$$\alpha = \frac{\left(\frac{\varepsilon}{\tau}\right)_p \sigma_c \left(\frac{\varepsilon}{\tau}\right)_s \sigma_i}{\left(\frac{\varepsilon}{\tau}\right)_p \sigma_c + \left(\frac{\varepsilon}{\tau}\right)_s \sigma_i} \tag{4.6}$$

In Equation 4.5, in addition to the previously defined variables, F is Faraday's constant, L is the membrane thickness, and P' and P" are the $CO_2$ partial pressures of the feed and sweep gas, respectively. In Equation 4.6, p and s are subscripts used to identify the porosity to tortuosity ratio of the support pores and solid phases, respectively, while $\sigma_c$ and $\sigma_i$ represent the conductivity of the carbonate and ceramic phases, respectively. Equation 4.6 shows how the relationship of the membrane microstructure and conductivities of the ceramic and carbonate phases, respectively, contribute to the permeation properties of $CO_2$ through the dual-phase membrane. The porosity to tortuosity ratio of the ceramic and carbonate phases are directly related, as molten carbonate infiltrates the entirety of the support pores. Qualitatively speaking, the carbonate conductivity is much greater than the ionic conductivity of the ceramic phase for the temperature range in question. Therefore, $CO_2$ permeation will be limited by oxygen ion transport through the ceramic phase, as the reaction of $CO_2$ with oxygen ions on the membrane surface is necessary to transport carbonate ions across the membrane thickness.

For a ceramic-carbonate membrane at a given temperature, a higher $CO_2$ partial pressure gradient across the membrane results in a larger driving force for $CO_2$ permeation and, therefore, a higher $CO_2$ permeation flux. Figure 4.8 shows the effect of $CO_2$ feed partial pressure on LCGFA-carbonate membranes at high temperature. The feed $CO_2$ partial pressure was varied from 0.25-0.9 atm, while maintaining a feed and sweep flow rate of 100 $mL \cdot min^{-1}$ at 900°C. The $CO_2$ permeation flux increases from 0.024-0.032 $mL \cdot cm^{-2} \cdot min^{-1}$. As predicted by the model, $CO_2$ permeation increases linearly with a logarithmic increase in $CO_2$ partial pressure gradient across the membrane, i.e.,

increasing the feed $CO_2$ partial pressure from low initial concentration will have more effect than increasing from high initial concentration, since this results in a greater change in the driving force across the membrane. This trend is also observed experimentally for $CO_2/N_2$ separation for $Bi_{1.5}Y_{0.3}Sm_{0.2}O_{3-\delta}$ (BYS)-carbonate membranes at 650°C and $La_{0.6}Sr_{0.4}Co_{0.8}Fe_{0.2}O_{3-\delta}$ (LSCF)-carbonate membranes at 900°C [Rui et al., 2012; Norton et al., 2013]. The $CO_2$ permeation flux through the LCGFA-carbonate dual-phase membrane is significantly lower than that of LSCF-carbonate dual-phase membranes because of the lower oxygen ionic conductivity of LCGFA (0.03 $S \cdot cm^{-1}$ at 900°C) compared to LSCF (0.1 $S \cdot cm^{-1}$ at 900°C) [Dong et al., 2009; Anderson and Lin, 2010]. Table 4.5 shows a comparison of the permeance of LCGFA compared to other dual-phase membranes reported in the literature.

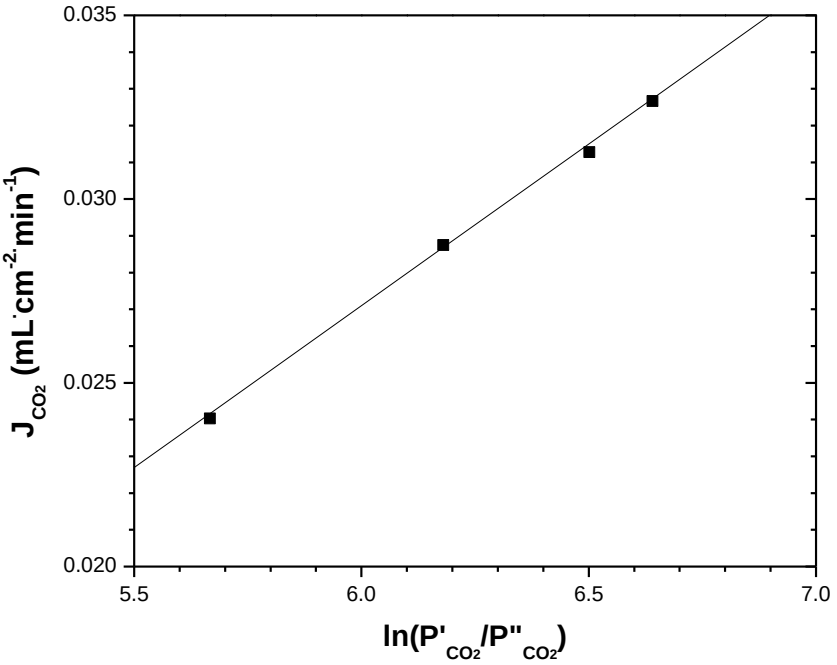


*Figure 4.8 Effect of $CO_2$ partial pressure gradient on $CO_2$ permeation flux of LCGFA-carbonate membranes (thickness = 1.5 mm, feed and sweep flow rate = 100 mL·min$^{-1}$, feed $CO_2$ = 0.25-0.9 atm, T = 900°C)*

*Table 4.5 Comparison of $CO_2$ permeance through various dual-phase disk membranes*

| Ceramic Phase | Thickness (μm) | Temp (°C) | $CO_2$ Permeance ($10^{-8}$ mol·m$^{-2}$·s$^{-1}$·Pa$^{-1}$) | Reference |
|---|---|---|---|---|
| LSCF | 375 | 900 | 4.7 | Anderson & Lin, 2010 |
| YSZ | 200-400 | 850 | 2.0 | Wade et al., 2011 |
| GDC | 200-400 | 850 | 3.0 | Wade et al., 2011 |
| BYS | ~50 | 650 | 1.1 | Rui et al., 2012 |
| SDC | 1200 | 700 | 13.5 | Zhang et al., 2012 |
| YSZ | ~10 | 650 | 7.69 | Lu et al., 2013 |
| LCGFA | 750 | 900 | 0.6 | This Work |

Figure 4.9 shows the $CO_2$ permeation flux through a LCGFA-carbonate membrane at 900°C as a function of exposure time to experimental conditions. The membrane exhibits a stable permeation flux between 0.021-0.025 $mL \cdot cm^{-2} \cdot min^{-1}$ for 275 hours of exposure at 900°C. Figure 4.10 shows XRD patterns of the LCGFA-carbonate membrane after 275 hours of exposure to experimental conditions at 900°C. The feed and sweep sides of the membrane still exhibit a fully developed perovskite structure. However, the $CeO_2$ peak appears more intense when compared to fresh membranes and membranes tested for 24 hours (Figure 4.1 and Figure 4.5). This is the result of partial decomposition of the ceramic phase at the membrane surface exposed to low $CO_2$ partial pressure for the duration of the long-term experiment. Previous membranes have been reported to develop large leaks after long periods of exposure likely resulting from carbonate decomposition or rapid decreases in permeation properties due to decomposition of the ceramic phase after continuous exposure to $CO_2$. Rui et al., however, reported increasing permeation performance of $Bi_{1.5}Y_{0.3}Sm_{0.2}O_{3-\delta}$-carbonate membranes for the first 50 hours of testing at 700°C due to a change in ceramic support structure before reaching steady state for the remainder of the study [Rui et al., 2012]. In addition, LSCF-carbonate has shown decreasing stability for 110 hours in a $CO_2$ gradient for temperatures ranging between 800-900°C [Norton et al., 2013]. To this point, however, these are the only other known reports of dual-phase membrane $CO_2$ permeation stability data.

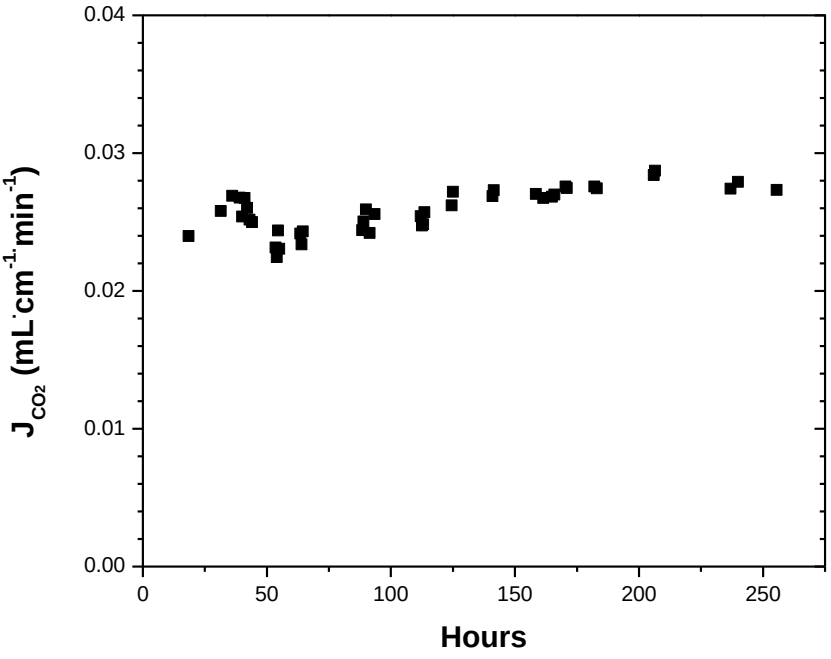


*Figure 4.9 Time dependence of $CO_2$ permeation flux of LCGFA-carbonate membrane (thickness = 1.5 mm, feed and sweep flow rate = 100 mL·min$^{-1}$, feed $CO_2$ = 0.5 atm, T = 900°C)*

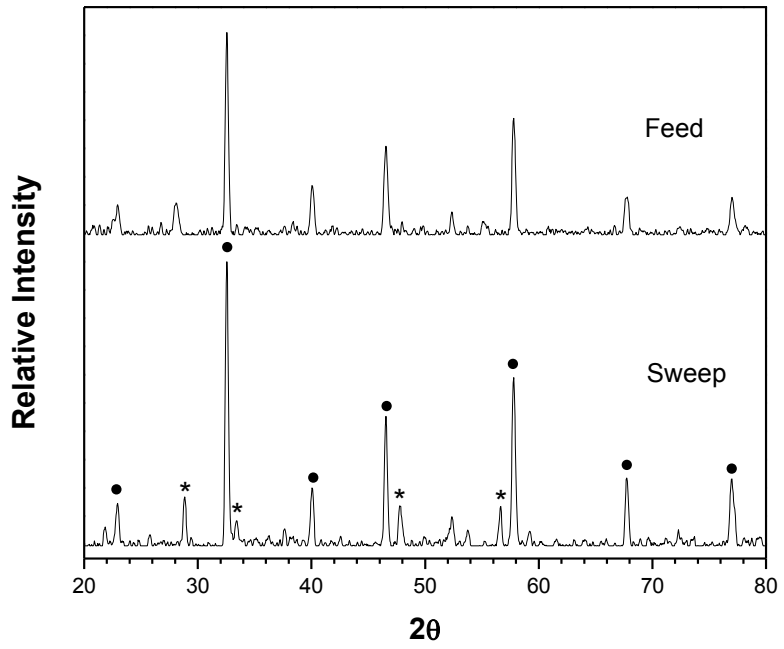


*Figure 4.10 XRD patterns of the feed and sweep side of LCGFA-carbonate membrane after 280 hours of exposure of experimental conditions at 900ºC (peak identification: • = perovskite, * = $CeO_2$ phase)*

4.4 Conclusions

Ceramic-carbonate dual-phase membranes made of ionically conducting porous $La_{0.85}Ce_{0.1}Ga_{0.3}Fe_{0.65}Al_{0.05}O_{3-\delta}$ (LCGFA) support with a Li/Na/K molten carbonate mixture were prepared by the direct infiltration method. Molten carbonate completely infiltrated into the ceramic support pores resulting in a decrease in helium permeance by four orders of magnitude down to $10^{-10}$ $mol \cdot m^{-2} \cdot s^{-1} \cdot Pa^{-1}$. LCGFA-carbonate membranes exhibit thermal and chemical stability by maintaining a perovskite structure when exposed to experimental conditions ranging from pure $N_2$ to various concentrations of $CO_2$, and under reducing conditions such as simulated syngas. $CO_2$ permeation through

the LCGFA-carbonate membrane exhibits exponential dependence to increasing temperature reaching a maximum permeation flux of 0.032 $mL \cdot cm^{-2} \cdot min^{-1}$ at 900°C. Decreasing the membrane thickness by 50% resulted in a 100% increase in $CO_2$ permeation flux while maintaining the same apparent activation energy which confirms that $CO_2$ transport was limited by bulk diffusion for the membrane thicknesses tested. In addition, the theoretical model accurately predicts a linear dependence in $CO_2$ permeation flux with a logarithmic increase in $CO_2$ partial pressure gradient across the membrane, reaching a maximum permeation flux of 0.033 $mL \cdot cm^{-2} \cdot min^{-1}$ at a feed partial pressure of 0.9 atm at 900°C. Finally, LCGFA-carbonate membranes showed very stable $CO_2$ permeation performance of 0.021-0.025 $mL \cdot cm^{-2} \cdot min^{-1}$ for more than 275 hours of exposure to experimental conditions at 900°C because LCGFA is resistant to formation of carbonate when exposed to $CO_2$. In Chapter 5, a new fluorite-type ceramic support is chosen for the dual-phase membrane in order to improve the poor permeation properties of LCGFA-carbonate membranes while maintaining the chemical and permeation stability and extending them to exposure to simulated syngas.

# CHAPTER 5

# STABILITY OF Ce-Sm OXIDE-CARBONATE DUAL-PHASE MEMBRANE UNDER PRE-COMBUSTION CONDITIONS AT HIGH TEMPERATURE

## 5.1 Introduction

The development of $CO_2$ selective membranes for pre-combustion capture is a considerable challenge, as it requires the separation of larger $CO_2$ from smaller $H_2$. In addition, both polymeric and inorganic membranes are both limited in their separation performance at high temperatures. To improve upon these limitations, the use of a dense ceramic-carbonate dual-phase membrane has been shown to selectively separate $CO_2$ from a gas mixture at high temperature. Early experimental studies, however, have focused on inert separation from gases such as $N_2$. In addition, the literature shows that little work has been done to examine the chemical and permeation stability of the dual-phase membrane. In Chapter 2, the permeation stability of LSCF-carbonate was examined in $CO_2$-rich environments with and without the presence of $O_2$. This membrane showed poor stability without the presence of $O_2$, as the membrane surface reacted with $CO_2$, resulting in a carbonate surface layer that limited the surface exchange reaction between $CO_2$ and lattice oxygen. In Chapter 3, LCGFA-carbonate membranes were shown high chemical stability in the presence of simulated syngas conditions. In addition, stable $CO_2$ permeation was measured for one month at high 900$^oC$ in a $CO_2$:$N_2$ environment. However, limited ionic conductivity of the ceramic phase resulted in a relatively low $CO_2$ permeance relative to other materials previously reported in the literature.

In an effort to improve the stability of the dual-phase membrane in harsh experimental conditions and maintain a high $CO_2$ permeation flux, the fluorite-type ceramic material samarium doped ceria (SDC) with composition $Ce_{0.8}Sm_{0.2}O_{1.9}$ was chosen as the ceramic support for the dual-phase membrane. This material has been shown to have very high permeation properties in the presence of molten carbonate at intermediate temperatures [Zhang et al., 2012]. Moreover, this material has been extensively studied as a material for oxygen permeation [Huang et al., 1997]. The objective of this current work is to synthesize the dual-phase membrane and examine the chemical and permeation stability of the membrane under inert and simulated syngas conditions at high temperature.

## 5.2 Experimental Methods

### *5.2.1 Preparation of porous and dense $Ce_{0.8}Sm_{0.2}O_{1.9}$ supports*

Samarium-doped ceria (SDC) powder of composition $Ce_{0.8}Sm_{0.2}O_{1.9}$ was prepared based on the citrate method previously described by Yin and Lin [Yin & Lin, 2007]. Stoichiometric amounts of metal nitrate precursors $Ce(NO_3)_3 \cdot 6H_2O$ (99.5%, Alfa Aesar) and $Sm(NO_3)_3 \cdot 6H_2O$ (99.9%, Alfa Aesar) were weighed out in a 0.05 mole basis and mixed with a 100 percent excess of citric acid (99.5%, Alfa Aesar). The precursors were dissolved in 1000 mL of de-ionized water and heated to 105$^oC$ and covered for four hours to prevent evaporation and promote polymerization. Evaporation was then implemented by uncovering and heating the solution at 110$^oC$ for 3-4 hours. The resulting viscous solution was dried in a furnace (Thermolyne, 46100) at 110$^oC$ for 24 hours. Self-ignition of the dried gel was then performed at 400$^oC$ to burn out the organic compounds. The resulting powder was then ground with a mortar and pestle to reduce the particle size.

The powder was then calcined at 550°C in air for 10 hours with heating and cooling ramping rates of $10^{o}C \cdot min^{-1}$. The calcined powder was again ground using a mortar and pestle. Approximately 3 grams of powder was placed in a 30 mm stainless-steel mold and pressed to 160 MPa for 5 minutes using a hydraulic press (Carver, Model #3853). The green disks were then sintered at temperatures ranging from 950-1150°C for 20 hours with heating and cooling ramping rates of $2^{o}C \cdot min^{-1}$ resulting in porous SDC disk supports.

*5.2.2 Synthesis of $Ce_{0.8}Sm_{0.2}O_{2-x}$ -carbonate dual phase membrane*

Synthesis of SDC-carbonate dual-phase membranes was achieved by direct infiltration of molten carbonate into the pores of sintered SDC support via the direct infiltration technique previously described by Chung et al. [Chung et al., 2005]. The carbonate powders $Li_2CO_3$ (99.2%, Fischer Scientific), $Na_2CO_3$ (99.9%, Fischer Scientific), and $K_2CO_3$ (99.8%, Fischer Scientific) were weighed in a 42.5/32.5/25 mol% ratio, respectively, and heated to 550°C in a furnace. Porous ceramic supports were preheated above the molten carbonate mixture to prevent thermal shock before being lowered into contact with carbonate. Supports were left in contact with molten carbonate for 5-10 minutes to ensure complete infiltration via capillary forces. The membrane was then lifted and slowly removed from the furnace and cooled. Residual carbonate on the membrane surface was removed using SiC polishing paper.

*5.2.3 Characterization of ceramic supports and ceramic-carbonate dual-phase membranes*

The porosity of the membranes was measured by the Archimedean method previously described [Harry & Johnson, 2004]. To briefly summarize, membrane samples

were weighed at three stages: dry, immersed in liquid nitrogen (measured once the weight reached steady state), and saturated in liquid nitrogen (measured once immediately lifted from liquid $N_2$). Using these three weights, the porosity of the sample can be estimated using the Archimedean principle by using the following equation:

$$P = \frac{S - D}{S - I} \tag{5.1}$$

where P is the porosity fraction, S is the saturated sample weight, D is the dry sample weight, and I is the immersed sample weight. Three samples for each sintering temperature were measured each four times to establish mean porosity. Room temperature helium permeation was used to determine the average pore size of porous supports as well as verifying the gas tightness of dense ceramic and ceramic-carbonate dual-phase membranes. The phase structure of the SDC powder and membranes were characterized using X-ray diffraction (XRD) (Bruker, $CuK_{\alpha 1}$) evaluated in the 2θ range of $20^o$ to $80^o$. Scanning electron microscopy (SEM) imaging was performed to confirm the porous nature of ceramic supports as well as the dense nature of dense ceramic and ceramic-carbonate samples.

*5.2.4 Carbon Dioxide Permeation measurements*

A Probostat high temperature permeation system (Probostat, Norwegian Electro Ceramics AS) was used for carbon dioxide permeation experiments. For each experiment an alumina spacer attached to a spring force assembly, a dense SDC-carbonate disk membrane, and silver seal were placed on top of a 20 mm alumina tube, which was then enclosed by a 40 mm diameter alumina tube. Argon was introduced inside the 20 mm alumina tube serving as the sweep gas at the bottom of the membrane while carbon

dioxide and nitrogen was introduced to the space between the two alumina tubes serving as the feed gas to the top of the membrane. The assembled apparatus was then placed in a vertical tube furnace and was heated to approximately 950$^{o}$C to reach the softening temperature of silver at a ramping rate of 1$^{o}$C·min$^{-1}$. Once the softening point of silver was reached, the spring assembly attached to the alumina spacer above the disk membrane forced the membrane into the silver ring forming a seal between the membrane and the 20 mm alumina tube. The quality of the seal was determined by measuring the nitrogen content in the argon sweep gas using a gas chromatograph (Agilent, 6890N). After reaching minimization of helium leakage, the system was cooled to either 700$^{o}$C or 900$^{o}$C at a rate of 1$^{o}$C·min$^{-1}$.

For carbon dioxide permeation experiments, the feed gas consisted of a variable carbon dioxide flow mixed with a balance of nitrogen to reach 100 mL·min$^{-1}$ for a carbon dioxide partial pressure varying between 0.1-0.9 atm. Argon was flowed as the sweep gas at a flow rate range between 25-200 mL·min$^{-1}$. The temperature was varied between 700-900$^{o}$C. Gas flow rates were regulated using mass flow controllers (MKS, Model 1179) and a four-channel readout (MKS, Type 247). Samples were taken three hours after a change in gas composition and one hour after a temperature change to allow the system to reach steady state. Table 5.1 shows the system parameters for tests with varying temperature, $CO_2$ partial pressure, and sweep flow rate. A mass balance on the measured sweep side gases was used to calculate the carbon dioxide permeation flux through each membrane. The $CO_2$ error in the permeate gas caused by seal leaks were corrected by measuring the presence of nitrogen and subtracting the corresponding carbon dioxide

from the calculated carbon dioxide permeation flux. The error in determining the carbon dioxide permeation flux using this procedure is approximately $\pm$ 10%.

*Table 5.1 System parameters for carbon dioxide permeation flux experiments*

| Variable Parameter | System Temp (°C) | Feed $CO_2$ Partial Pressure (atm) | Sweep Flow ($mL \cdot min^{-1}$) |
|---|---|---|---|
| Temperature | 500-900 | 0.5 | 100 |
| $CO_2$ Partial Pressure | 900 | 0.1-0.9 | 100 |
| Stability | 900 | 0.5 | 100 |

## 5.3 Results and discussion

### *5.3.1 Membrane synthesis*

Figure 5.1 shows XRD patterns of SDC powder after calcination as well as membrane supports sintered in 50 degree intervals from 950-1150°C. A minimum sintering temperature of 950°C was chosen for two main reasons. The previously described procedure for sealing membranes requires a system temperature of approximately 950°C. In addition, lowering the sintering temperature below 950°C results in a support that does not have adequate strength to be practically utilized for further testing. The XRD patterns of each support tested shows the presence of a fully developed fluorite phase without the presence of secondary phases, indicating that the minimum sintering temperature of 950°C is sufficient to achieve the desired structure. Therefore, from a structural standpoint, each of the sintering temperatures would be suitable for use as a support for the dual-phase membrane.

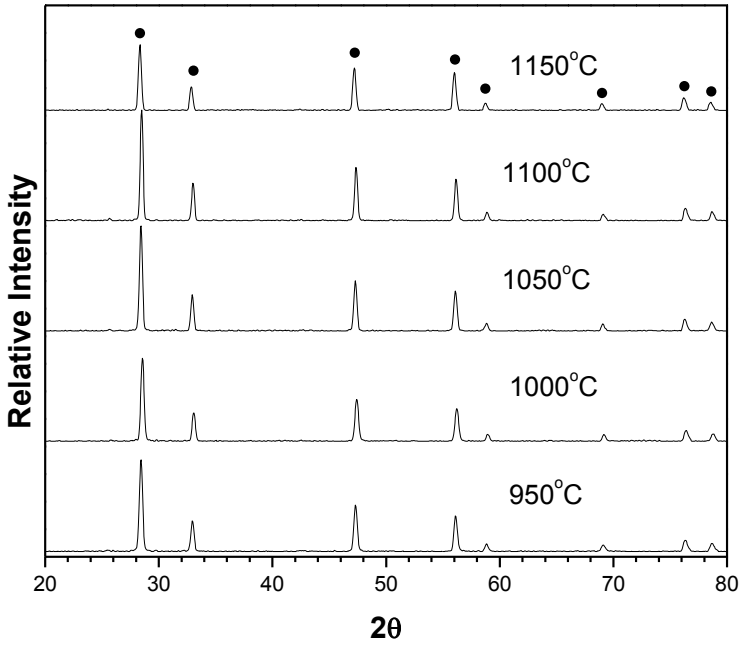


*Figure 5.1 XRD patterns of SDC porous supports sintered in 50°C intervals from 950-1150°C (peak identification: • = fluorite)*

A non-destructive liquid nitrogen Archimedean method was used to estimate the porosity of SDC supports prepared at sintering temperatures from 950-1150°C, as shown in Figure 5.2. As the sintering temperature increases, the support strength increases and the porosity decreases, as previously shown for $La_{0.6}Sr_{0.4}Co_{0.8}Fe_{0.2}O_{3-\delta}$ and $La_{0.85}Ce_{0.1}Ga_{0.3}Fe_{0.65}Al_{0.05}O_{3-\delta}$ porous supports prepared for use in the dual-phase membrane [Ortiz-Landeros et al., 2013]. At 950°C, an open porosity of 39% is measured followed by a decrease with increasing sintering temperature until reaching 33% at 1150°C. Previous work has shown that an optimal support porosity of 40-50% results in a maximum $CO_2$ permeation performance for $La_{0.6}Sr_{0.4}Co_{0.8}Fe_{0.2}O_{3-\delta}$-carbonate membranes at high temperature [Ortiz-Landeros et al., 2013]. A sufficiently high porosity is necessary to ensure connected pores throughout the thickness of the membrane support,

as $CO_2$ permeation relies on transport of carbonate ions through the molten carbonate phase which occupies the open pores of the ceramic support.

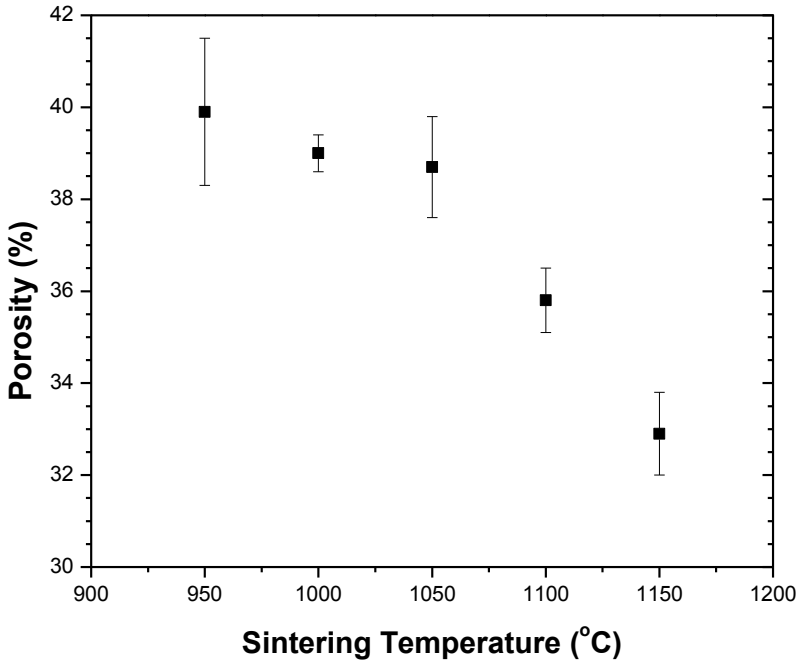


*Figure 5.2 Open porosity of SDC supports sintered from 950-1150°C as measured by the Archimedean method*

As addressed in Chapters 3 and 4, Rui et al. recently reported a model for $CO_2$ permeation through ceramic-carbonate membranes at high temperature based on driving forces provided by the oxygen ion conducting phase of the ceramic support as well as the carbonate ion conducting phase of the molten carbonate phase [Rui et al., 2009]. The $CO_2$ permeation flux through a bulk dual-phase membrane is predicted by:

$$J_{CO_2} = \frac{\alpha RT}{4F^2L} ln\left(\frac{P"_{CO_2}}{P'_{CO_2}}\right) \tag{5.2}$$

where α is a permeance coefficient (or referred to as total conductance) defined by:

$$\alpha = \frac{\left(\frac{\varepsilon}{\tau}\right)_p \sigma_c \left(\frac{\varepsilon}{\tau}\right)_s \sigma_i}{\left(\frac{\varepsilon}{\tau}\right)_p \sigma_c + \left(\frac{\varepsilon}{\tau}\right)_s \sigma_i} \tag{5.3}$$

In Equation 5.2, R is the ideal gas constant, T is the system temperature, F is Faraday's constant, L is the membrane thickness, P' and P" are the feed and sweep $CO_2$ partial pressures, respectively. In Equation 5.3, ε and τ denote the porosity and tortuosity of either the molten carbonate phase which occupies the ceramic support pore (p) or the solid ceramic phase (s).

In an attempt to optimize the permeation flux for the system at a given temperature, it is necessary to optimize Equation 5.3, as the relationship between the membrane microstructure and conductivity of the respective phases determines the conductive properties of the membrane. It is difficult, however, to predict the transport of the oxygen and carbonate ions through the ceramic and carbonate phases, respectively, due to the irregular dual-phase structure, which is accounted for by the geometric parameter, tortuosity (τ).

In an effort to simplify Equation 5.2, the Bruggeman relation has been previously shown to relate transport properties of multiphase electrodes:

$$\tau = \gamma \varepsilon^{1-\alpha} \tag{5.4}$$

where γ and α are constants dependent on the morphology, porosity, and particle-size distribution of the porous structure [Fongy et al., 2010, Zacharias et al., 2013]. In porous electrode modeling, it is common to assume a uniform, spherical particle size, leading to the approximations of γ = 1 and α = 1.5 [Lei et al., 1995, Doyle et al., 1996]. However, in real systems, higher tortuosities are observed than those calculated using the idealized approximations [Fongy et al., 2010, Zacharias et al., 2013]. Therefore, it is necessary to

use experimental data to estimate values for the parameters shown in Equation 5.3. Ortiz-Landeros et al. has shown the porosity and porosity/tortuosity ratios for a range of sintering temperatures for LSCF [Ortiz-Landeros et al., 2013]. From this data, the parameters γ and α will be estimated for the ceramic SDC powder for the porosity range in question as shown in Figure 5.2. This assumes that SDC and LSCF powder have similar morphology and particle-size distribution, which is reasonable considering both are prepared using a similar synthesis technique. The porosity/tortuosity data previously published in the porosity range of 20-50% results in the following approximated values γ = 0.53 and α = 3.4:

$$\tau = 0.53\varepsilon^{-2.4} \tag{5.5}$$

Since the ceramic network occupies the non-porous space, the following approximation is made:

$$\varepsilon_p + \varepsilon_s = 1 \tag{5.6}$$

Combining equations 5.3, 5.5, and 5.6 results in the following approximation:

$$\alpha = \frac{1}{0.53}\frac{\varepsilon_p^{3.4}\sigma_c(1-\varepsilon_p)^{3.4}\sigma_i}{\varepsilon_p^{3.4}\sigma_c + (1-\varepsilon_p)^{3.4}\sigma_i} \tag{5.7}$$

At 900ºC, the oxygen ionic conductivity ($\sigma_i$) of the ceramic phase and the carbonate conductivity ($\sigma_c$) of the molten carbonate phase are 0.17 and 3.5, respectively [Zhang et al., 2012, Janz et al., 1979]. Therefore, for a SDC-carbonate membrane at 900ºC, a support porosity of roughly 34% should be chosen to maximize the permeance coefficient as defined in Equation 5.7. SDC supports sintered at 1100ºC have a measured porosity of approximately 36% based on the results presented in Figure 5.2. A support sintering temperature of 1100ºC was chosen for the duration of this study.

After preparing SDC supports with the desired support properties, supports were infiltrated with molten carbonate at 550$^{o}$C. After cooling the membranes to room temperature, helium permeance testing was used to confirm the dense nature of the membranes. Dual-phase membranes show a decrease in helium permeance by four orders of magnitude from $10^{-6}$ to $10^{-10}$ $mol \cdot m^{-2} \cdot s^{-1} \cdot Pa^{-1}$ when compared to porous supports, confirming complete infiltration of the support pores.

*5.3.2 High temperature $CO_2$ permeation measurements in $CO_2$:$N_2$*

The effect of temperature on the $CO_2$ permeation flux through 1.5 mm thickness SDC-carbonate membranes is shown in Figure 5.3. A feed $CO_2$ partial pressure of 0.5 atm was maintained with a balance of $N_2$ in the temperature range of 700-950$^{o}$C. A maximum permeation flux of 0.86 was measured at 950$^{o}$C. The measured permeate $CO_2$ partial pressure, as well as the permeation flux at each temperature, is given in Table 5.2. The $CO_2$ permeation flux exhibits an exponential dependence to increasing temperature as shown by the linear behavior of the Arrhenius plot as shown in Figure 5.3, resulting in an apparent activation energy of 63 $kJ \cdot mol^{-1}$. This result is slightly lower than previously reported for SDC-carbonate dual-phase membranes on the order of 74-80 $kJ \cdot mol^{-1}$ [Zhang et al., 2012]. However, this result more closely matches the estimated activated energy for prepared SDC powders, which showed an activation energy ranging from 60 to 74 $kJ \cdot mol^{-1}$, depending on the particle morphology [Mori et al., 2004]. This result suggests that $CO_2$ transport is mostly controlled by the oxygen conductivity through the ceramic phase of the dual-phase membrane, which is expected given that the carbonate conductivity of the molten carbonate phase is higher than the ionic conductivity of the ceramic phase in the temperature range investigated.

*Table 5.2 $CO_2$ permeation flux and permeate $CO_2$ partial pressure of SDC-carbonate membrane with a feed $CO_2$ partial pressure of 0.5 atm.*

| Temp. (°C) | α ($S \cdot cm^{-1}$) | P' (atm) | P'' (atm) | Theor. $CO_2$ Flux ($mL \cdot cm^{-2} \cdot min^{-1}$) | Actual $CO_2$ Flux ($mL \cdot cm^{-2} \cdot min^{-1}$) |
|---|---|---|---|---|---|
| 700 | 0.007 | 0.5 | 0.0036 | 0.07 | 0.17 |
| 750 | 0.011 | 0.5 | 0.0054 | 0.11 | 0.27 |
| 800 | 0.017 | 0.5 | 0.0077 | 0.17 | 0.40 |
| 850 | 0.026 | 0.5 | 0.0099 | 0.25 | 0.52 |
| 900 | 0.037 | 0.5 | 0.0127 | 0.35 | 0.68 |
| 950 | 0.051 | 0.5 | 0.0160 | 0.47 | 0.86 |

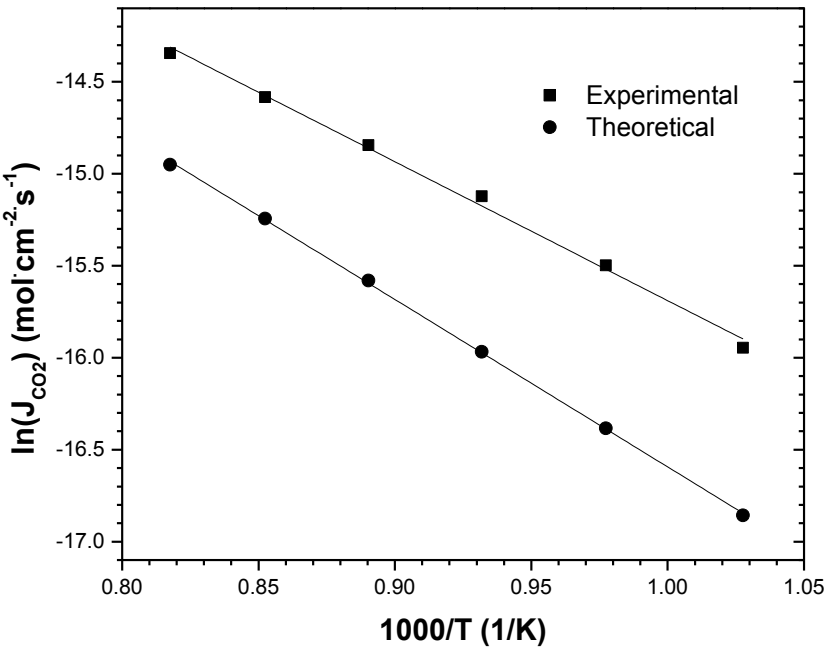


*Figure 5.3 Effect of temperature on $CO_2$ permeation flux of SDC-carbonate membranes of 1.5 mm thickness (feed and sweep flow rate = 100 $mL \cdot min^{-1}$, feed $CO_2$ = 0.5 atm, T = 700-950°C)*

Previous studies have demonstrated a $CO_2$ permeability that is two orders of magnitude greater than other gases present in the feed gas as reported in the literature and as shown in Chapter 4 [Anderson & Lin, 2010]. Based on the proposed transport mechanism, the dense dual-phase membrane is only permeable to $CO_2$. Any detectable feed gas in the permeate stream, other than $CO_2$, results from a membrane defect or seal leak. The concentration of $N_2$ in the permeate stream is roughly 50-65 ppm in the entire temperature range tested resulted in a very similar $CO_2$:$N_2$ selectivity on the order of 100. During one particular experiment, the $CO_2/N_2$ selectivity was determined to be more than 1000. Therefore, it is assumed that a defect or imperfect sealing is the limiting factor in maximizing the measured $CO_2$ selectivity over other feed gases.

In addition to providing insight to the permeation properties of the membrane at various temperatures, it is also important to determine the effect a wide range of $CO_2$ pressure gradients has on the permeation performance. Figure 5.4 shows the effect of varying the $CO_2$ partial pressure gradient across the membrane. As shown, the permeation flux increases linearly with a logarithmic increase in $CO_2$ partial pressure gradient across the membrane. As the gradient across the membrane increases, the driving force also increases, resulting in a larger permeation flux. This dependence is predicted by the model described in Equation 5.2, and is consistent with dual-phase membranes as reported in the literature [Rui et al., 2012] and compared to the results previously reported in Chapters 3 and 4.

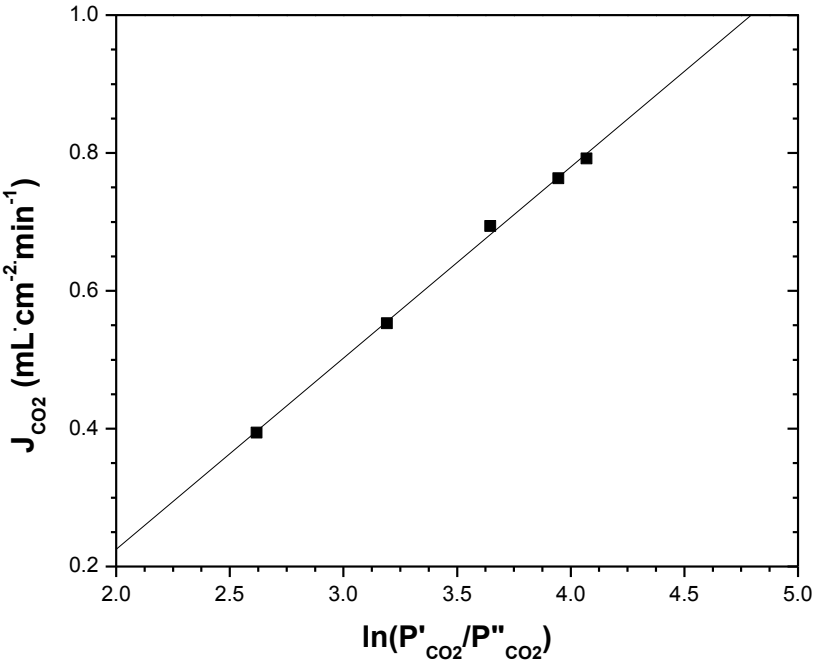


*Figure 5.4 Effect of $CO_2$ partial pressure gradient on $CO_2$ permeation flux of SDC-carbonate membrane (thickness = 1.5 mm, feed and sweep flow rate = 100 mL·min$^{-1}$, feed $CO_2$ = 0.1-0.9 atm, T = 900$^o$C)*

The $CO_2$ permeation stability of SDC-carbonate membranes was examined under steady-state conditions for 14 days. Figure 5.5 shows the long-term stability of a 1.5 mm thick membrane exposed to a 0.5 atm $CO_2$ feed partial pressure at 900$^o$C. The membrane exhibits remarkably stable permeation behavior for two full weeks of testing with a high $CO_2$ permeation flux between 0.68-0.74 mL·cm$^{-2}$·min$^{-1}$ for more than 330 hours of exposure. Of the previous studies on the permeation stability of the dual-phase membrane, only LCGFA-carbonate membranes have been shown to maintain chemical and permeation stability after long term exposure to a high $CO_2$ concentration feed gas without the presence of $O_2$. The oxygen permeation flux for SDC-carbonate membranes,

however, is roughly 30 times higher than that measured for LCGFA-carbonate, due to the increased ionic conductivity of the ceramic phase of the membrane. LSCF-carbonate membranes showed long-term permeation stability, however, the presence of $O_2$ was required to maintain the structural integrity of the ceramic phase. Without the presence of $O_2$, the ceramic phase rapidly decomposes into oxide and carbonate phases on the membrane surfaces, resulting in a substantial drop in $CO_2$ flux. $Bi_{1.5}Y_{0.3}Sm_{0.2}O_{3-\delta}$ (BYS)-carbonate membranes have shown transient $CO_2$ permeation behavior for the first 50 hours of testing at 700°C due to a change in ceramic support structure before reaching steady-state for the remainder of the study [Rui et al., 2012].

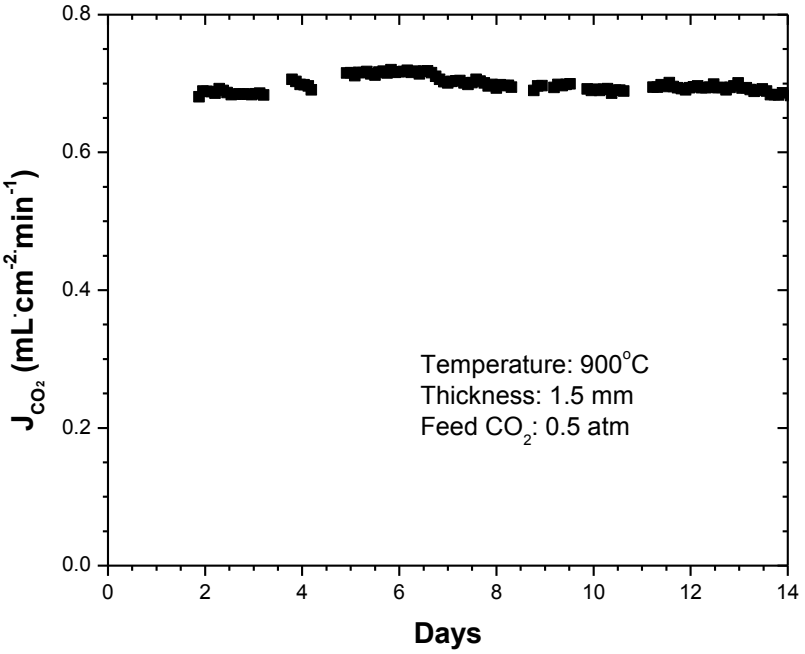


*Figure 5.5 Time dependence of $CO_2$ permeation flux of SDC-carbonate membrane*

Figure 5.6 shows XRD patterns of the SDC-carbonate membrane after one month of exposure to experimental conditions at 900°C. The feed and sweep sides of the

membrane both maintain a fluorite structure with no sign of formation of secondary phases. However, a peak intensity shift is observed for the 200 and 400 peaks, likely resulting from a change in orientation of the ceramic phase on the membrane surface after long-term exposure to experimental conditions at high temperature. Further examination is required in order to determine the significance of this finding. Previous work for LSCF-carbonate dual-phase membranes has shown degradation of the sweep side surface after long-term exposure to experimental conditions. LCGFA-carbonate membranes maintained chemical stability with the exception of enhanced detection of $CeO_2$, likely resulting from slight decomposition at the membrane surface, after long-term exposure to a $CO_2$:$N_2$ feed gas mixture at 900°C.

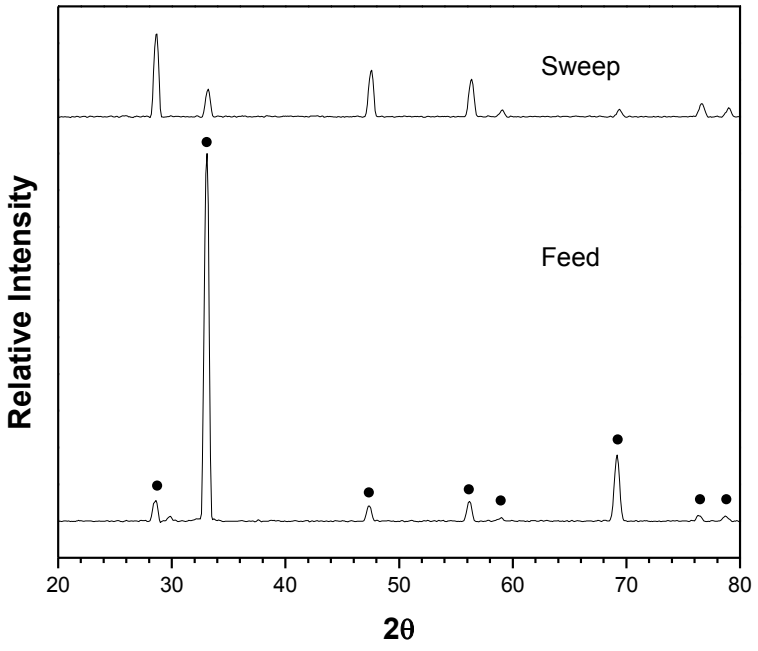


*Figure 5.6 XRD patterns of the feed and sweep side of SDC-carbonate membrane after 30 days of exposure to $CO_2$ at 900°C (peak identification: • = fluorite phase)*

Figure 5.7 shows a comparison of the $CO_2$ permeation flux of LSCF-carbonate, LCGFA-carbonate, and SDC-carbonate membranes at different temperatures. The $CO_2$ permeation flux of SDC-carbonate membranes is significantly higher than that measured for LSCF-carbonate and LCGFA-carbonate membranes, which is a result of using a ceramic phase with a high conductivity and high chemical stability. While previous reports have shown higher permeation results for LSCF-carbonate membranes [Anderson & Lin, 2010], data for all three materials was taken after the $CO_2$ permeation reached steady state in order to account for any changes to the membrane surface that affected the permeation properties.

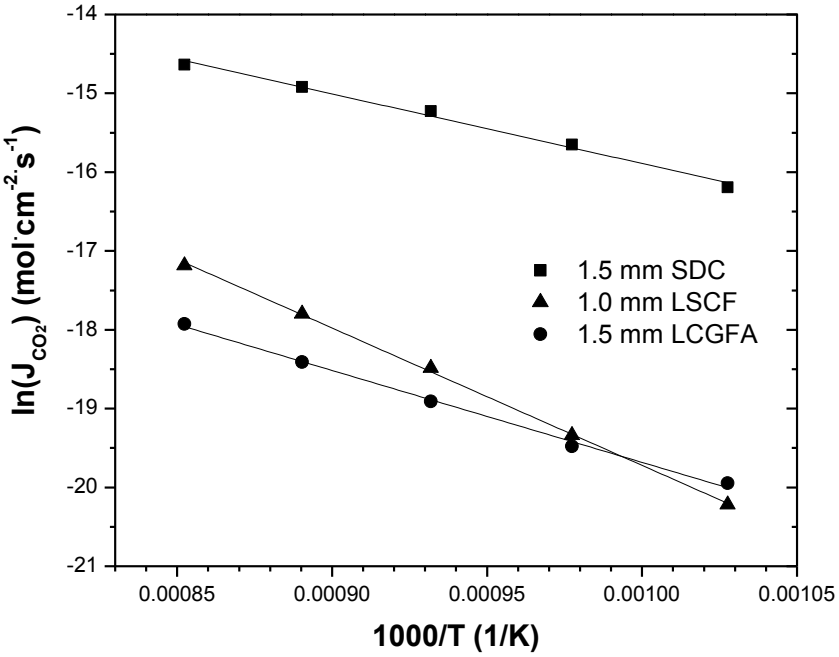


*Figure 5.7 Comparison of $CO_2$ permeation flux of LSCF-carbonate, LCGFA-carbonate, and SDC-carbonate membranes from 700-900°C*

In Chapter 3, $CO_2$ permeation through LSCF-carbonate membranes was shown to rapidly decrease upon exposure to $CO_2$ at high temperature without the presence of $O_2$. In Chapter 4, $CO_2$ permeation through LCGFA-carbonate membranes was shown to be steady under $CO_2$:$N_2$ environments for hundreds of hours. The results for SDC-carbonate show, however, a membrane that is not only stable for more than two weeks exposure to experimental conditions at 900ºC, but also a permeation flux which has more than a factor of 10 improvement over the ceramic-carbonate membranes previously studied.

*5.3.3 High temperature $CO_2$ permeation measurements in simulated syngas*

In addition to establishing tolerance in varying $CO_2$ environments, it is important to demonstrate whether dual-phase membranes are able to withstand harsh conditions in order to serve as potential alternatives for pre-combustion $CO_2$ capture. Figure 5.8 shows the effect of temperature on the $CO_2$ permeation flux through 1.5 mm thick SDC-carbonate membranes exposed to simulated syngas of composition 50% CO, 35% $CO_2$, 10% $H_2$, 5% $N_2$ in the temperature range of 500-900ºC. A $CO_2$ permeation flux of 0.10 and 0.79 $mL \cdot cm^{-2} \cdot min^{-1}$ was measured at 500 and 900ºC, respectively. As shown by the Arrhenius plot, the membrane exhibits an exponential dependence to increasing temperature for the entire temperature range in question, resulting in a measured apparent activation energy of 54 $kJ \cdot mol^{-1}$.

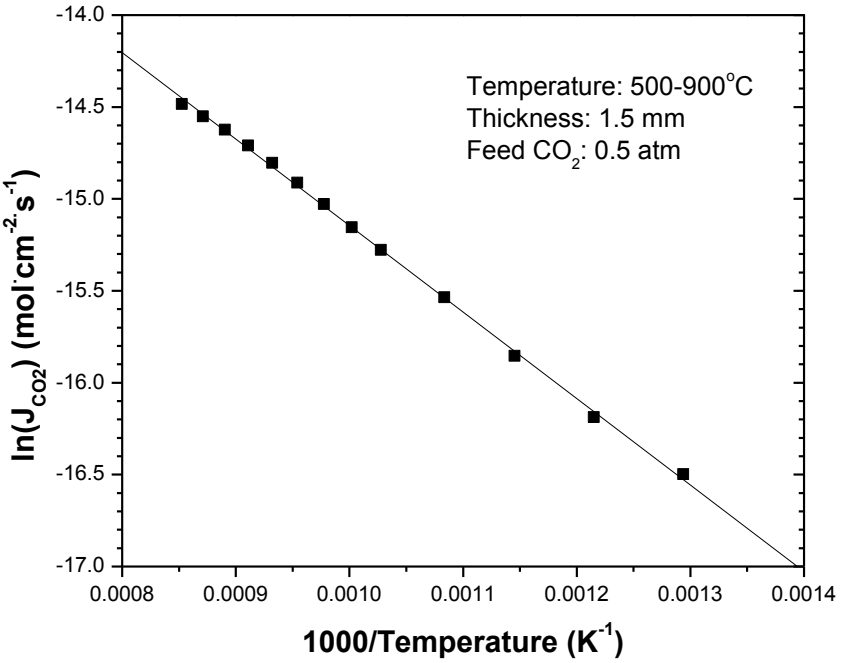


*Figure 5.8 Effect of temperature on $CO_2$ permeation flux of SDC-carbonate membranes of 1.5 mm thickness exposed to simulated syngas*

The $CO_2$ permeation stability of SDC-carbonate exposed to simulated syngas was examined under steady state conditions for more than 30 days. Figure 5.9 shows the long-term stability of the membrane exposed to 50% CO, 35% $CO_2$, 10% $H_2$, and 5% $N_2$ at 700°C. The permeation flux varies throughout the study, ranging from 0.26-0.35 $mL \cdot cm^{-2} \cdot min^{-1}$ before stabilizing at approximately 0.31 $mL \cdot cm^{-2} \cdot min^{-1}$ for the last 10 days of the study. LCGFA-carbonate membranes have shown chemical stability after 24 hours of exposure to simulated syngas, but this is the first reported permeation stability data in reducing conditions. Zhang et al. reported $CO_2$ permeation data for SDC-carbonate exposed to $H_2$, but observed rapid decomposition likely resulting from decomposition of the molten carbonate phase at high temperature [Zhang et al., 2012].

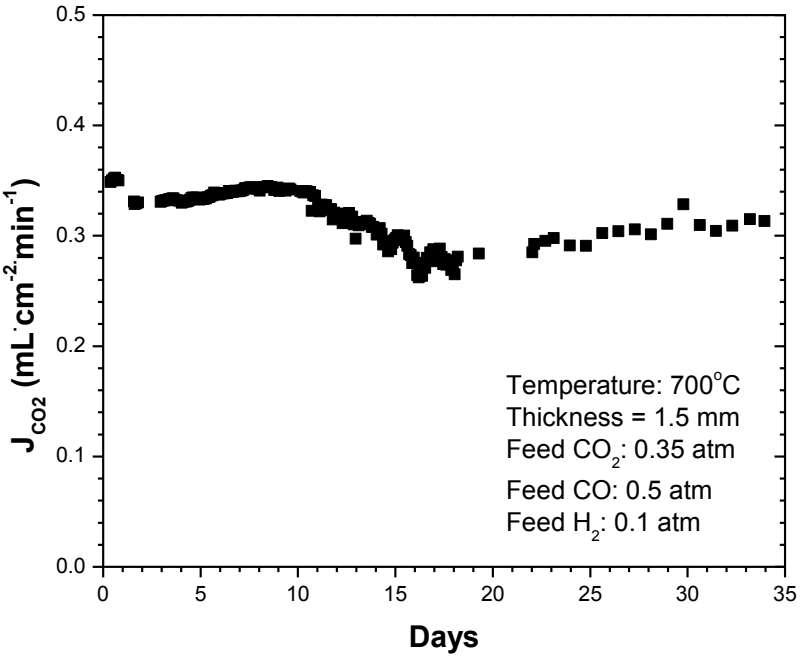


*Figure 5.9 Time dependence of $CO_2$ permeation flux of SDC-carbonate membrane in simulated syngas*

Figure 5.10 shows XRD patterns of the SDC-carbonate membrane after 35 days of exposure to simulated syngas at 700°C. As shown, both the feed and sweep sides of the membrane maintain a fluorite structure. As shown in Figure 5.6, a peak intensity shift is observed for the membrane after long term exposure to experimental conditions. However, after exposure to simulated syngas, a shift in the 111 and 222 peaks is observed. This is, again, likely resulting from a change in orientation of the ceramic phase on the membrane surface after long-term testing at high temperature. Further analysis is required to provide an explanation and determine the significance. On the feed side of the membrane, $Sm_2O_3$ peaks are also present: these result from decomposition of the fluorite structure on the immediate membrane surface after long term exposure to $H_2$-

containing environments. This decomposition would explain the transient behavior of the long-term permeation flux shown in Figure 5.8. Figure 5.11 shows a comparison of SDC-carbonate membranes exposed to $CO_2$ and simulated syngas for one month or more. The surface appears to be dense, for the membrane exposed to a $CO_2$:$N_2$ feed, and is consistent with what is observed prior to exposure to experimental conditions at high temperature. The membrane surface exposed to simulated syngas shows a porous network, which undoubtedly affects the permeation properties of the membrane at high temperature. While the membrane shows signs of decomposition into metal oxide phases after long-term exposure, the SDC-carbonate membrane maintained long-term permeation flux stability after more than one month of exposure to $H_2$-containing simulated syngas at 700$^o$C.

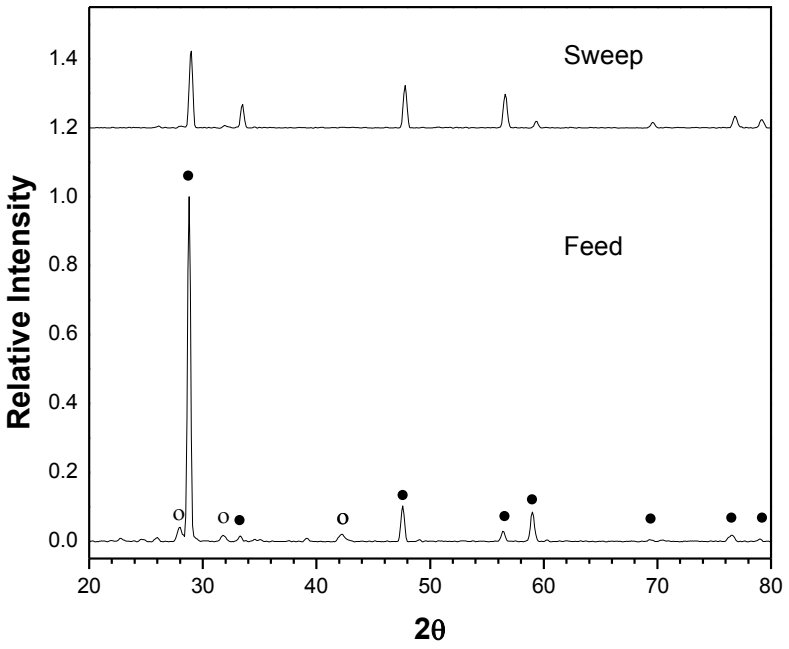


*Figure 5.10 XRD patterns of the feed and sweep side of SDC-carbonate membrane after 36 days of exposure to simulated syngas at 700°C (peak identification: • = fluorite, ° = $Sm_2O_3$ phase)*

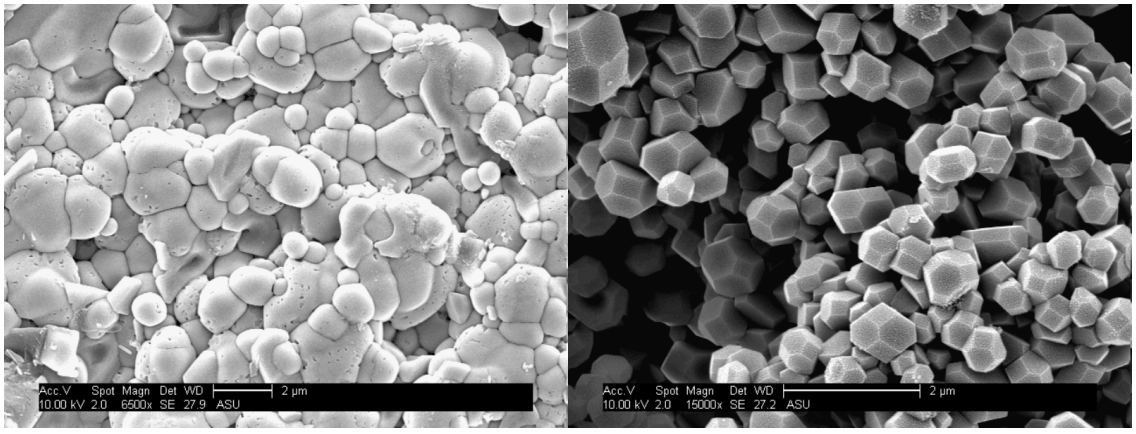


*Figure 5.11 SEM of SDC-carbonate membrane: (a) after one month of exposure to $CO_2$ + $N_2$ at 900°C, and (b) after 36 days exposure to simulated syngas at 700°C*

## 5.4. Conclusions

Ceramic-carbonate dual-phase membranes made of the ionically conducting porous material samarium doped ceria (SDC) with composition $Ce_{0.8}Sm_{0.2}O_{1.9}$ support and a Li/Na/K molten carbonate mixture were prepared by the direct infiltration method. SDC-carbonate membranes exhibit chemical and permeation stability when exposed to a $CO_2$:$N_2$ feed with varying system temperature, varying $CO_2$ partial gradient, and stability under long-term steady-state exposure to experimental conditions at 900°C for two weeks. SDC-carbonate membranes exhibit exponential dependence to increasing temperature and linear dependence to a logarithmic increase in $CO_2$ partial pressure gradient as predicted by the theoretical model. A maximum $CO_2$ permeation flux of 0.86 $mL \cdot cm^{-2} \cdot min^{-1}$ was measured at 950°C. A stable permeation flux of 0.68-0.74 was measured during the two-week stability test. SDC-carbonate membranes exposed to simulated syngas of composition 50% CO, 35% $CO_2$, 10% $H_2$, 5% $N_2$ were also studied under varying system temperature in the range of 500-900°C. Even in $H_2$-containing simulated syngas, the permeation flux still shows exponential dependence to increasing system temperature, with a maximum measured permeation flux of 0.79 $mL \cdot cm^{-2} \cdot min^{-1}$ at 900°C. A stability study, lasting more than one month, resulted in a variable permeation flux between 0.26-0.35 $mL \cdot cm^{-2} \cdot min^{-1}$ at 700°C that stabilized for the last 10 days of testing at approximately 0.31 $mL \cdot cm^{-2} \cdot min^{-1}$. For each membrane tested, SDC-carbonate membranes maintained chemical and permeation stability after long-term exposure to experimental conditions at high temperature.

# CHAPTER 6

# SUMMARY AND RECOMMENDATIONS

## 6.1 Summary

The research presented in this dissertation focused on the fundamental study of the chemical and permeation stability of dual-phase membranes for pre-combustion carbon capture. Specifically, the $Ce_{0.8}Sm_{0.2}O_{1.9}$-carbonate dual-phase membrane was developed and showed improved chemical stability and permeation performance when compared to other ceramic-carbonate membranes. In addition, the LCGFA-carbonate was found to be a dual-phase membrane with good chemical stability in various experimental conditions including simulated syngas at high temperature. Finally, LSCF-carbonate membranes were found to exhibit stable long-term permeation properties in the presence of oxygen to maintain the structural stability of the ceramic phase.

The first objective of this work was to determine the permeation stability of membranes containing the perovskite material $La_{0.6}Sr_{0.4}Co_{0.8}Fe_{0.2}O_{3-\delta}$ (LSCF). In Chapter 2, the oxygen permeation stability of dense LSCF membranes was studied in inert and reducing conditions. The surface catalytic properties of the membrane exposed to reducing conditions changed with exposure time, resulting in transient oxygen permeation behavior before reaching steady state after approximately 200 hours of exposure. The increased driving force for oxygen permeation provided by the reducing conditions on the permeate side of the membrane resulted in an increased oxygen permeation flux when compared to the membrane exposed to inert conditions, despite degradation of the immediate membrane surface into $SrCO_3$ and CoO. Under the studied experimental conditions, the membrane reached steady state for continuous operation.

In Chapter 3, LSCF-carbonate membranes were examined in a $CO_2$-rich environment with and without the presence of $O_2$ to examine the long term permeation stability of the dual-phase membrane. $CO_2$ permeation flux decreased considerably for temperatures ranging from 800-900$^oC$ in the presence of $CO_2$:$N_2$ before reaching steady state after approximately 65 hours. This is caused by adsorption of $CO_2$ on the membrane surface resulting in decomposition of the membrane surface and a decrease in the partial-pressure driving force across the membrane. The addition of $O_2$ on the feed side of the membrane with $CO_2$ maintained the stability of the ceramic LSCF phase. In addition, the introduction of $O_2$ provided a second chemical driving force that also resulted in a change in the transport mechanism, as carbonate ions were formed by the reaction of $CO_2$ with $O_2$ on the feed side of the membrane rather than from oxygen ions in the carbonate phase. This change in transport mechanism resulted in a drastic increase in $CO_2$ permeation, as transport was no longer limited by the ionic conductivity of the LSCF phase. LSCF-carbonate membranes exposed to a $CO_2$ and $O_2$ gradient resulted in high, stable $CO_2$ permeation at temperatures between 850-950$^oC$ for continuous operation.

The second objective was to introduce a known $CO_2$-tolerant ceramic phase in the dual-phase membrane in an effort to prove stability of the dual-phase membrane as well as to verify the permeation mechanism for selective $CO_2$ separation. $La_{0.85}Ce_{0.1}Ga_{0.3}Fe_{0.65}Al_{0.05}O_{3-\delta}$ (LCGFA) membranes were successfully prepared and exposed to various experimental conditions at high temperature. LCGFA-carbonate membranes exhibit thermal and chemical stability by maintaining a perovskite structure when exposed to experimental conditions ranging from pure $N_2$ to various concentrations of $CO_2$, and under reducing conditions such as simulated syngas. $CO_2$ permeation

through LCGFA-carbonate is thermally activated and permeation is inversely proportional to membrane thickness, which confirmed the assumption that $CO_2$ permeation through the membrane was limited by bulk diffusion. In addition, the theoretical model accurately predicted a linear dependence in $CO_2$ permeation flux with a logarithmic increase in $CO_2$ partial pressure gradient across the membrane. Finally, LCGFA-carbonate membranes showed very stable $CO_2$ permeation performance for more than 275 hours of exposure to experimental conditions at 900$^o$C, though the permeance was low when compared to other dual-phase membranes in the literature.

The final objective of this work was to demonstrate the use of a dual-phase membrane to separate $CO_2$ from a simulated syngas mixture. Due to the low permeance of LCGFA-carbonate membranes, the ceramic phase was switched to the fluorite type material samarium doped ceria (SDC) with composition $Ce_{0.8}Sm_{0.2}O_{1.9}$. SDC-carbonate membranes were first exposed to $CO_2$:$N_2$ to test the membrane properties observed for the stable LCGFA-carbonate membranes. Membranes exhibit chemical and permeation stability when exposed to a $CO_2$:$N_2$ feed with varying system temperature, varying $CO_2$ partial pressure gradient, and stability under steady-state, long-term exposure to experimental conditions at 900$^o$C for two weeks. $CO_2$ permeation was thermally activated and shows linear dependence to a logarithmic increase in $CO_2$ partial pressure gradient as predicted by the theoretical model for SDC-carbonate. Following confirmation of stability in $CO_2$:$N_2$, the membrane was exposed to simulated syngas with composition: 50% CO, 35% $CO_2$, 10% $H_2$, and 5% $N_2$. $CO_2$ permeation was thermally activated in the temperature range of 500-900$^o$C. A stability study in simulated syngas showed stable permeation for more than one month of exposure to experimental conditions at 700$^o$C.

For each membrane tested, SDC-carbonate membranes maintained chemical and permeation stability after long-term exposure to experimental conditions at high temperature.

## 6.2 Recommendations

Based on the experimental and theoretical results reported in this dissertation, the following recommendations for future research are suggested.

### *6.2.1 Optimization of ceramic pore structure*

Porous ceramic supports used in this dissertation were prepared by sintering compressed powder at a temperature below the densification temperature for each material. While this method resulted in supports that could be successfully infiltrated and tested at high temperature, steps can be taken in an attempt to optimize the pore structure. For example, Zhang et al. have demonstrated a two-step co-precipitation and sacrificial-template technique for preparing porous SDC supports for use in the dual-phase membrane. While there are other factors that have been previously addressed that also contributed, the $CO_2$ permeation properties through SDC-carbonate membranes prepared by this method are much better than other membranes reported in the literature [Zhang et al., 2012]. Not only does this method improve the pore structure of the ceramic support, but it also allows for greater sintering temperatures when preparing the support which provides potential advantages in terms of support conductivity and mechanical strength. In addition, a fundamental study on the ceramic:carbonate ratio for an optimized pore structure would lead to improvements in $CO_2$ permeation properties.

### *6.2.2 Improving ceramic support geometry*

Early development of the dual-phase membrane, including the work presented here, has focused on proving the concept of the dual-phase membrane. In particular, the focus of this work has been to prove that a dual-phase membrane can selectively separate $CO_2$ under a wide range of experimental conditions while maintaining chemical and structural stability. The work presented was limited to membranes having a disk-like geometry that are relatively thick (0.75-1.5 mm) with a low permeation area (1-2 $cm^2$). In order to improve permeation performance, the geometry of the membrane can be improved. This can be done by decreasing the membrane thickness or increasing the permeation area. Thinner dual-phase membranes on the order of ~10 μm are being currently developed in the Membrane and Energy Laboratory by preparing a thin dual-phase membrane film on a porous support to minimize bulk diffusion resistance (Lu and Lin, 2013). To increase the permeation area, tubular membranes with an order of magnitude increase in surface area relative to membrane disks are also being developed (Dong et al., 2013). The ability to fabricate a dual-phase membrane with a large permeation area and a thin $CO_2$ selective layer would result in the highest permeation properties for a given ceramic-carbonate membrane. While these options present unique challenges, development of a thin membrane film on a supported tubular geometry should be examined.

*6.2.3 Molten carbonate phase optimization*

The work presented here as well as a majority of the dual-phase membranes presented in the literature have reported using the same molten carbonate composition. The eutectic mixture of molten carbonate used in this study was composed of $Li_2CO_3$, $Na_2CO_3$, and $K_2CO_3$ in a 42.5/32.5/25% mol% mixture. Based on early development of the $CO_2$

permeation model, it was assumed that $CO_2$ permeation was limited by the ionic-carbonate conductivity of the ceramic phase, as the carbonate ion conductivity of the molten carbonate phase is greater than the oxygen ionic conductivity of the ceramic phases that have been tested to this point in the temperature range of 500-900$^oC$ (Rui et al., 2009; Anderson and Lin, 2010). However, recent adjustments of the $CO_2$ permeation model showed a more complicated relationship between the physical structure and conductivities of the respective phases (Ortiz-Landeros et al., 2013). The ternary Li/Na/K carbonate mixture was initially chosen due to its low melting temperature (397$^oC$) when compared to single or binary carbonate mixtures (Chung et al., 2005). However, this mixture had a higher decomposition partial pressure and lower conductivity at a given temperature when compared to binary mixtures that have been previously studied (Janz et al., 1979). Therefore, potential replacements of the molten carbonate phase could be studied in an effort to maximize the carbonate phase conductivity and overall stability at high temperature under a wide range of experimental conditions.

# REFERENCES


Aaron, D., Tsouris, C. (2005). Separation of CO2 from Flue Gas: A Review. *Separation Science and Technology*, 40, 321-348.

Aasland, S., Tangen, I. L., Wiik, K., Odegard, R. (2000). Oxygen permeation of $SrFe_{0.67}Co_{0.33}O_{3-d}$. *Solid State Ionics*, 135, 713-717.

Adler, S. B., Chen, X. Y., Wilson, J. R. (2007). Mechanisms and rate laws for oxygen exchange on mixed-conducting oxide surfaces. *Journal of Catalysis*, 245, 91-109.

Akin, F. T., Lin, Y. S., Zeng, Y. (2001). Comparative study on oxygen permeation and oxidative coupling of mehane on disk-shaped and tubular dense ceramic membrane reactors. *Ind. Eng. Chem. Res.*, 40, 5908-5916.

Anderson, M., Lin, Y.S. (2006). Synthesis and Characterization of Carbonate-Ceramic Dual-Phase Membranes for Carbon Dioxide Separation. *Proc. 9th Internal. Conf. on Inorganic Membranes*.

Anderson, M., Lin, Y. S. (2010). Carbonate-ceramic dual-phase membrane for carbon dioxide separation. *Journal of Membrane Science*, 357, 122-129.

Anderson, M., Wang, H., Lin, Y.S. (2012). Inorganic membranes for carbon dioxide and nitrogen separation, *Rev. Chem. Eng.* 28, 101-121.

Anderson, M., Lin, Y.S. (2013). Carbon dioxide separation and dry reforming of methane for synthesis of syngas by a dual-phase membrane reactor. *AIChE J*., 59, 2207-2218.

Arashi, H., Naito, H. (1992). Oxygen permeability in $ZrO_2$-$TiO_2$-$Y_2O_3$ system. *Solid State Ionics*, 53-56 431-435.

Arnold, M., Wang, H. H., Feldhoff, A. (2007). Influence of $CO_2$ on the oxygen permeation performance and the microstructure of perovskite-type $(Ba_{0.5}Sr_{0.5})(Co_{0.8}Fe_{0.2})O_{3-\delta}$ membranes. *Journal of Membrane Science*, 293, 44.

Bernardo, P., Drioli, E., Golemme, E. (2009). Membrane Gas Separation: A Review/State of the Art. *Ind. Eng. Chem. Res.*, 48 , 4638-4663.

Bounaceur, R., Lape, N., Roizard, D., Vallieres, C., Favre, E. (2006). Membrane processes for poste-combustion carbon dioxide capture: A parametric study. *Energy*, 31, 2556-2570.

Bouwmeester, H. J. M. (2003). Dense ceramic membranes for methane conversion. *Catalysis Today*, 82, 141-150.

Burggraaf, A. J., Cot, L. (1996). Fundamentals of Inorganic Membrane Science and Technology. Elsevier, Amsterdam, New York.

Caro, J., Wang, H. H., Tablet, C., Kleinert, A., Feldhoff, A., Schiestel, T., Kilgus, M., Kolsch, P., Werth, S. (2006). Evaluation of perovskites in hollow fibre and disk geometry in catalytic membrane reactors and in oxygen separators. *Catalysis Today*, 118, 128-135.

Carolan, M. F., Dyer, P. N., Fine, S. M., LaBar Sr., J. M., Thorogood, R. M. (1993). Process for restoring permeance of an oxygen-permeable ion transport membrane utilized to recover oxygen from oxygen-containing gaseous mixtures, U.S. Patent 5,240,473.

Carolan, M. F., Dyer, P. N., Fine, S. M., LaBar Sr., J. M., Thorogood, R. M. (1993). Process for recovering oxygen from gaseous mixtures containing water or carbon dioxide which process employs barium-containing ion transport membranes, U.S. Patent 5,269,822.

Carolan, M. F., Dyer, P. N., Fine, S. M., LaBar Sr., J. M., Thorogood, R. M. (1993). Process for recovering oxygen from gaseous mixtures containing water or carbon dioxide which process employs ion ion transport membranes, U.S. Patent 5,261,932.

Carolan, M. F., Motika, S. A., Dyer, P. N., Alba, P. B. (1996). Novel compositions capable of operating under high carbon dioxide partial pressures for use in solid-state oxygen producing devices. E.P. Patent 0,732,306.

Chung, S.J., Park, J.H., Li, D., Ida, J.I., Kumakiri, I., Lin, Y.S. (2005). Dual-Phase Metal-Carbonate Membrane for High-Temperature Carbon Dioxide Separation. *Ind. Eng. Chem. Res.*, 44, 7999-8006.

Cook, R. L., Sammells, A. F. (1991). On the systematic selection of perovskite solid electrolytes for intermediate temperature fuel cells. *Solid State Ionics*, 45, 311-321.

Cooper, C. A., Lin, Y. S. (2002). Microstructural and gas separation properties of CVD modified mesoporous γ-alumina membranes. *Journal of Membrane Science*, 195, 35-50.

Dong, H., Shao, Z., Xiong, G., Tong, J.;,Sheng, S., Yang, W. (2001). Investigation on POM reaction in a new perovskite membrane reactor. *Catalysis Today*, 67, 3-13.

Doyle, M., Newman, J., Sozdz, A. S., Schmutz, N., Tarascon, J.-M. (1996). Comparison of Modeling Predictions with Experimental Data from Plastic Lithium Ion Cells. *Journal of the Electrochemical Society*, 143, 1890-1903.

Dyer, P. N., Carolan, M. F., Butt, D., Van Doorn, R. H. E., Culter, R. A. (2002). *Patent No. 6.492,290*. US.

Favre, E. (2007). Carbon dioxide recovery from post-combustion processes: Can gas permeation membranes compete with absorption? *Journal of Membrane Science*, 294, 50-59.

Figueroa, J.D., Fout, T., Plasynski, S., McIlvried, H., Srivastava R.D. (2008). Advances in $CO_2$ capture technology-The U.S. Department of Energy's Carbon Sequestration Program. *International Journal of Greenhouse Gas Control*, 2 9-20.

Fongy, C., Gaillot, A.C., Jouanneau, S., Guyomard, D., Lestriez, B. (2010). Ionic vs Electronic Power Limitations and Analysis of the Fraction of Wired Grains in $LiFePO_4$ Composite Electrodes. *Journal of the Electrochemical Society*, 157, A885-A891.

Goldschmidt, V. M. (1946). Ionic radius of divalent copper. *Nature*, 157, 192-193.

Han, J., Zeng, Y., Lin, Y.S. (1997). Oxygen permeation through fluorite type bismuth-yttrium-copper oxide membranes. *Journal of Membrane Science*, 132, 235-243.

Harry, K. G., Johnson, A. (2004). A non-destructive technique for measuring ceramic porosity using liquid nitrogen. *Journal of Archaeological Science*, 31, 1567-1575.

Hsieh, H.P. (1996). Inorganic Membranes for Separation and Reaction, Amsterdam: Elsevier Science B.V.

Huang, W., Shuk, P., Greenblatt, M. (1997). Properties of sol-gel prepared $Ce_{1-x}Sm_xO_{2-x/2}$ solid electrolytes. *Solid State Ionics*, 100, 23-27.

Ishihara, T., Kilner, J. A., Honda, M., Sakai, N., Harumi, Y., Yusaku, T. (1998). Oxygen surface exchange and diffusion in LaGaO3 based perovskite type oxides. *Solid State Ionics*, 113-115, 593-600.

Ishihara, T., Yamada, T., Arikawa, H., Nishiguchi, H., Takita, Y. (2000). Mixed electronic-oxide ionic conducting and oxygen permeation property of Fe-, Co- or Ni-doped $LaGaO_3$ perovskite oxide, *Solid State Ionics*, 135, 631-636.

Janz, J., Allen, C., Bansal, P., Murphy, R., Tomkins, R. (1979). Physical Properties Data Compilations Relevant to Energy Storage; Molten Salts: Data on Single and Multi Component Salt System. Washington, DC: National Bureau of Standards.

Kharton, V. V., Yaremchenko, A. A., Kovalevsky, A. V., Viskup, A. P., Naumovich, E. N., Kerko, P. F. (1999). Perovskite-type oxides for high-temperature oxygen separation membranes. *Journal of Membrane Science*, 163, 307-317.

Kharton, V. V., Viskup, A. P., Kovalevsky, A. V., Jurado, J. R., Naumovich, E. N., Vecher, A. A., Frade, J. R. (2000). Oxygen ionic conductivity of Ti-containing strontium ferrite. *Solid State Ionics*, 133, 57-65.

Kim, J., Lin, Y. S. (1999). Synthesis and Characterization of Suspension-Derived, Porous Ion-Conducting Ceramic Membranes. *J. Am. Ceram. Soc.*, 82, 2641-2646.

Kniep, J., Yin, Q., Kumakiri, I., Lin, Y. S. (2010). Electrical conductivity and oxygen permeation properties of $SrCoFeO_x$ membranes. *Solid State Ionics*, 180, 1633-1639.

Kniep, J., Lin, Y. S. (2010). Effect of zirconium doping on hydrogen permeation through strontium cerate membranes. *Ind. Eng. Chem. Res.*, 49, 2768-2774.

Kniep, J., Lin, Y. S. (2010). Oxygen- and hydrogen-permeable dense ceramic membranes. In V.V. Kharton (Ed.), *Solid state electrochemistry II: electrodes, interfaces, and ceramic membranes*, Wiley-VCH, 467-500.

Koresh, J. E., Sofer, A. (2006). Molecular Sieve Carbon Permselective Membrane. Part I. Presentation of a New Device for Gas Mixture Separation. *Separation Science and Technology*, 18, 723-734.

Kruidhof, H., Bouwmeester, H. J. M., Doorn, R. H. E. v., Burggraaf, A. J. (1993). Influence of order-disorder transitions on oxygen permeability through selected nonstoichiometric perovskite-type oxides. *Solid State Ionics*, 63-65, 816-822.

Kusakabe, K., Kuroda, T., Murata, A., Morooka, S. (1997). Formation of a Y-Type Membrane on a Porous [alpha]-Alumina Tube for Gas Separation. *Ind. Eng. Chem. Res.*, 36, 649-655.

Lane, J. A., Kilner, J. A. (2000). Oxygen surface exchange on gadolinia doped ceria. *Solid State Ionics*, 136-137, 927-932.

Lei, Y., Wang, C., Yang, X., Pan, H., Wu, J., Wang, Q. (1995). A mathematical model for the cycle life of hydride electrodes. *Proceedings of the International Symposium on Metal-Hydrogen Systems-Fundamentals and Applications*, 231, 611-615.

Leo, A., Liu, S., Diniz da Costa, J. C. (2009). Development of mixed conducting membranes for clean coal energy delivery. *International Journal of Greenhouse Gas Control*, 3, 357-367.

Li, K. (2007). *Ceramic Membranes for Separation and Reaction*; West Sussex; Wiley.

Li, S.; Jin, W.; Huang, P.; Xu, N.; Shi, J., Lin, Y. S., Hu, M. Z.-C., Payzant, E. A. (1999). Comparison of Oxygen Permeability and Stability of Perovskite Type $La_{0.2}A_{0.8}Co_{0.2}Fe_{0.8}O_{3-\delta}$ (A = Sr, Ba, Ca) Membranes. *Ind. Chem. Eng. Res*, 38, 2963-2972.

Lin, Y. S., Burggraaf, A. J. (1993). Experimental Studies on Pore Size Change of Porous Ceramic Membranes after Modification. *Journal of Membrane Science*, 79, 65-82.

Lin, Y. S., Zeng, Y. (1996). Catalytic properties of oxygen semipermeable perovskite type ceramic membrane materials for oxidative coupling of methane. *Journal of Catalysis*, 164, 220-231.

Lin, Y.S. (2001). Microporous and dense inorganic membranes: current status and prospective. *Separation and Purification Technology*, 25, 39-55.

Liu, S., Tan, X., Li, K., Hughes, R. (2002). Synthesis of strontium cerates-based perovskite ceramics via water-soluble complex precursor routes. *Ceram. Int.*, 28, 327-335.

Lu, B., Lin, Y.S. (2013). Synthesis and characterization of thin ceramic-carbonate dual-phase membranes for carbon dioxide separation. *Journal of Membrane Science*, 444, 402-411.

Luebke, D. R., Pennline, H. W. (2003). $CO_2$ selective hybrid membranes by silation of alumina. *Proc. A. Int. Pitts. Coal Conf*, 20, 787-805.

Luo, H., Wei, Y., Jiang, H., Yuan, W., Lv, Y., Caro, J., Wang, H. (2010). Performance of a ceramic membrane reactor with high oxygen flux Ta-containing perovskite for the partial oxidation of methane to syngas. *Journal of Membrane Science*, 350, 154-160.

Manning, P. S., Sirman, J. D., Kilner, J. A. (1996). Oxygen self-diffusion and surface exchange studies of oxide electrolytes having the fluorite structure. *Solid State Ionics*, 93, 125-132.

Mori, T., Wang, Y., Drennan, J. Auchterlonie, G., Li, J.-G., Ikegami T. (2004). Influence of particle morphology on nanostructural feature and conducting property in Sm-doped $CeO_2$ sintered body. *Solid State Ionics*, 175, 641-649.

Nigara, Y., Mizusaki, J., Ishigame, M. (1995). Measurement of oxygen permeability in $CeO_2$ doped CSZ. *Solid State Ionics*, 79, 208-211.

Nigara, Y., Kosaka, Y., Kawamura, K., Mizusaki, J., Ishigame, M. (1996). Oxygen permeability in $ZrO_2$-$CeO_2$MgO at high temperature. *Solid State Ionics*, 86-88, 739-744.

Norton, T., Lin, Y.S. (2012). Transient Oxygen Permeation and Surface Catalytic Properties of Lanthanum Cobaltite Membrane under Oxygen-Methane Gradient. *Ind. Eng. Chem. Res.*, 51, 12917-12925.

Norton, T., Ortiz-Landeros, J., Lin, Y.S. (2013). Long Term Permeation Stability of $La_{0.6}Sr_{0.4}Co_{0.8}Fe_{0.2}O_{3-\delta}$-Carbonate Dual-Phase Membranes for $CO_2$ Separation at High Temperatures. To Be Submitted.

Ortiz-Landeros, J., Norton, T., Lin, Y.S. (2013). Effects of Pore Structure of Supports on Carbon Dioxide Permeation of Ceramic-Carbonate Dual-Phase Membranes. *Chem. Eng. Sci.*, accepted for publication.

Osada, K., Ohnishi, T., Shin, Y., Yoshino, J., Kurpishi, N. (1999). Development of inorganic membranes by sol-gel method for $CO_2$ separation. *Proc Int. Conf. Greenhouse Gas Control Technology*, 2, 43-45.

Pei, S., Kleefisch, M. S., Kobylinski, T. P., Faber, J., Udovich, C. A., Zhang-McCoy, V., Dabrowski, B., Balachandran, U., Mieville, R. L., Poeppel, R. B. (1995). Failure mechanisms of ceramic membrane reactors in partial oxidation of methane to synthesis gas. *Catalysis Letters*, 30, 201-212.

Perry, J. D., Nagai, K., Koros, W. J. (2006). Polymer membrane for hydrogen separations. *MRS Bulletin*, 31, 745-749.

Powell, C.E., Qiao, G.G. (2006). Polymeric CO2/N2 gas separation membranes for the capture of carbon dioxide from power plant flue gases. *Journal of Membrane Science*, 279, 1-49.

Prado, F., Grunbaum, N., Caneiro, A., Manthiram, A. (2004). Effect of $La^{3+}$ doping on the perovskite-to-brownmillerite transformation in $Sr_{1-x}La_xCo_{0.8}Fe_{0.2}O_{3-\delta}$ ($0 \leq x \leq 0.4$). *Solid State Ionics*, 167, 147-154.

Qi, X., Lin, Y. S., Swartz, S. L. (2000). Electric Transport and Oxygen Permeation Properties of Lanthanum Cobaltite Membranes Synthesized by Different Methods. *Ind. Eng. Chem. Res.*, 39, 646-653.

Qiu, L., Lee, T. H., Liu, L. M., Yang, Y. L., Jacobson, A. J. (1995). Oxygen permeation studies of $SrCo_{0.8}Fe_{0.2}O_{3-\delta}$. *Solid State Ionics*, 76, 321-329.

Rui, Z, Li, Y., Lin, Y. S. (2009). Analysis of oxygen permeation through dense ceramic membranes with chemical reactions of finite rate. *Chemical Enginnering Science*, 64, 172-179.

Rui, Z., Anderson, M., Lin, Y.S., Li, Y. (2009). Modeling and analysis of carbon dioxide permeation through ceramic-carbonate dual phase membranes. *Journal of Membrane Science*, 345, 110-118.

Rui, Z., Ji, H., Lin, Y. S. (2011). Modeling and analysis of ceramic-carbonate dual-phase membrane reactor for carbon dioxide reforming with methane. *International Journal of Hydrogen Energy*, 36, 8292-8300.

Rui, Z., Anderson, M., Li, Y., Lin, Y.S. (2012). Ionic conducting ceramic and carbonate dual phase membranes for carbon dioxide separation. *Journal of Membrane Science*, 417-418, 174-182.

Ruiz-Trejo, E., Sirman, J. D., Baikov, Y. M., Kilner, J. A. (1998). Oxygen ion diffusivity, surface exchange and ionic conductivity in single crystal Gadolina doped Ceria. *Solid State Ionics*, 113-115, 565-569.

Scholes, C. A., Smith, K. H., Kentish, S. E., Stevens, G. W. (2010). $CO_2$ capture from pre-combustion processes-Strategies for membrane gas separation. *International Journal of Greenhouse Gas Control*. 4, 739-755.

Schwartz, M., White, J. H., Sammells, A. F. (2000). *Patent No. 6,033,632*. US.

Schwartz, M., White, J. H., Sammells, A. F. (2001). *Patent No. 6,214,757*. US.

Shao, Z., Yang, W., Cong, Y., Dong, H., Tong, J., Xiong, G. (2000). Investigation of the permeation behavior and stability of a $Ba_{0.5}Sr_{0.5}Co_{0.8}Fe_{0.2}O_{3-\delta}$ oxygen membrane. *Journal of Membrane Science*, 175, 177-188.

Shao, Z., Xiong, G., Dong, H., Yang, W., Lin, L. (2001). Synthesis, oxygen permeation study and membrane performance of a $Ba_{0.5}Sr_{0.5}Co_{0.8}Fe_{0.2}O_{3-\delta}$ oxygen-permeable dense ceramic reactor for partial oxidation of methane to syngas. *Separation and Purification Technology*, 25, 97-116.

Shekhawat, Luebke, D. R., Pennline, H. W. (2003). A Review of Carbon Dioxide Selective Membranes. National Energy Technology Laboratory, Morgantown, WV, 2003.

Sirman, J. (2006). The evolution of materials and architecture for oxygen transport membranes. *Nonporous Inorganic Membranes*, Weinheim, Wiley-VCH Verlag, 165-184.

Steel, B. C. H. (1992). Oxygen ion conductors and their technological applications. *Materials Science and Engineering*, 13, 79-87.

Steeneveldt, R., Berger, B., Torp, T. A. (2006). $CO_2$ capture and storage. Closing the knowing-doing gap. *Chem. Eng. Res. Des.*, 84, 739-763.

Sunarso, J., Baumann, S., Serra, J. M., Meulenberg, W. A., Liu, S., Lin, Y. S., Diniz da Costa, J. C. (2008). Mixed ionic-electronic conducting (MIEC) ceramic-based membranes for oxygen separation. *Journal of Membrane Science*, 320, 13-41.

Tan, X., Liu, N., Meng, B., Sunarso, J., Zhang, K., Liu, S. (2012). Oxygen permeation behavior of $La_{0.6}Sr_{0.4}Co_{0.8}Fe_{0.2}O_3$ hollow fibre membranes with highly concentrated $CO_2$ exposure. *Journal of Membrane Science*, 389, 216-222.

Taniguchi, N., Nishimura, C., Kato, J. (2001). Endurance against moisture for protonic conductors of perovskite-type ceramics and preparation of practical conductors. *Solid State Ionics*, 145, 349-355.

ten Elshof, J. E., Bouwmeester, H. J. M., Verweij, H. (1995). Oxidative coupling of methane in a mixed-conducting perovskite membrane reactor. *Applied Catalysis A: General*, 130, 195-212.

ten Elshof, J. E., Bouwmeester, H. J. M., Verweij, H. (1996). Oxygen transport through $La_{1-x}Sr_xFeO_{3-\delta}$ membranes II. Permeation in air/CO, $CO_2$ gradients. *Solid State Ionics*, 89, 81-92.

Teraoka, Y., Zhang, H. M., Furukawa, S., Yamozoe, N. (1985). Oxygen Permeation Through Perovskite-type Oxides. *Chemistry Letters*, 1743-1746.

Teraoka, Y., Nobunaga, T., Yamazoe, N. (1988). Effect of Cation Substitution on the Oxygen Semipermeability of Perovskite-type Oxides. *Chemistry Letters*, 503-506.

Teraoka, Y., Honbe, Y., Ishii, J., Furukawa, H., Moriguchi, I. (2002). Catalytic effects in oxygen permeation through mixed-conductive LSCF perovskite membranes. *Solid State Ionics*, 152-153, 681-687.

Thambimuthu, K., Soltanieh, M., Abandas, J. C. (2005). IPCC Special Report on Carbon Dioxide Capture and Storage. Series Cambridge University Press, Cambridge.

Thursfield, A., Metcalf, I. S. (2007). Air separation using catalytically modified mixed conducting hollow fibre membrane module. *Journal of Membrane Science*, 288, 175-187.

Tong, J., Yang, W., Zhu, B., Cai, R. (2002). Novel and ideal zirconium-based dense membrane reactors for partioal oxidation of methane to syngas. *Catalysis Letters*, 78, 129-137.

Tong, J., Yang, W., Cai, R., Zhu, B., Lin, L. (2002). Novel and ideal zirconium-based dense membrane reactors for partial oxidation of methane to syngas. *Catalysis Letters*, 78, 129-137.

Trunec, M., Cihlar, J. (2006). Tubular $La_{0.7}Ca_{0.3}Fe_{0.85}Co_{0.15}O_{3-\delta}$ Perovskite Membranes, Part II: Performance and Stability. *J. Am. Ceram. Soc.*, 89, 955-959.

Tsai, C.-Y., Dixon, A. G., Moser, W. R., Ma, Y. H. (1997). Dense Perovskite Membrane Reactors for Partial Oxidation of Methane to Syngas. *Ceramics Processing*, 43, 2741-2750.

U.S. Environmental Protection Agency (2012). Draft Inventory of U.S. Greenhouse Gas Emissions and Sinks: 1990-2010. Environmental Protection Agency, Washington, DC.

Uhlhorn, R. J. R., Keizer, K., Burggraaf, A. J. (1989). Gas and surface diffusion in modified γ-alumina systems. *Journal of Membrane Science*, 26, 225-241.

Van Roosmalen, J. A. M., Cordfunke, E. H. P. (1991). A new defect model to describe the oxygen deficiency in perovskite-type oxides. *Journal of Solid State Chemistry*, 93, 212-219.

Wade, J.L., Lackner, K.S., West, A.C. (2007). Transport model for a high temperature, mixed conducting $CO_2$ separation membrane. *Solid State Ionics*, 178, 1530-1540.

Wade, J.L., Lee, C., West, A.C., Lackner, K.S. (2011). Composite electrolyte membranes for high temperature $CO_2$ separation, *Journal of Membrane Science*. 369, 20-29.

Wang, H. Tablet, C., Feldhoff, A., Caro, J. (2005). A cobalt-free oxygen permeable membrane based on the perovskite type oxide $Ba_{0.5}Sr_{0.5}Zn_{0.2}Fe_{0.8}O_{3-\delta}$. *Advanced Materials*, 17, 1785-1788.

Zhu, X., Wang, H., Yang, W. (2006). Partial oxidation of methane to syngas in $BaCe_{0.15}Fe_{0.85}O_{3-\delta}$ membrane reactors. *Catalysis Letters*, 111, 179-185.

Zhu, X., Cong, Y., Yang, W. (2006). Effects of synthesis methods on oxygen permeability of $BaCe_{0.15}Fe_{0.85}O_{3-\delta}$ ceramic membranes. *Journal of Membrane Science*, 283, 158-163.

Zhu, X., Cong, Y., Yang, W. (2006). Oxygen permeability and structural stability of $BaCe_{0.15}Fe_{0.85}O_{3-\delta}$ membranes. *Journal of Membrane Science*, 283, 38-44.

Waindich, A., Mobius, A., Muller, M. (2009). Corrosion of $Ba_{1-x}Sr_xCo_{1-y}Fe_yO_{3-\delta}$ and $La_{0.3}Ba_{0.7}Co_{0.2}Fe_{0.8}O_{3-\delta}$ materials for oxygen separating membranes under oxycoal conditions. *Journal of Membrane Science*, 337, 182-187.

Wu, Z., Jin, W., Xu, N. (2006). Oxygen permeability and stability of $Al_2O_3$-doped $SrCo_{0.8}Fe_{0.2}O_{3-\delta}$ mixed conducting oxides. *Journal of Membrane Science*, 279, 320-327.

Xu, N., Li, X., Franks, M.A., Zhao, H., Huang, K. (2012). Silver-molten carbonate composite as a new high-flux membrane for electrochemical separation of $CO_2$ from flue gas. *Journal of Membrane Science*, 401-402, 190-194.

Xu, Q., Huang, D. P., Chen, W., Lee, J. H., Kim, B. H., Wang, H., Yann, R. Z. (2004). Influence of sintering temperature on microstructure and mixed electronic-ionic conduction properties of perovskite-type $La_{0.6}Sr_{0.4}Co_{0.8}Fe_{0.2}O_3$ ceramics. *Ceramics International*, 30, 429-433.

Xu, Q., Huang, D. P., Chen, W., Lee, J. H., Wang, H., Yann, R. Z. (2004). Citrate method synthesis characterization and mixed electronic-ionic conduction properties of $La_{0.6}Sr_{0.4}Co_{0.2}Fe_{0.8}O_3$ perovskite-type complex oxides. *Scripta Materialia*, 50, 165-170.

Xu, S. J., Thomson, W. J. (1998). Stability of $La_{0.6}Sr_{0.4}Co_{0.2}Fe_{0.8}O_{3-\delta}$ Perovskite Membranes in Reducing and Nonreducing Environments. *Ind. Eng. Chem. Res.*, 37, 1290-1299.

Xu, S. J., Thomson, W. J. (1999). Oxygen permeation rates through ion-conducting perovskite membranes. *Chemical Engineering Science*, 54, 3839-3850.

Yan, A. Y., Maragou, V., Arico, A., Cheng, M. J., Tsiakaras, P. (2007). Investigation of a $Ba_{0.5}Sr_{0.5}Co_{0.8}Fe_{0.2}O_{3-\delta}$ based cathode SOFC II. The effect of $CO_2$ on the chemical stability. *Appl. Catal. B: Environ.*, 76, 320-327.

Yang, H., Xu, Z., Fan, M., Gupta, R., Slimane, R. B., Bland, A. E., Wright, I. (2008). Progress in carbon dioxide separation and capture: A review. *Journal of Environmental Sciences*, 20, 14-27.

Yang, Q., Lin, Y. S., Bulow, M. (2006). High temperature sorption separation of air for producing oxygen-enriched $CO_2$ stream. *AICHE Journal*, 52, 574-581.

Yang, W., Wang, H., Zhu, X., Lin, L. (2005). Development and application of oxygen permeable membrane in selective oxidation of light alkanes. *Topics in Catalysis*, 35, 155-167.

Yaremchenko, A. A., Kharton, V. V., Viskup, A. P., Naumovich, E. N., Lapchuk, N. M., Tikhonovich, V. N. (1999). Oxygen ionic and electronic transport in $LaGa_{1-x}Ni_xO_{3-\delta}$ perovskites. *Journal of Solid State Chemistry*, 142, 325-335.

Yi, J. X., Feng, S. J., Zuo, Y. B., Liu, W., Chen, C. S. (2005). Oxygen permeability and stability of $Sr_{0.95}Co_{0.8}Fe_{0.2}O_{3-\delta}$ in a $CO_2$- and $H_2O$-containing atmosphere. *Chem. Mater.*, 17, 5856-5861.

Yi, J., Schroeder, M., Weirich, T., Mayer, J. (2010). Behaviour of $Ba(Co,Fe,Nb)O_{3-\delta}$ perovskite in $CO_2$-containing atmosphere: degradation mechanism and material design. *Chem. Mater.*, 22, 6246-6253.

Yi, J., Schroeder, M. (2011). High temperature degradation of $Ba_{0.5}Sr_{0.5}Co_{0.8}Fe_{0.2}O_{3-\delta}$ membranes in atmospheres containing concentrated carbon dioxide. *Journal of Membrane Science*, 378, 163-170.

Yin, Q., Lin, Y. S. (2007). Beneficial effect of order-disorder phase transition on oxygen sorption properties of perovskite-type oxides. *Solid State Ionics*, 178, 83-89.

Yuan, W., Hu, X., Li, L. (2006). Preparation and Characterization of Single-Phase Perovskite $La_{0.6}Sr_{0.4}Co_{0.8}Fe_{0.2}O_{3-\delta}$. *Journal of Natural Gas Chemistry*,15, 58-62.

Zacharias, N. A., Nevers, D. R., Skelton, C., Knackstedt, K., Stephenson, D. E., Wheeler, D. R. (2013). Direct Measurements of Effective Ionic Transport in Porous Li-Ion Electrodes. *Journal of The Electrochemical Society*, 160, A306-A311.

Zeng, Y., Lin, Y. S., Swartz, S. L. (1998). Perovskite-type ceramic membrane: synthesis, oxygen permeation and membrane reactor performance for oxidative coupling of methane. *Journal of Membrane Science*, 150, 87-98.

Zeng, P., Ran, R., Chen, Z., Zhou, W., Gu, H., Shao, Z., Liu, S. (2008). Efficient stabilization of cubic perovskite $SrCoO_{3-\delta}$ by B-site low concentration scandium doping combined with sol-gel synthesis. *Journal of Alloys and Compounds*, 144, 465-470.

Zhang, K., Sunarso, J., Shao, Z., Zhou, W., Sun, C., Wang, S., Liu, S. (2011) Research progress and materials selection guidelines on mixed conducting perovskite-type ceramic membranes for oxygen production. *RSC Advances*, 1, 1661-1676.

Zhang, L., Li, X., Wang, S., Romito, K. G., Huang, K. (2011). High conductivity mixed oxide-ion and carbonate-ion conductors supported by a prefabricated porous solid-oxide matrix. *Electrochemistry Communications*, 13, 554-557.

Zhang, L., Mao, Z., Thomason, J. D., Wang, S., Huang, K. (2012). Synthesis of a Homogenously Porous Solid Oxide Matrix with Tunable Porosity and Pore Size. *Journal of the American Ceramic Society*, 95, 1832-1837.

Zhang, L., Xu, N., Li, X., Wang, S., Huang, K., Harris, W.H., Chiu, W.K.S. (2012). High $CO_2$ permeation flux enabled by highly interconnected three-dimensional ionic channels in selective $CO_2$ separation membranes. *Energy & Environmental Science*, 5, 8310-8317.

Zhu, X., Wang, H., & Yang, W. (2004). Novel cobalt-free oxygen permeable membrane. *Chemical Communications*, 1130-1131.

Zhu, X., Wang, H., Cong, Y., Yang, W. (2006). Partial oxidation of methane to syngas in $BaCe_{0.15}Fe_{0.85}O_{3-\delta}$ membrane reactors. *Catalysis Letters*, 111, 179-185.

Zhu, X., Li, Q., Cong, Y., Yang, W. (2008). Syngas generation in a membrane reactor with a highly stable ceramic composite membrane. *Catalysis Communications*, 10, 309-312.

Zolochevsky, A., Grabovskiy, A. V., Parkhomenko, L., Lin, Y. S. (2012). Coupling effects of oxygen surface exchange kinetics and membrane thickness on chemically induced stresses in perovskite-type membranes. *Solid State Ionics*, 212, 55-65.

# APPENDIX A

# SYNTHESIS OF PEROVSKITE TYPE LANTHANUM STRONTIUM COBALT IRON OXIDE MEMBRANES BY CITRATE METHOD

1. To synthesize $La_{0.6}Sr_{0.4}Co_{0.8}Fe_{0.2}O_{3-\delta}$ powder, weight out the appropriate amount of nitrate metal precursors. Table A.1 shows the weight of each precursor for the synthesis of 0.05 moles of product. Excess citric acid is added with the nitrate metal precursors to ensure complete reaction of the reactants.

*Table A.1 Constituents of $La_{0.6}Sr_{0.4}Co_{0.8}Fe_{0.2}O_{3-\delta}$*

| *Material* | *Weight (g)* |
|---|---|
| $La(NO_3)_3 \cdot 6H_2O$ | 12.993 |
| $Sr(NO_3)_2$ | 4.236 |
| $Co(NO_3)_3 \cdot 6H_2O$ | 11.642 |
| $Fe(NO_3)_3 \cdot 9H_2O$ | 4.040 |
| Citric acid | 38.524 |

2. Dissolve the nitrate metal precursors and citric acid in 1000 ml of de-ionized water.
3. Heat the solution on the hot plate to about 95 - 100$^{o}$C to carry out the polymerization reaction. Place a glass cover over the beaker to limit evaporation of water. Make sure the solution is not boiling during the process. Keep the solution at this temperature for 4 hours.
4. Remove the lid and evaporate the excess water from the solution at 100°C. This is known as the condensation process and will last for 3-4 hours, depending on the temperature and amount of water added at the start of the process.

5. At the end of condensation process, a viscous, gel-like substance should be obtained.
6. The gel is then dried in an oven at 120$^{o}$C for 24 hours.
7. After drying, the resulting brittle, porous material is self-ignited in a heating mantle at 400$^{o}$C to remove the organics that were present. Make sure air is supplied into the beaker so that the most of the organic components can be burned off.
8. Grind the resulting powder with a mortar and pestle for 10 minutes.
9. Calcine the powder at 600$^{o}$C for 20 hours (ramp rate = 2°C/min) to burn off the organic residues.
10. Regrind the powder for 10 minutes using a mortar and pestle.
11. Place approximately 3 grams of the calcined powder in a 2.3 cm diameter die and press the powder to 180 MPa.
12. Sinter the green disk in air at desired temperature for 24 hours (ramp rate = 2$^{o}$C/min).
13. The resulting membrane should be characterized with X-ray diffraction to verify the crystal structure and a room temperature unsteady state helium permeance test.

# APPENDIX B

# SYNTHESIS OF PEROVSKITE TYPE LANTHANUM CERIUM GALLIUM IRON ALUMINUM OXIDE MEMBRANES

1. To synthesize $La_{0.85}Ce_{0.1}Ga_{0.3}Fe_{0.653}Al_{0.05}O_{3-\delta}$ powder, weigh out the appropriate amount of metal oxide precursors. Table B.1 shows the weight of each precursor for the synthesis of 0.2 moles of product.

*Table B.1 Constituents of $La_{0.85}Ce_{0.1}Ga_{0.3}Fe_{0.653}Al_{0.05}O_{3-\delta}$*

| *Material* | *Weight (g)* |
|---|---|
| $La_2O_3$ | 27.694 |
| $CeO_2$ | 3.442 |
| $Ga_2O_3$ | 5.623 |
| $Fe_2O_3$ | 10.380 |
| $Al_2O_3$ | 0.510 |

2. Dissolve the metal oxide precursors in 1000 ml of de-ionized water.
3. Combine the slurry with zirconia balls in the ball miller canister.
4. Seal the canister and ball mill the solution for 24 hours.
5. After ball milling, transfer the solution to a beaker and allow the solution to dry.
6. Grind the resulting sample with a mortar and pestle for 10 minutes.
7. Calcine the powder at 950$^{o}$C for 10 hours (ramp rate = 2$^{o}$C/min).
8. Grind the resulting powder for another 10 minutes using a mortar and pestle.
9. Add 5 drops of water to 5 grams of powder followed by grinding in mortar and pestle prior to pressing.
10. Place approximately 4 grams of powder in a 2.3 cm diameter die and press the powder to 400 MPa.
11. Sinter the green disk in air at 1100$^{o}$C for 10 hours (ramp rate = 2$^{o}$C/min).

12. The resulting porous membrane should be characterized with X-ray diffraction to verify the crystal structure and a room temperature unsteady state helium permeance test.

# APPENDIX C

# SYNTHESIS OF FLUORITE TYPE SAMARIUM DOPED CERIUM OXIDE MEMBRANES

1. To synthesize $Ce_{0.8}Sm_{0.2}O_{1.9}$ powder, weigh out the appropriate amount of nitrate metal precursors. Table C.1 shows the weight of each precursor for the synthesis of 0.1 moles of product. Excess citric acid is added with the nitrate metal precursors to ensure complete reaction of the reactants.

*Table C.1 Constituents of $Ce_{0.8}Sm_{0.2}O_{1.9}$*

| *Material* | *Weight (g)* |
|---|---|
| $Ce(NO_3)_3 \cdot 6H_2O$ | 34.738 |
| $Sm(NO_3)_3 \cdot 6H_2O$ | 8.889 |
| Citric acid | 76.84 |

2. Dissolve the nitrate metal precursors and citric acid in 1000 ml of de-ionized water.
3. Heat the solution on the hot plate to about 95 - 100°C to carry out the polymerization reaction. Place a glass cover over the beaker to limit evaporation of water. Make sure the solution is not boiling during the process. Keep the solution at this temperature for 4 hours.
4. Remove the lid and evaporate the excess water from the solution at 100°C. This is known as the condensation process and will last for 3-4 hours, depending on the temperature and amount of water added at the start of the process.
5. At the end of condensation process, a viscous, gel-like substance should be obtained.
6. The gel is then dried in an oven at 120°C for 24 hours.

7. After drying, the resulting brittle, porous material is self-ignited in a heating mantle at 400$^{o}$C to remove the organics that were present. Make sure air is supplied into the beaker so that the most of the organic components can be burned off.
8. Grind the resulting powder with a mortar and pestle for 10 minutes.
9. Calcine the powder at 550$^{o}$C for 10 hours (ramp rate = 2°C/min) to burn off the organic residues.
10. Regrind the powder for 10 minutes using a mortar and pestle.
11. Place approximately 3 grams of the calcined powder in a 2.3 cm diameter die and press the powder to 180 MPa.
12. Sinter the green disk in air at desired temperature for 24 hours (ramp rate = 2$^{o}$C/min).
13. The resulting membrane should be characterized with X-ray diffraction to verify the crystal structure and a room temperature unsteady state helium permeance test.

# APPENDIX D

# UNSTEADY STATE MEMBRANE ROOM TEMPERATURE HELIUM PERMEATION

1. Mount the membrane in the stainless steel permeation cell (PC). If performing permeation at room temperature, be sure to seal the side of each membrane with a rubber O-ring. A schematic of the unsteady state system can be found in Figure D.1.

1. 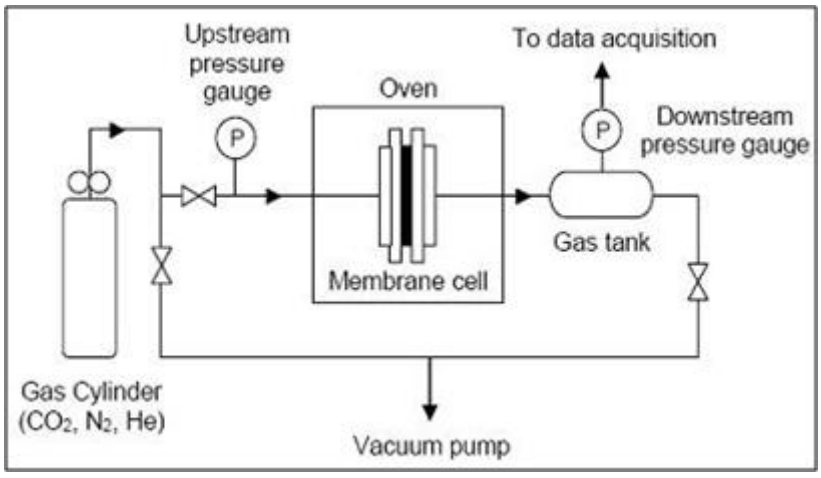


*Figure D.1 Unsteady state helium permeance test apparatus*

2. Be sure to tighten the bolts along the edges of the permeation cell so that the membrane is completely sealed. However, do not tighten the cell so much that is causes your membrane to break.
3. Evacuate the system with the vacuum pump. Leave the vacuum pump on until the pressure in the system reaches a minimum value. At this point, close the valves to seal the system under the vacuum
4. Once finished using the vacuum pump, turn it off. Leaving it on can cause the pump to either overheat or emit fumes into the surrounding area.
5. Before gathering permeance data, it is a good idea to check and make sure that there is no leak within the permeation cell by isolating the permeation cell. Let the system set for a couple of minutes and monitor the pressure readout (PR). If

the pressure does not change or the change is very minimal, then there is no leak and you can proceed to check the permeance of the membrane.

6. Open the valve which will allow helium gas to enter the system. Increase or decrease the pressure in the system by adjusting the flow rate of helium in the system. Monitor the upstream pressure gauge until the pressure in the system has reached the desired value.
7. On the computer that is attached to the unsteady state system, open Labview.
8. Type in a name that you want to save the file as. Keep in mind, it is usually a good idea to indicate some important parameters in the test file, such as the permeating gas, the gauge pressure of the system and the temperature at which the test was conducted.
9. Indicate the desired time step for data collection.
10. Click $\rightarrow$ and after about 1 second, open the valve to let the helium gas permeation through the membrane. Allow the system to take data for as long as it is necessary to gain an accurate measure of dP/dt, which is the slope of the line in the Labview window. Stop collecting data by clicking the red stop sign in the Labview window.
11. Export the data to a program, such as Excel, and graph it. Fit a line to the data and get the slope. As mentioned previously, the slope of this line is the dP/dt. Be sure to remember that dP/dt from this data is in units of mmHg/s.
12. Using the following equation, one can solve for the permeance of the membrane:

$$Q = \left(\frac{dP}{dt}\right)\left(\frac{V_c}{S \cdot R \cdot T \cdot (P_h - P_l)}\right) \qquad \text{(B.1)}$$

$Q \equiv$ permeance (*usually in moles/$m^2 \cdot Pa \cdot s$*)

$dP/dt \equiv$ change in pressure versus time

$V_c \equiv$ volume of the cylinder (*in this case, the cylinder is 1L or $10^{-3} m^3$*)

$S \equiv$ area of the membrane that is exposed to the permeating gas

$R \equiv$ gas constant for chosen units

$T =$ temperature

$P_h \equiv$ upstream pressure

$P_l \equiv$ downstream pressure

13. After completing all of the necessary experiments, be sure to relieve the pressure on the system. To do this, shut off the helium to the system and open all valves to the atmosphere.

# APPENDIX E

# DIRECT INFILTRATION OF MOLTEN CARBONATE IN CERAMIC MEMBRANE SUPPORTS

1. The LSCF membranes can be infiltrated with molten carbonate to form the LSCF-carbonate dual-phase membrane. This process can be dangerous and should be done with the utmost care. To begin, molten carbonate should be placed into one of the crucible cups. The cup should be placed into the vertical tube furnace and heated to 500°C.
2. Always wear a lab coat and a protective face shield when working with the molten carbonate. It is best to use high temperature gloves for this purpose.
3. At 500°C, the molten carbonate will be a very hot liquid. As such, it is prone to spill if one bumps the vertical furnace hard enough. Spilling of the hot liquid could start a fire if spilled on paper, or burn you or another lab member. Therefore, you should do your best to keep from bumping the furnace and causing such incidents.
4. Suspend your membrane about 1-2 cm above the molten carbonate. Allow the membrane to preheat for 10-20 min.
5. Slowly raise the crucible using the designed apparatus at the bottom of the furnace. Once the liquid barely touches the bottom surface of the membrane, let it remain for 15 min. A good sign that infiltration is complete is when the top surface of the membrane has a shiny look to it.
6. Lower the molten carbonate until it is about 1-2 cm below the membrane. Slowly remove the membrane from the furnace. Removing too fast can cause thermal shock which can cause the membrane to break.
7. Allow the membrane to cool to room temperature
8. Remove any excess carbonates with SiC polishing paper.

# APPENDIX F

# TOTAL CONDUCTIVITY MEASUREMENT

1. Polish the ceramic disk into a bar shape with a desired dimension about 2×10×16 mm for measurement. Four short silver wires (with 2-3 cm long end) were connected to the ends of the sample bar by a silver conductive paint.
2. Load the sample in a quartz tube and connect the four silver ends of the sample to the four wires in the system (see Figure 2.1). Connect the two outer end wires to the Potentiostat (Radiometer AIS, PG2O1), which is providing a direct electrical current through the sample bar, and connect the two inner wires to the digital multimeter (Protek, B-845), which measures the voltage drop along the inner section of the bar.
3. Heat the system to 900ºC with a temperature ramping rate of 5ºC/min in air.
4. Introduce the gas or gases into the system, under which the conductivity will be measured. The total gas flow for any environment is set at l00 ml/min.
5. Set the internal voltage of Potentiostat at 0 mV, and keep at standby mode to wait for steady state of the sample in the gas flow.
6. When both the display of the Potentiostat E (free) and the multimeter voltage are zero at standby mode, measurements can be started. Usually it takes three hours to reach steady state conditions in a new gas environment and 30 minutes at a new temperature.
7. For measurements, set the Potentiostat in operation mode with the voltage of 100mV, read the current value on the Potentiostat and the voltage value on the multimeter at the same time. The electrical resistance R of the inner section of the sample can be calculated by these two values. Combined with the distance of the inner section L, the width X and thickness Y of the bar, the conductivity σ can be calculated by the equation: $\sigma = L/(XYR)$.

# APPENDIX G

# HIGH TEMPERATURE GAS PERMEATION

1. Place a gas-tight membrane (verified by room temperature unsteady state helium permeance test) and silver seal on top of the inner alumina tube of the Probostat module (Norwegian Electro Ceramics AS) (see Figure 2.2). The membrane and seal are held in place by spring pressure applied by an alumina spacer on top of the membrane.
2. Heat the system to 950°C (ramp rate = 60°C/hr) with 30 ml/min of helium (He) and argon (Ar) flowing on either side of the membrane. The flow rate of the gases was regulated by mass flow controllers (MKS, Model 1179) and a four-channel readout (MKS, Type 247).
3. Once the system reached 950°C, a gas sample was taken from the Ar stream and the amount of He in the Ar stream (and therefore, the leakage rate through the seal) was determined by running the sample through a gas chromatographer (Aglient, 6890N) with a packed column (2836PC, Alltech) and a TCD detector.
4. If the He content in the Ar stream is quite high, the system is ramped up 1°C, allowed to dwell for an hour, and then additional gas samples are taken to determine if the He content has been lowered.
5. Step 4 is repeated until the He content in the Ar stream has been minimized.
6. Once the He leak has been minimized, the system can be ramped down (ramp rate = 60°C/hr) to experimental conditions.
7. Once the system has reached the temperature for experiments, the different gas mixtures can be introduced in the system. Steady state conditions are usually achieved after 3 hours for a gas mixture change or 1 hour after a temperature change.
8. The component make-up of the effluent feed or sweep gases were measured by running samples through the gas chromatograph.